

# Intelligent Signal Processing for Digital Healthcare Monitoring

Von der Fakultät für Elektrotechnik und Informatik  
der Gottfried Wilhelm Leibniz Universität Hannover  
zur Erlangung des akademischen Grades

Doktor-Ingenieur  
(abgekürzt: Dr.-Ing.)

genehmigte

**Dissertation**

von

M.Sc. Javier Conte Alcaraz

2022

Referent : Prof. Dr. Jürgen Peissig

Korreferent : Assist. Prof. Dr.-Ing. Sanam Moghaddamnia

Tag der Promotion : 17.12.2021

M.Sc. Javier Conte Alcaraz: *Intelligent Signal Processing for Digital  
Healthcare Monitoring*, Dissertation, © 2022

First of all, I would like to thank Prof. Dr. Jürgen Peissig for offering me a research position at the institute of communications technology (IKT) and for his valuable support, encouragement, and guidance throughout my research work.

Further, I would like to express my sincere gratitude and appreciation to my supervisor Prof. Dr. -Ing. Sanam Moghaddamnia for her insightful guidance, great encouragement, and endless support to me throughout the course of my Ph.D. program. Whenever there were difficulties and obstacles in my research work, she always gave me the advice to help me solve these hurdles. I have appreciated her constant encouragement and motivation, which I needed during my Ph.D. journey at the IKT.

Also, I would like to express my deep appreciation and thank you, Mr. Marwan Hammouda, Mr. Martin Fuhrwerk, and Mr. Maxim Penner for all the valuable feedback and excellent advice on various topics related to this thesis.

During my stay at the IKT, I had the opportunity to supervise several students for their master projects and theses. I would like to thank them for their work on data collection and experiments. Additionally, I would like to thank all the participants of the experiments and measurements conducted in this thesis.

This thesis is dedicated to my father, my mother, and my brother for their endless love, intellectual guidance, never-ending support (through the hard times), and tremendous encouragement and support along the journey of my education. They have given me incredible opportunities to further my overseas education, and without them, all the achievements in my life would not be possible.





---

## ABSTRACT

---

Healthy gait is a complex process and requires a balance between various neurophysiological systems in the body and is considered an essential indicator of a subject's physical and cognitive health status. Consequently, applications in bioinformatics and healthcare would significantly profit from the information of a prolonged period or constant monitoring of subjects' gait, habits, and behavior in their natural living conditions and everyday daily activities using smart devices.

Comparing inertial measurement and fixed sensors systems, the first ones provide excellent capabilities for gait analysis applications and offer several advantages such as small size, low price, mobility, and are easily integrated into wearable systems. The second ones are considered the gold standard, but they are costly and unsuitable for outdoor measurements.

This thesis focuses on improving the gait rehabilitation time and quality after an operation using inertial measurement units by providing a novel metric to objectively assess the gait rehabilitation progress in real-life settings and reducing the number of applied sensors for practical, real-life scenarios. Therefore, the experimental measurements for such analysis have been performed in a highly controlled setting to guarantee the data quality. This thesis presents a new gait metric that quantifies and tracks the rehabilitation progress using kinematic gait data from activities carried out in indoor and outdoor environments. The thesis investigates how signal processing and machine learning can be formulated and utilized to develop robust methods to tackle real-life challenges. It is shown that the proposed approach can be personalized to track the gait rehabilitation progress. Another issue addressed in this thesis is the successful machine learning methods applied to gait analysis due to the high amount of data generated by the wearable sensor systems. The thesis introduces the novel concept of "digital twins", which reduces the applied wearable sensors in a system or case of sensor failure.

The evaluation of the proposed metric with healthy participants and patients using statistical signal processing and machine learning methods showed that incorporating the extracted signal features is robust in real-life scenarios, especially for the scenario involving rehabilitation gait exercises in indoor settings. The methodology was also evaluated in a clinical study and delivered a good performance in monitoring the rehabilitation progress of different patients. This thesis presents a prototype mobile application for objective assessment of the gait rehabilitation progress in real-life settings.

**Keywords:** Gait parameter estimation, nonlinear Modeling, IMU, Tracking, Rehabilitation, Gait Analysis, Neural Network, Machine Learning, Deep Learning.

---

## ZUSAMMENFASSUNG

---

Ein gesunder Gang ist ein komplexer Prozess und erfordert ein Gleichgewicht zwischen verschiedenen neurophysiologischen Systemen im Körper und gilt als wesentlicher Indikator für den physischen und kognitiven Gesundheitszustand einer Person. Folglich würden Anwendungen im Bereich der Bioinformatik und des Gesundheitswesens erheblich von den Informationen profitieren, die sich aus einer längeren oder ständigen Überwachung des Gangs, der Gewohnheiten und des Verhaltens von Personen unter ihren natürlichen Lebensbedingungen und bei ihren täglichen Aktivitäten mit Hilfe intelligenter Geräte ergeben.

Vergleicht man Trägheitsmess- und stationäre Sensorsysteme, so bieten erstere hervorragende Möglichkeiten für Ganganalyseanwendungen und bieten mehrere Vorteile wie geringe Größe, niedriger Preis, Mobilität und sind leicht in tragbare Systeme zu integrieren. Die zweiten gelten als der Goldstandard, sind aber teuer und für Messungen im Freien ungeeignet.

Diese Arbeit konzentriert sich auf die Verbesserung der Zeit und Qualität der Gangrehabilitation nach einer Operation unter Verwendung von Inertialmessgeräten, indem sie eine neuartige Metrik zur objektiven Bewertung des Fortschritts der Gangrehabilitation in realen Umgebungen liefert und die Anzahl der verwendeten Sensoren für praktische, reale Szenarien reduziert. Daher wurden die experimentellen Messungen für eine solche Analyse in einer stark kontrollierten Umgebung durchgeführt, um die Datenqualität zu gewährleisten. In dieser Arbeit wird eine neue Gangmetrik vorgestellt, die den Rehabilitationsfortschritt anhand kinematischer Gangdaten von Aktivitäten in Innen- und Außenbereichen quantifiziert und verfolgt. In dieser Arbeit wird untersucht, wie Signalverarbeitung und maschinelles Lernen formuliert und genutzt werden können, um robuste Methoden zur Bewältigung von Herausforderungen im realen Leben zu entwickeln. Es wird gezeigt, dass der vorgeschlagene Ansatz personalisiert werden kann, um den Fortschritt der Gangrehabilitation zu verfolgen. Ein weiteres Thema dieser Arbeit ist die erfolgreiche Anwendung von Methoden des maschinellen Lernens auf die Ganganalyse aufgrund der großen Datenmenge, die von den tragbaren Sensorsystemen erzeugt wird. In dieser Arbeit wird das neuartige Konzept des "digitalen Zwillings" vorgestellt, das die Anzahl der verwendeten Wearable-Sensoren in einem System oder im Falle eines Sensorausfalls reduziert.

Die Evaluierung der vorgeschlagenen Metrik mit gesunden Teilnehmern und Patienten unter Verwendung statistischer Signalverarbeitungs- und maschineller Lernmethoden hat gezeigt, dass die Einbeziehung der extrahierten Signalmerkmale in realen

Szenarien robust ist, insbesondere für das Szenario mit Rehabilitations-Gehübungen in Innenräumen. Die Methodik wurde auch in einer klinischen Studie evaluiert und lieferte eine gute Leistung bei der Überwachung des Rehabilitationsfortschritts verschiedener Patienten. In dieser Arbeit wird ein Prototyp einer mobilen Anwendung zur objektiven Bewertung des Rehabilitationsfortschritts in realen Umgebungen vorgestellt.

**Schlagwörter:** Gangparameterschätzung, nichtlineare Modellierung, IMU, Tracking, Rehabilitation, Ganganalyse, Neuronales Netzwerk, Maschinelles Lernen, Deep Lernen.

---

## CONTENTS

---

<b>Dissertation</b>	1
<b>1 INTRODUCTION</b>	3
1.1 Motivation . . . . .	4
1.2 Open issues . . . . .	5
1.3 Contributions . . . . .	6
1.4 Thesis outline . . . . .	7
<b>2 HUMAN GAIT</b>	9
2.1 The gait process . . . . .	9
2.2 Gait signals . . . . .	11
2.2.1 Temporal-spatial . . . . .	12
2.2.2 Electrical . . . . .	12
2.2.3 Kinetic . . . . .	12
2.2.4 Kinematic . . . . .	12
2.3 Measurement systems . . . . .	13
2.3.1 Electromyography . . . . .	13
2.3.2 Force pressure sensors and switches . . . . .	14
2.3.3 Camera systems . . . . .	15
2.3.4 Micro-electro-mechanical system . . . . .	15
2.4 Wearable IMU system . . . . .	19
2.5 Concluding remarks . . . . .	20
<b>3 DATA ACQUISITION</b>	21
3.1 Android application . . . . .	21
3.1.1 Android structure . . . . .	22
3.1.2 Application components . . . . .	22
3.1.3 Activities . . . . .	23
3.1.4 Priority . . . . .	23
3.1.5 Life cycle . . . . .	23
3.1.6 Services . . . . .	24
3.1.7 Threads . . . . .	25
3.1.8 Bluetooth . . . . .	26
3.1.9 Application implementation . . . . .	27
3.2 Data measurements . . . . .	28
3.2.1 Healthy participant measurements . . . . .	29

3.2.2	Rehabilitation clinic . . . . .	30
3.3	Concluding remarks . . . . .	31
4	SIGNAL PREPROCESSING . . . . .	33
4.1	Sensor fusion . . . . .	33
4.1.1	Discrete-time system representation . . . . .	34
4.1.2	Assumptions in Kalman filtering . . . . .	35
4.1.3	Estimation procedure . . . . .	36
4.1.4	Zero velocity update . . . . .	39
4.1.5	Lower body joint angle estimation . . . . .	42
4.1.6	Quaternions and reference system . . . . .	43
4.2	Concluding remarks . . . . .	45
5	OBJECTIVE GAIT ASSESSMENT . . . . .	47
5.1	Feature extraction . . . . .	48
5.1.1	Time domain . . . . .	48
5.1.2	Regularity and symmetric features . . . . .	49
5.1.3	Frequency domain . . . . .	51
5.1.4	Time-frequency domain . . . . .	56
5.2	Feature selection and dimension reduction . . . . .	58
5.2.1	Principal component analysis . . . . .	60
5.2.2	Linear discriminant analysis . . . . .	61
5.2.3	Student's t-test . . . . .	62
5.2.4	SNR ranking . . . . .	63
5.3	Grading System . . . . .	64
5.3.1	Results . . . . .	65
5.3.2	Acoustic feedback for rehabilitation . . . . .	67
5.4	Concluding Remarks . . . . .	70
6	DIGITAL TWINS OF GAIT KINEMATICS . . . . .	73
6.1	Related work . . . . .	74
6.2	Modeling approaches . . . . .	75
6.2.1	Physical models . . . . .	76
6.2.2	Behavioral models . . . . .	76
6.3	Polynomial models for joint estimation . . . . .	76
6.3.1	Volterra model and special cases . . . . .	76
6.3.2	Comparison to MPM . . . . .	77
6.3.3	The memory-polynomial model for joint estimation . . . . .	78
6.3.4	Memory polynomial model identification . . . . .	79
6.3.5	Results . . . . .	80
6.4	Neuronal networks for joint estimation . . . . .	84
6.4.1	Generalized regression neural networks . . . . .	85

6.4.2	Recurrent neural networks . . . . .	85
6.5	Deep neuronal networks for joint estimation and rehabilitation monitoring . . . . .	88
6.5.1	Long short-term memory network for joint estimation . . . . .	88
6.5.2	Results . . . . .	92
6.5.3	Convolutional neuronal networks for rehabilitation monitoring . . . . .	95
6.5.4	Results . . . . .	98
6.6	Concluding remarks . . . . .	100
7	CONCLUSIONS AND FUTURE WORK . . . . .	103
	BIBLIOGRAPHY . . . . .	105
	PUBLICATIONS . . . . .	117
	CURRICULUM VITAE . . . . .	119

---

## LIST OF FIGURES

---

Figure 2.1	Illustration of the three principal anatomical planes of the human body. . . . .	9
Figure 2.2	Gait events and gait phases in one gait cycle. The two phases of stance and swing define a gait cycle. The IC initiates the stance phase, and the TOE terminates it. 60% of a gait cycle is contained in the stance phase. The swing phase starts when the toe has no contact with the ground and terminates right before the next IC. The other 40% of the gait cycle is the swing phase. . . . .	10
Figure 2.3	Flexion and extension direction of the lower body joint angles in the sagittal plane. . . . .	11
Figure 2.4	Typical hip, knee and ankle joint angle trajectories in a complete normal gait cycle. . . . .	13
Figure 2.5	Example of muscle activity measurement using electrodes that measures the potential differences between two points. . . . .	14
Figure 2.6	Example of a force plate and pressure insoles from AMTI Force and Motion [9]. . . . .	14
Figure 2.7	Illustration of a OptiTrack camera system [10]. . . . .	15
Figure 2.8	Illustration of a 3D IMU. . . . .	16
Figure 2.9	Example of a three-dimensional acceleration signal. . . . .	17
Figure 2.10	Example of a three-dimensional gyroscope signal. . . . .	17
Figure 2.11	Example of a three-dimensional magnetometer signal. . . . .	18
Figure 2.12	Illustration of the Wearable Sensor System [19]. . . . .	19
Figure 2.13	Shimmer component diagram [18]. . . . .	19
Figure 3.1	Illustration of Android's structure . . . . .	21
Figure 3.2	Illustration of activity life cycle . . . . .	24
Figure 3.3	Illustration of separate thread and handler . . . . .	25
Figure 3.4	Illustration of Shimmer class for communications management. . . . .	27
Figure 3.5	Illustration of ObjectCluster . . . . .	28
Figure 3.6	Illustration of application overview . . . . .	28
Figure 3.7	Illustration of the data flow between threads. . . . .	28
Figure 3.8	Data flow between the UI thread and the CSound thread . . . . .	29
Figure 3.9	Walking route for the measurements. . . . .	29



Figure 3.10	Knee brace and modification of the support point of the foot. Support points: (A) Caput des Os metatarsae I, (B) Caput des Os metatarsae V and (C) Tuber calcanei . . . . .	30
Figure 3.11	Sequence of measurements and intervention in the intervention study on patients for system assessment. . . . .	30
Figure 4.1	Gait analysis process. . . . .	33
Figure 4.2	PDR diagram applying KF. . . . .	34
Figure 4.3	Processing and measurement models. . . . .	35
Figure 4.4	KF recursive processes. . . . .	36
Figure 4.5	Prediction and update processes. . . . .	38
Figure 4.6	Illustration of the angular velocity in the sagittal plane from different locations. The IC and TOE events are obtained from the foot angular velocity. The red triangle, green circle and black square markers represent the MS, IC and TOE, respectively.	41
Figure 4.7	Block diagram of the indirect Kalman Filter. . . . .	42
Figure 4.8	Lower body joint angles in the sagittal plane compared to the reference system. . . . .	43
Figure 4.9	Shimmer (white) and reference (orange) sensor system platform.	43
Figure 4.10	IMU Block diagram of the orientation filter. . . . .	43
Figure 4.11	(a) Comparison between the acceleration in the sensor frame (S) and the earth frame E. (b) Quaternion used to rotate the signal from the sensor frame (S). . . . .	44
Figure 5.1	Overview of the objective gait assessment process . . . . .	48
Figure 5.2	Illustration of peak asymmetric factor . . . . .	49
Figure 5.3	Autocorrelation function of acceleration data during normal walking. . . . .	50
Figure 5.4	Example of the entropy function for an event with two equiprobable states . . . . .	54
Figure 5.5	Example of the periodic and stochastic parts for the knee joint angle. . . . .	55
Figure 5.6	IMF signal decomposition for the foot angular velocity in the sagittal plane which, is used as input for the networks. . . . .	59
Figure 5.7	Grading system block diagramm. . . . .	63
Figure 5.8	Efficiency of the grading system based on SNR . . . . .	64
Figure 5.9	Efficiency of the grading system based on LDA . . . . .	65
Figure 5.10	Efficiency of the grading system based on PCA . . . . .	65
Figure 5.11	Assessment of the rehabilitation training. . . . .	67
Figure 5.12	Wearable system setup consisting of seven IMUs, an Android tablet and headphones. . . . .	68

Figure 5.13	Gait speed comparison between the experimental and the control patient group with and without RTAF during the rehabilitation sessions. Striped bars represent the experimental patient group with real-time acoustic feedback. . . . .	68
Figure 5.14	Gait cadence comparison between the experimental and the control patient group with and without RTAF during the rehabilitation sessions. Striped bars represent the experimental patient group with real-time acoustic feedback. . . . .	69
Figure 5.15	Gait length comparison between the experimental and the control patient group with and without RTAF during the rehabilitation sessions. Striped bars represent the experimental patient group with real-time acoustic feedback. . . . .	69
Figure 5.16	Individual performance comparison between an experimental and a control patient during the two weeks study . . . . .	69
Figure 5.17	Individual performance comparison between an experimental and a control patient during the two weeks study . . . . .	70
Figure 6.1	Overall system concept: The gait kinematic data $x(n)$ are collected and processed with ML methods in the Android application for digital and biomedical healthcare systems. On the left side, the traditional sensor fusion algorithm based on KF estimates the lower limb joint signals using the information from several IMUs. On the right side, the novel ML approach estimates the lower limb joint angles based on the information of only one IMU placed on the foot. The dashed line represents the reference data $y(n)$ for the training and test phases of the ML approaches. . . . .	73
Figure 6.2	The memory polynomial model. . . . .	78
Figure 6.3	MPM implementation . . . . .	79
Figure 6.4	Performance comparison of MPM for different nonlinearity orders $K$ . Triangle markers represent the all-order terms. Circle markers represent the even-order terms. Square markers represent the odd-order terms. The optimal values can be found, where the NMSE is minimized. . . . .	81
Figure 6.5	Performance comparison of MPM for different values of the memory depth parameter $Q$ using the optimal values of $K$ . Triangle markers represent the all-order terms. Circle markers represent the even-order terms. Square markers represent the odd-order terms. . . . .	82

Figure 6.6	Estimation of the joint angles using the MPM and the optimal values for K and Q. The blue solid line represents the reference signal. The red dashed line represents the estimation. . . . .	83
Figure 6.7	Cross-validation estimation results of the joint angles using the proposed MPM and the optimal values for K and Q. The blue solid line represents the reference signal. The red dashed line represents the estimation. . . . .	84
Figure 6.8	Architecture of a RNN with an input, a hidden and an output layer. The network maps the input sequence $x_{D_i,t}$ to a hidden sequence $h_{n,t}$ and to a sequence of outputs $y_{m,t}$ . The parameters $D_i$ , $n$ and $m$ are the number of signals, the number of hidden units and the number of outputs, respectively. $W_{xh}$ , $W_{hh}$ and $W_{hy}$ are the input to hidden, hidden to hidden and hidden to output matrices, respectively. The bias vectors of the network are represented by $b_h$ for the hidden layer and by $b_y$ for the output layer. . . . .	86
Figure 6.9	A NARX network with series to parallel architecture. The TDL blocks introduce past values (memory effect) of the input and output signals to the network . . . . .	87
Figure 6.10	LSTM cell. The cell can process data sequentially and keeps its hidden state $h$ over the time. . . . .	89
Figure 6.11	Estimated lower limb joint angles in the sagittal plane using the GRNN with the input set 4 and the reference lower limb joint angles from the wearable system. Blue solid lines and red dashed lines are the reference and the estimated joints angles, respectively. . . . .	93
Figure 6.12	Estimated lower limb joint angles in the sagittal plane using the NARX with the input set 4 and the reference lower limb joint angles from the wearable system. Blue solid lines and red dashed lines are the reference and the estimated joints angles, respectively. . . . .	94
Figure 6.13	Estimated lower limb joint angles in the sagittal plane using the LSTM with the input set 4 and the reference lower limb joint angles from the wearable system. Blue solid lines and red dashed lines are the reference and the estimated joints angles, respectively. . . . .	94

Figure 6.14	Wearable System Concept: the gait kinematic data are collected and processed with ML methods in an Android application for digital and biomedical healthcare systems. First step, data collection from patients with hip unilateral arthroplasty surgery. Second step, segmentation of kinematic signals in GC. Third step, use of different IMUs and kinematic signals to train the proposed DCNN for rehabilitation progress monitoring. . . . .	96
Figure 6.15	Classification accuracy of one IMU applying the proposed DCNN for Pelvis (P), Left Upper Leg (LUL), Left Lower Leg (LLL) and Left Foot (LF). . . . .	97
Figure 6.16	Classification accuracy of multiple IMUs applying the proposed DCNN. . . . .	99

---

## LIST OF TABLES

---

Table 2.1	Sensor configuration for kinematic data acquisition . . . . .	19
Table 5.1	Signal Features . . . . .	60
Table 5.2	Classification results . . . . .	67
Table 6.1	Optimal parameters for the MPM of different joint angles based on an IMU located at one foot. . . . .	83
Table 6.2	Input sets of the neural networks. . . . .	90
Table 6.3	Average RMSE performance comparison of the different neu- ral networks and inputs sets. . . . .	92
Table 6.4	Proposed DCNN architecture and hyperparameters. . . . .	98

---

## ACRONYMS

---

<b>ADAM</b>	adaptive moment estimation
<b>ADC</b>	analogue-to-digital converter
<b>AMD</b>	acceleration magnitude detection
<b>AMS</b>	acoustic model sequences
<b>AMVD</b>	acceleration moving variance detector
<b>ANN</b>	artificial neural network
<b>ANR</b>	application not responding
<b>AP</b>	anterior posterior
<b>API</b>	application programming interface
<b>ARED</b>	angular rate energy detector
<b>BN</b>	batch normalization
<b>CNN</b>	convolutional neural network
<b>D</b>	dropout
<b>DC</b>	direct current
<b>DCNN</b>	deep convolutional neural network
<b>DFT</b>	discrete Fourier transform
<b>DL</b>	deep learning
<b>DNN</b>	deep neural network
<b>DT</b>	digital twin
<b>EKF</b>	extended Kalman filter
<b>EMD</b>	empirical mode decomposition
<b>EMG</b>	electromyography
<b>FDR</b>	Fisher's discriminant ratio
<b>FFT</b>	fast Fourier transform
<b>FNN</b>	feedforward neural network
<b>FT</b>	Fourier transform
<b>GC</b>	gait cycle
<b>GRNN</b>	generalized regression neural network
<b>HHT</b>	Hilbert-Huang transformation
<b>HT</b>	Hilbert transform
<b>IA</b>	instantaneous amplitude
<b>IC</b>	initial contact
<b>IDFT</b>	inverse discrete Fourier transform
<b>IE</b>	instantaneous energy
<b>IF</b>	instantaneous frequency
<b>IKT</b>	institute of communications technology
<b>IMF</b>	intrinsic mode function
<b>IMU</b>	inertial measurement unit
<b>INS</b>	inertial navigation system
<b>ISM</b>	industrial, scientific and medical
<b>KF</b>	Kalman filter
<b>KL</b>	Karhunen-Loève
<b>LDA</b>	linear discriminant analysis

<b>LS</b>	least squares
<b>LSTM</b>	long short-term memory
<b>LTI</b>	linear time invariant
<b>MEMS</b>	micro-electro-mechanical system
<b>MI</b>	motion intensity
<b>ML</b>	machine learning
<b>MLP</b>	multilayer perceptron
<b>MPM</b>	memory polynomial model
<b>MRC</b>	maximum ratio combining
<b>MS</b>	mid-swing
<b>NARX</b>	nonlinear autoregressive network with exogenous inputs
<b>NB</b>	naive Bayes
<b>NMSE</b>	normalized mean square error
<b>NMSE</b>	normalized mean square error
<b>NN</b>	neural network
<b>OS</b>	operating system
<b>PCA</b>	principal component analysis
<b>PDF</b>	probability density function
<b>PDR</b>	pedestrian dead recognition
<b>PSD</b>	power spectral density
<b>ReLU</b>	rectified linear unit
<b>RFCOMM</b>	radio frequency communication
<b>RMP</b>	randomly modulated periodicity
<b>RMS</b>	root mean square
<b>RMSE</b>	root mean square error
<b>RNN</b>	recurrent neural network
<b>RTAF</b>	real-time acoustic feedback
<b>SE</b>	spectral entropy
<b>SEMG</b>	surface electromyography
<b>SMNR</b>	sum signal-to-noise-modulation-ratio
<b>SNR</b>	signal to noise ratio
<b>SOD</b>	stance optimal detector
<b>SSL</b>	secure socket layer
<b>STM</b>	state transition matrix
<b>TDL</b>	taped delay line
<b>TOE</b>	toe off
<b>TS</b>	time series
<b>UI</b>	user interface
<b>WE</b>	wavelet entropy
<b>WS</b>	wearable sensors
<b>WSS</b>	wearable sensor system
<b>WT</b>	wavelet transformation
<b>XML</b>	eXtensible Markup language
<b>ZUPT</b>	zero velocity update





# DISSERTATION



---

## INTRODUCTION

---

Due to diseases, signs of aging, accidents, and surgical interventions, the gait characteristics of normal humans can change. Also, the mobility of individual limbs or the coordination of movement sequences can be restricted. In the long term, this results in a variety of severe consequential damages to the hip and spine and, accordingly, a significant reduction in quality of life. Intensive and long-term physiotherapy is necessary to restore the physiological mobility of patients. Concurrent therapy is often time-consuming and cost-intensive and depends on the findings. In exceptional cases, methods of objective gait analysis are used to supplement subjective biomechanical findings, but their application is complex.

For healthy persons, walking is part of daily life. To the question: How do you walk correctly? There is no answer at first. Walking is controlled by the subconscious and seems to work by itself. Walking is a highly complex task and has to be learned during childhood over a relatively long period.

The human gait results from a complex interaction between the central and peripheral nervous systems as well as the supporting and locomotor systems. The gait analysis proves to be a more sensitive indicator for disturbances in this complex interaction. Therefore, the gait evaluation is an excellent diagnostic tool for such disorders.

After the failure of parts of the locomotor system due to illness or accident, the patient has to relearn how to walk. He adapts to the changed conditions and changes its course. For example, if the patient's walking is painful due to a leg injury, this will develop a gait modification. The aching leg is relieved and tries to develop other body parts by increasing activity, to compensate for the failure. It is not uncommon, especially during more extended periods of injury, that the modified gait is maintained after healing. This faulty pattern sequence can cause permanent damage after a more extended period of time, e.g., to the spinal column lead. This can be avoided by proper rehabilitation treatment.

Mobile and customizable methods of objective gait analysis and gait training are only available to a minimal extent. Due to the increasing shortage of time at work and in daily life, the use of a mobile objective gait analysis system has great potential as a rehabilitation or therapy aid as well as a means of evaluating the course of rehabili-

tation. With such a procedure, a more effective, time- and cost-efficient rehabilitation process can be achieved, which can also be supplemented by independent training appointments at the patient's own home. With the novel mobile instruction and feedback method investigated in this thesis, the rehabilitation period is significantly shortened, especially in the case of the knee and hip prosthetics, and the follow-up costs of the rehabilitation are significantly reduced.

After an illness or accident, sometimes permanent damage to the musculoskeletal system occurs, so walking is not possible or only possible to a minimal extent. The use of rehabilitation technology enables compensation for this damage. The loss of, e.g., a leg can be partially compensated by a leg prosthesis as an individual adaptation of the limb for the patient. The quality of the aid only becomes apparent during use when walking.

### 1.1 MOTIVATION

The previous Section illustrates that gait analysis is essential for orthopedics, surgery, neurology, occupational, accident, and sports medicine, and many related fields. The gait analysis is suitable for use as a diagnostic tool and monitoring therapy. Especially, it can be used as a means of quality control of rehabilitation measures and for the evaluation of rehabilitation methodology.

The most frequently used method for assessing gait is the visual subjective gait analysis, whereby the evaluation is based on the observer's (physician, master orthopedic surgeon, etc.) experience and Know-How of gait. However, subjective gait analysis has its limits. On the one hand, it provides excellent qualitative statements. On the other hand, it depends strongly on the observer's wealth of experience. Important aspects relevant to gait analysis are entirely removed from the visual assessment, e.g., the degree of strain on the legs during walking. The instrumental gait analysis enables the limits mentioned above to be overcome. In principle, the objective measurement of gait parameters is independent of the observer and serves as an important addition to the subjective gait analysis. Although, as a result of technical progress, the possibilities of gait analysis have been enormously advanced in the past years, the current application in practice is still unsatisfactory. Most measuring stations for gait analysis consider either small training paths, or their use is too time-consuming for practical and routine operation. Last but not least, the high acquisition costs are one of the reasons for the low penetration of the measuring systems.

With the fast-growing healthcare and biomedical data, the field of biomedical informatics is emerging and is an excellent scenario for the application of artificial intelligence and machine learning for its exceptional chances, and scenarios [1]. The data contain different types and ranges of information going from individuals to groups of people and have connected diverse organisms in healthcare systems. These data

are becoming an enabling resource to use for scientific knowledge discovery and clinical decision-making. Simultaneously, the vast amount and complex relationships within the information present significant obstacles to their application into effective practical clinical actions. In particular, biomedical and healthcare information is frequently characterized by vast amounts of data, high dimensionality, disproportion across classes, diverse sources, distortion, and incompleteness, which demand the application of existing machine learning and optimization methods. Therefore, there is a huge demand for novel algorithms, including machine learning, data mining, and optimization, that specifically address the unique challenges associated with biomedical and healthcare data allowing better interpretation and exploiting the data.

This thesis aims to help overcome the technical limitations of previous research work by developing a novel rehabilitation tracking framework using advanced feature extraction techniques and machine learning methods. By providing additional information obtained from gait monitoring results, this framework can be used for both healthy people and patients to understand, monitor the gait performances, and classify and evaluate the progress during the rehabilitation process.

## 1.2 OPEN ISSUES

As the background has shown, many open issues remain to be investigated. In particular, the most relevant issues regard the analysis of the collected data and the selection of the most appropriate methods for classification, quantification, and monitoring the rehabilitation. The issues investigated in this work include the following:

- Quantitative statement on healthy and patient gait.
- Rehabilitation monitoring.
- Reduce the number of sensors and increase accuracy.
- How to develop and optimize a classification system for rehabilitation?
- How to measure the success of the exercises?
- How to grade the quality of the rehabilitation performance?
- Address the problem of the amount of data generated by the systems.

Additionally, this work provides open issues regarding the feedback:

- Which information from the gait kinematic signals needs to be conveyed to the user?
- Is acoustic feedback suited for walking rehabilitation?
- Is the feedback clear for the patient?

- Provided with acoustic feedback, does the patient reduce the rehabilitation duration?

### 1.3 CONTRIBUTIONS

In this work, while tackling the objectives mentioned above, the following contributions were achieved:

- Evaluation of the novel monitoring method: The proposed method is applied to quantify and evaluate the efficacy of the rehabilitation progress.
- Integration of the algorithm in small and unnoticeable tracking systems to supply valuable information. This will help to accurately determine the rehabilitation training for individuals with variable responses to the exercises.
- Quantification of the rehabilitation performance
- A novel "digital twins" modeling method for reducing the applied sensors in the system. The practical use of the sensor system for patients is increased due to the fewer sensors to be attached to the patient's lower limbs.
- A new deep convolutional neural network (DCNN) for monitoring the rehabilitation progress using the kinematic gait data from only one inertial measurement unit (IMU) placed at the foot.
- The novel algorithm can be integrated with patients' continuous monitoring systems. This will help evaluate the progress of individuals going through physical rehabilitation at home.
- Detection of subtle changes in an individual's range of motion. The tracking algorithm can provide valuable information about the performance of patients working and recovery path.
- A new long short-term memory (LSTM) network for the body lower limbs joints modeling using the kinematic gait data from only one IMU.
- Analysis, comparison, and development of different gait feature methods and models based on three-dimensional kinematic gait data captured from the lower body limbs with different sensors for gait pattern classification in terms of accuracy and robustness. The new models use the nonlinear relationships of the kinematic signals to increase the accurate estimation of the model
- A novel mobile prototype application for supporting digital healthcare and therapy. The prototype uses the state-of-the-art IMUs to obtain the kinematic data from the subjects and analyze the signals in real-time.

- Improvement of the time and progress in the rehabilitation process by applying signal processing and machine learning.

#### 1.4 THESIS OUTLINE

The structure of this thesis is organized as follows:

- In Chapter 2 basic terminologies required to describe the gait mechanism and an overview of the gait signals and measurement systems are provided. The different gait parameters and gait measurement systems are explained. In addition, the advantages and disadvantages of each method are also discussed.
- In Chapter 3, the fundamental components of the prototype Android application are briefly introduced, and gait data measurements campaigns are described, respectively. The application has the fundamental function of capturing and processing kinematic data. Further, the gait data measurements of healthy participants and patients will be used to perform different analyses.
- In Chapter 4, the preprocessing steps applied to the kinematic data are presented. Here, the main focus is made on preparing the kinematic signals for the feature extraction and the estimation of the lower body joint angles using sensor fusion techniques.
- In Chapter 5, a framework for the object gait assessment is provided. Here, the time, frequency, and time-frequency domain information is utilized to evaluate the performance and monitor the rehabilitation progress. Different features are extracted from the three-dimensional kinematic signals from seven different IMUs placed at the body lower limbs of healthy participants and patients. The novel grading metric and the acoustic feedback are investigated and analyzed with a clinical study.
- In Chapter 6, the concept “digital twin” is proposed for sensor reduction. The nonlinear modeling approach is utilized in estimating the lower body joint angles from one IMU. The proposed memory polynomial model (MPM) and deep neural networks (DNNs) are investigated and evaluated using kinematic data from healthy participants and patients.
- Chapter 7 provides a summary of the thesis outcomes and an outlook on some research issues for future work.





---

## HUMAN GAIT

---

This chapter introduces the basic terminologies required to describe the gait mechanism and provides an overview of the gait signals and measurement systems.

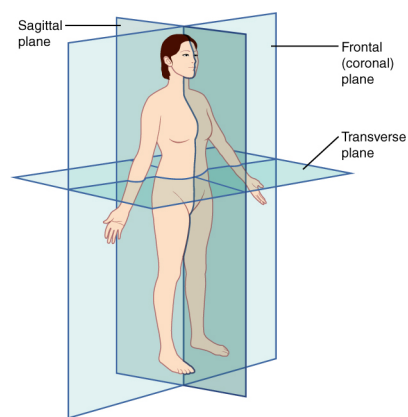


Figure 2.1: Illustration of the three principal anatomical planes of the human body.

### 2.1 THE GAIT PROCESS

The intentional and free movement pattern of the lower extremities during the locomotion process is defined as human gait. This process is two-footed and includes a two-phased forward movement, and is the outcome of a complex proceeding including muscles, peripheral nerves, and the brain, among others [2]. The field of gait analysis emerges from various science-based areas such as biomechanics, anatomy, and physiology. The systematic analysis of the walking process is called gait analysis [3]. Evaluating gait characteristics and patterns to provide better diagnosis and rehabilitation routines is one of the most relevant purposes of gait analysis. Prior to analyzing the gait in detail, it is necessary to introduce the basic terminologies of the human body used to describe the gait. As illustrated in Figure 2.1, three planes are within the human body:

- The sagittal plane splits the body into two symmetrical right and left halves.
- The frontal plane distinguishes the rear and frontal parts of the body.

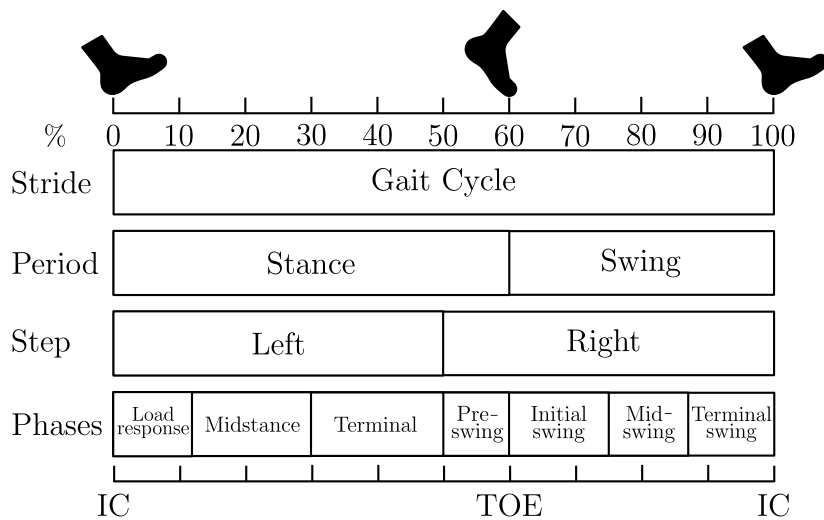


Figure 2.2: Gait events and gait phases in one gait cycle. The two phases of stance and swing define a gait cycle. The IC initiates the stance phase, and the TOE terminates it. 60% of a gait cycle is contained in the stance phase. The swing phase starts when the toe has no contact with the ground and terminates right before the next IC. The other 40% of the gait cycle is the swing phase.

- The transverse plane divides the upper body and lower body.

The repetition of a succession of forwarding movement patterns while simultaneously sustaining the body stability is called walking [4]. During the forward movement, the task of one extremity is to hold the body weight, and the other extremity serves to advance itself to a new forward position. There is a weight transfer when both extremities contact the ground. The gait cycle is the most basic concept in clinical gait analysis. As depicted in Figure 2.2, one gait cycle is delimited between two sequential initial contacts (ICs) from one foot. An IC event is defined at the point where the foot makes contact with the ground during walking [4]. The terms IC and heel contact are often used as synonyms in the literature due to the initial contact striking the ground with the heel in normal gait. A gait cycle contains in its most elemental description two phases: stance and swing phase. The contact between the foot and the ground occurs during the stance phase. The swing phase starts as the foot has no contact with the ground. The stance phase duration is about 60% of the total gait cycle, and the swing phase is about 40% [4].

The knowledge of the lower body segments implicated in the gait process is fundamental to understanding the gait cycle. Four principal segments actuate during the walking process. These are the ankle, the foot, the knee, and the hip. Figure 2.3 shows the flexion and extension direction of the lower body joint angles in the sagittal plane.

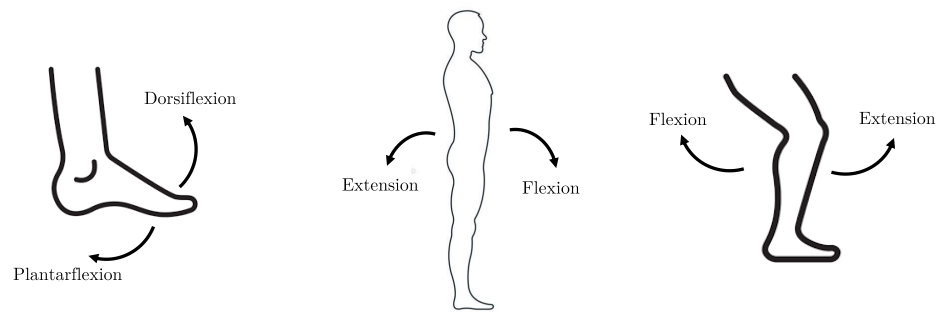


Figure 2.3: Flexion and extension direction of the lower body joint angles in the sagittal plane.

The point where one segment is in contact with another is called a joint. The proper action of the leg muscles is essential for the correctness of the segment movements. The function of these segments and the connection with the muscles through the gait process is as follows [5]:

- The ankle is the coupling between the foot and the shank. During the stance phase, the plantar-flexors are active, and the dorsi-flexors are active during the swing phase.
- Three sections form the foot: the metatarsophalangeal, the midtarsal, and the subtalar. These sections and their muscles have the principal function of shock absorption, stability, and forward movement control. These tasks occur sequentially as floor contact proceeds from IC to total forefoot support.
- The knee is the union of the Tibia and Femur, which constitute the significant segments of the lower extremities. In the stance phase, the extremity stability is determined by the knee. In the swing phase, the principal role of the knee is the free forward movement of the extremity.
- The hip is the junction between the upper body and the lower extremities. Consequently, it is designed to provide three degrees of movement with specific muscle control for each direction. During the stance phase, the role of the hip muscles is to stabilize the upper body parts. In the swing phase, the hip muscles perform the forward movement of the body.

## 2.2 GAIT SIGNALS

The evaluation of four different types of signals is expected to determine gait performance: temporal-spatial, electrical, kinetic, and kinematic signals. Those signals provide a natural intuition of the subject's walking and have been widely used for gait assessment. This work focuses on the analysis and process of temporal-spatial and kinematic signals.

### 2.2.1 *Temporal-spatial*

Temporal-spatial measurements examine the global aspects of gait measured in time and length. They are typically calculated based on time series (TS) signals (gyroscope, accelerometer, etc.) which vary during walking. These kinds of signals are typically considered in gait to be a semi-periodic behavior. The gait cycles possess an elevated similitude during steady walking, and the collected gait data is generally processed and analyzed by applying the information of several gait cycles. Standard temporal-spatial parameters are:

- Stride time is the total time to complete a gait cycle.
- Step distance is the length between the two heels contacts from the same foot.
- Cadence is the ratio between steps and time.
- Stride distance is the length traveled between two successive foot strikes of the same foot.
- Speed is the distance covered in a given time; speed is measured in meters per second [6].

### 2.2.2 *Electrical*

Electrical signals primarily determine the muscle activation between two points utilizing electrodes to measure the electric potential differences [5]. Typically, surface skin electrodes are applied to measure the electrical activities of muscles. For invasive cases, intramuscular wire electrodes are used for the measurements. It is possible to use this kind of signal to recognize the gait period by analyzing the muscle activation during the walking phases.

### 2.2.3 *Kinetic*

Kinetic measures refer to the joint torques or joint moments, which are the efforts to change the velocity of the segments [5]. The summation of different components at the joint such as the external, gravitational, inter-segment, and angular torques, result in the total torque [2, 3].

### 2.2.4 *Kinematic*

Kinematics is the study of body motion without considering the force that caused it [7]. The kinematic analysis components are the characterization and determination

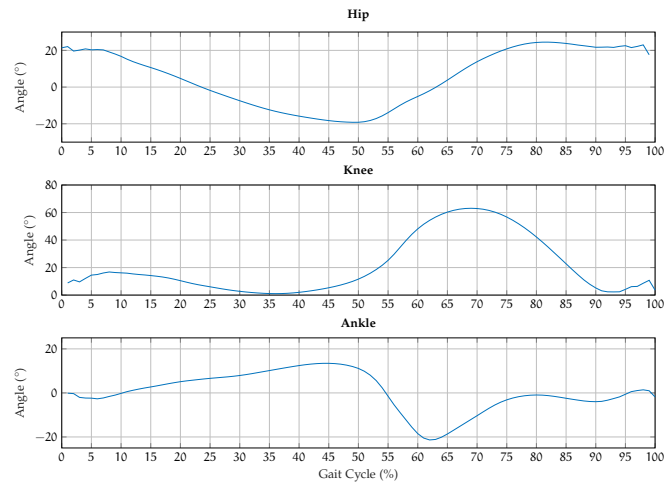


Figure 2.4: Typical hip, knee and ankle joint angle trajectories in a complete normal gait cycle.

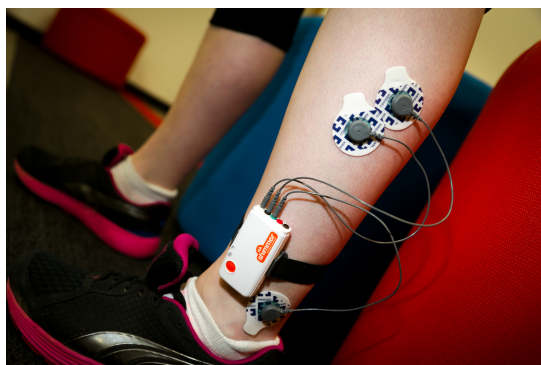
of the body movement patterns regarding how fast the change or how much distance travel. The kinematic measures of the body's lower extremities mainly refer to the hip, knee, and ankle joints and accelerations and angular velocity. Knowledge of the lower extremity angles implicated in the gait process is necessary to apply the signal processing methods in gait analysis correctly. The hip angle is the junction between the thigh and the trunk. During the flexion movement, the hip angle is positive and negative in extension movement. The junction between the foot and the Tibia defines the ankle angle. The range of motion varies for the different joints. For the ankle, the range for normal gait is around  $-15^{\circ}$  to  $+15^{\circ}$ . In typical cases, the knee possesses a broader range of motion from  $0^{\circ}$  to  $+70^{\circ}$  in typical cases. The average hip range of motion reaches from  $-30^{\circ}$  to  $+30^{\circ}$ . A detailed description of the complete angle trajectories and phases can be found in [4]. The hip, knee, and ankle joint angle trajectories for a normal gait cycle are illustrated in Figure 2.4.

## 2.3 MEASUREMENT SYSTEMS

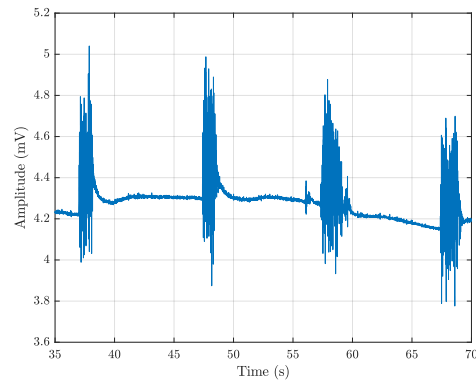
The assessment of the movement patterns of the human body during walking is often performed utilizing multiple sensors and recorded in a supervised environment. These sensors include electromyography (EMG), force pressure sensors, electromechanical switches, camera-based systems, micro-electro-mechanical system (MEMS) and IMUs. Each of these systems is introduced in this section.

### 2.3.1 Electromyography

EMG is an electrical manifestation of the contracting muscle, which can be either a voluntary or involuntary muscle contraction. The EMG signal is obtained from



(a) Shimmer EMG sensor



(b) EMG signal

Figure 2.5: Example of muscle activity measurement using electrodes that measures the potential differences between two points.



Figure 2.6: Example of a force plate and pressure insoles from AMTI Force and Motion [9].

the subject either by non-invasive measuring with surface electrodes (see Figure 2.5), or by invasive with wire or needle electrodes. For further analysis, the raw electrical signals have to be preprocessed. The preprocessing steps usually are amplification and conditioning, resulting in a better form and range which is more suitable for research and analytical purposes. The electromyography signals' non-stationary characteristics and minimal amplitude often cause difficulties when measuring these complex type analog signals. The practical use of surface electromyography (SEMG) for non-invasive measurements of pathophysiological and locomotor disorders has been demonstrated [8].

### 2.3.2 Force pressure sensors and switches

Footswitches are used to determine the timing of gait phase events precisely. They are located normally under the toe and the heel in order to detect the foot's contact with the ground. The principal application of pressure sensors is the distribution assessment of the foot pressure during walking [5]. The gait stability during walk-



Figure 2.7: Illustration of a OptiTrack camera system [10].

ing can be estimated by applying the information collected from these sensors. An example of the above mentioned sensors is depicted in Figure 2.6.

### 2.3.3 Camera systems

Camera-based systems offer a means for recording and reviewing the entire body's motion. This kind of system (see Figure 2.7) usually applies a high number of cameras in a limited indoor environment and detects the position of reflective markers fixed on predetermined positions on the body or lower extremities [10]. Camera systems are usually quite precise but are comparably more expensive and require more extensive space and longer setup time. The participant typically wears dark clothes with reflective markers attached to the Pelvis, thigh, shank, and foot for gait applications. The kinematic data related to the segments can be estimated and tracked using the markers. The images acquired during the measurement are used to look for the joints based on the locations of the reflective markers and later processed to estimate the angle. These systems are considered to be state-of-the-art. However, they are costly.

### 2.3.4 Micro-electro-mechanical system

Despite the fact that the detailed and accurate information provided by camera and pressure sensor systems, their use in outdoor environments, continuous daily activity monitoring, and long-time measurement is not appropriate [11]. For such objectives, inertial sensors developed using MEMS technology have excellent characteristics and a variety of factors such as cost, practical use, comfort, weight, mobility, and low power consumption. Thus, they are not limited to indoor spaces as seen in cameras (e.g., illumination effects) or pressure sensors. The MEMS features above mentioned

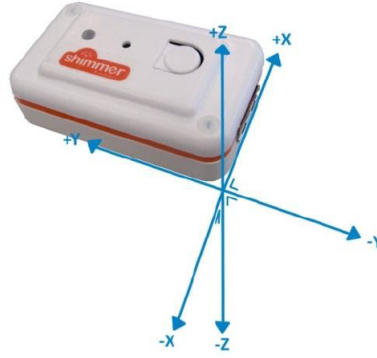


Figure 2.8: Illustration of a 3D IMU.

are used in the inertial/magnetic sensor units. By applying sensor fusion techniques, it is possible to estimate the orientation of each segment relative to an earth-fixed reference frame independently in real-time by placing these sensor modules in each of the significant extremities of the human body. It is also possible to generate a human body model from the information transferred independently from the extremities without knowing their relative orientation. There are several studies in the area of gait analysis and tracking based on MEMS [12–16]. Nevertheless, the major problem related to MEMS-based inertial sensors is the noise, which causes errors in calibration, bias, thermo-mechanical distortion, and other non-desired effects, etc. [17].

#### 2.3.4.1 *Inertial measurement unit*

IMUs generally consist of three different MEMS sensors: accelerometers, gyroscopes and magnetometers. Depending on the application, the sensors have one, two, or three axes.

#### 2.3.4.2 *Accelerometer*

The forces applied to an object are directly proportional to the object's acceleration. The acceleration is defined as the variation of velocity with respect to time [18]. It is measured in units of  $m/s^2$ . An accelerometer is a device capable of measuring all accelerations applied to it. The two principal components of acceleration are inertial and gravitational acceleration. The resulting acceleration,  $\mathbf{a}_T$ , measured by the device is [18]:

$$\mathbf{a}_T = \mathbf{a}_I + \mathbf{g}, \quad (2.1)$$

where  $\mathbf{a}_I$  is the inertial component and  $\mathbf{g}$  is the gravitational component [18]. Inertial acceleration manifests itself when forces other than gravity are applied. There are inertial forces actuating on a body, except if the body is not moving or possesses constant speed. When an accelerometer is completely stationary (i.e., there is no in-



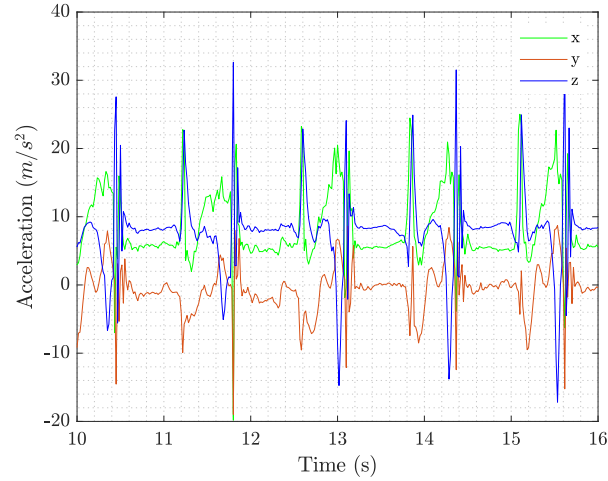


Figure 2.9: Example of a three-dimensional acceleration signal.

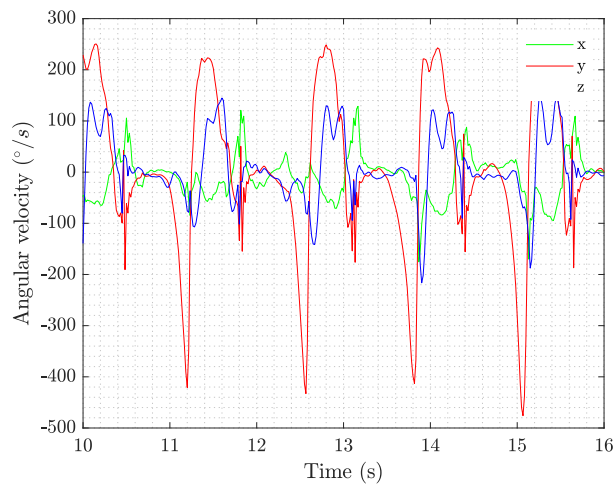


Figure 2.10: Example of a three-dimensional gyroscope signal.

ertial acceleration acting on the device), it measures a constant acceleration equal in magnitude to the acceleration due to gravity ( $9.81 \text{ m/s}^2$  approx). This is often referred to in units labeled "g", where  $1g \approx 9.81 \text{ m/s}^2$ . A 3D accelerometer is formed of three mutually orthogonal mono-axial accelerometers. Each axis measures a certain proportion of both gravitational acceleration and inertial acceleration [19].

#### 2.3.4.3 Gyroscope

The angular change of one object concerning the time around an axis is defined as angular velocity [18]. A device capable of measuring angular velocity is called a gyroscope. The angular velocity measured by the gyroscope is given by [18]:

$$\omega = \omega \cos(\alpha), \quad (2.2)$$

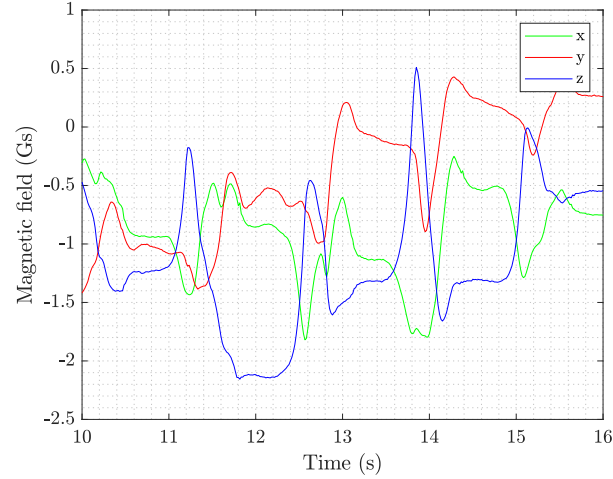


Figure 2.11: Example of a three-dimensional magnetometer signal.

where  $\omega$  is the resulting angular velocity vector along the measuring axis,  $\alpha$  is the angle between  $\omega$  and the angular velocity vector  $\mathbf{w}$  [18]. If  $\omega$  is aligned with  $\mathbf{w}$ , the measured angular velocity is equal to  $\mathbf{w}$ . On the other hand, if  $\omega$  is perpendicular to  $\mathbf{w}$ , the angular velocity is zero. A 3D gyroscope is formed of three mutually orthogonal mono-axial gyroscopes [19].

#### 2.3.4.4 Magnetometer

Magnetic materials and electric circulation create a local magnetic field affecting the objects and devices around them [18]. The Earth generates a constant magnetic field that flows from the South pole to the North pole, which affects all magnetic devices. Large metal objects and electromagnetic sources can interfere with the Earth's local magnetic field, creating heading errors. The measurement of a device's heading or the strength of the surrounding magnetic field is performed by a magnetometer. The magnetic field measured by the magnetometer, whose measurement axis  $\mathbf{m}$  makes an angle,  $\beta$ , with the magnetic field vector  $\mathbf{b}$  is given by

$$m = \mathbf{b}\cos(\beta), \quad (2.3)$$

where  $m$  is the magnitude of the magnetic field vector component along the measuring axis of the magnetometer,  $\beta$  is the angle between the magnetometer measuring axis and the magnetic field vector, and  $\mathbf{b}$  is the magnitude of the magnetic field acting on the sensor [18]. If  $\mathbf{m}$  is aligned parallel with  $\mathbf{b}$ , the measured magnetic field component is equal to  $\mathbf{b}$ . On the other hand, if  $\mathbf{m}$  is perpendicular to  $\mathbf{b}$ , the measurement of the magnetic field is zero. 3D Magnetometers have three orthogonal mono-axis [19].

## 2.4 WEARABLE IMU SYSTEM



Figure 2.12: Illustration of the Wearable Sensor System [19].

The wearable IMU system of Shimmer shown in Figure 2.12 is a small wireless sensor platform well suited for wearable applications [19]. Emerging research fields in motion capture, continuous monitoring, and data acquisition for long periods are possible due to the characteristics of the integrated sensors, such as low-power consumption, and low-energy communication standards, among others. Figure 2.13 presents a block diagram of the Shimmer mainboard with core components and interconnections between integrated device components illustrated. The central element of the platform is the low-power microprocessor, which controls the operation of the device. The CPU configures and controls various integrated peripherals through I/O pins, some of which are available on the internal/external-expansion connectors.

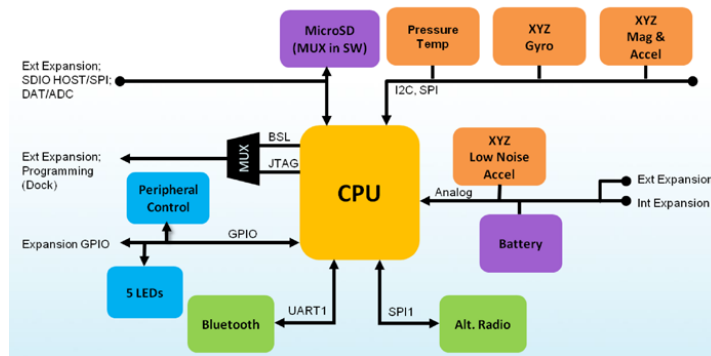


Figure 2.13: Shimmer component diagram [18].

Table 2.1: Sensor configuration for kinematic data acquisition

Sensor type	Range	Resolution
3DoF Accelerometer	$\pm 20$ g ( $m/s^2$ )	16 bit
3DoF Gyroscope	$\pm 2000$ dps ( $^\circ/s$ )	16 bit
3DoF Magnetometer	$\pm 1.3$ Gs ( $100 \mu T$ )	16 bit

The CPU has an integrated 16 channels 16 bits analogue-to-digital converter (ADC) to capture sensor kinematic data [18]. Table 2.1 provides information on the range and resolution of the IMUs used in this work. The external communication with other devices occurs through the docking station and the expansion slot. A built-in microSD slot offers additional storage capacity. The devices are equipped with a low-energy Bluetooth chip to transfer the kinematic data wirelessly.

## 2.5 CONCLUDING REMARKS

This chapter explicitly introduces and explains the basic concepts of human gait. This knowledge is essential for applying signal processing methods and machine learning architectures correctly. It is then followed by introducing several measurement systems for gait analysis and the different types of signals typically used for gait analysis. In the following chapters, the signal processing methods and machine learning approaches applied in this work for gait analysis and rehabilitation monitoring are detailed, as well as validation work and experimental and practical outcomes from real scenarios.

---

## DATA ACQUISITION

---

This chapter introduces the Android framework, the developed application for receiving and processing the kinematic gait data from the IMUs and the data acquisition measurements performed in different scenarios with healthy and patient participants in the rehabilitation clinic. The gathered data was employed to develop robust methods for gait rehabilitation monitoring and gait analysis. The goal is to develop a reliable, transparent, and validated solution for gait analysis and rehabilitation monitoring that is easy to use in real scenarios.

### 3.1 ANDROID APPLICATION

This section provides an overview of the Android operating system and the basic understanding of building an application. Android is a multifunctional and open software and offers many tools to create an application. Some valuable characteristics of Android are: open code operating system (OS), open development platform, a vast amount of devices using the same OS and a big programmer community [20].

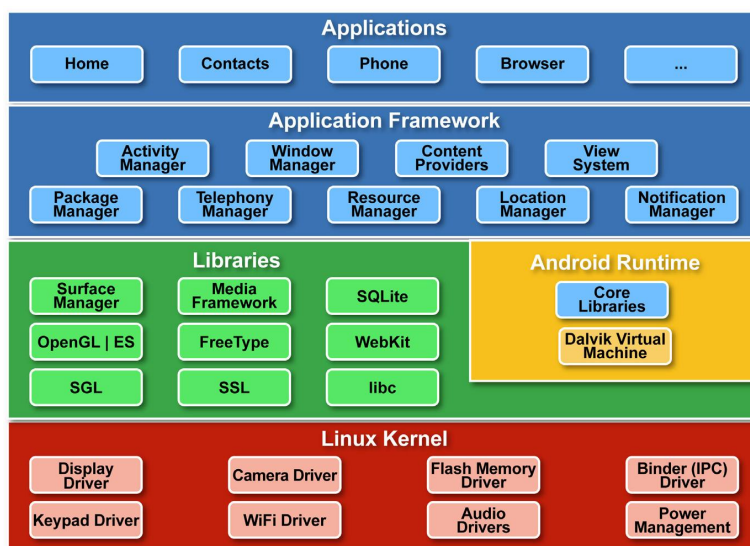


Figure 3.1: Illustration of Android's structure

### 3.1.1 *Android structure*

The different layers in which Android is built are shown in Figure 3.1. The most important layers are given below [21]:

- The Linux kernel contains the low-level drivers for all the Android hardware components. This layer also has security services, processor management, and a protocol stack.
- The libraries include all code that contains the main functionalities of the Android OS. Some main libraries are: SQLite, Webkit, FreeType, secure socket layer (SSL), etc.
- The Runtime contains the core libraries that allow developers to create their own applications using Java. The Dalvik Virtual Machine is also in this layer and allows running each application in a separate process using a virtual machine instance. This virtual machine was specially designed for Android, and it is optimized to work on mobile devices with battery, low memory, and processor capacity, and it can execute multiple machine instances.
- The application framework includes the different application managers, e.g., activity manager, notification manager, Resources manager [22].
- The applications are on the top of the stack, and they can be the native and also the non-native applications.

### 3.1.2 *Application components*

The first step to understanding how to program a signal processing application is to know its components and how they communicate themselves to obtain the goal functionality. Android has a set of basic components [20] as follows:

- Activities extend the Activity class, use the screen, and have a visual representation.
- Views are components of the user interface (UI). Views are defined by design layouts that are eXtensible Markup language (XML) files where the visual content is defined.
- Services are processed in the background, without the user's control and UI. There are local services, which are used from our device, and there are also remote services, which can be used from remote devices. Services update data and activities, send notifications and create intents.

For a list with all components refer to [22].

### 3.1.3 *Activities*

An Activity is an application component that provides a screen with which users can interact in order to do something, such as receive the kinematic data from the IMUs, perform preprocessing, extract features from the signals [20]. Each activity has a window to draw its UI. An application usually consists of several activities that work together to perform the desired action [20]. In order to perform different actions, activities can start other activities.

### 3.1.4 *Priority*

Android is a system that maximizes users' attention. The system manages the resources looking for the best user experience [20]. Android will stop other applications from prioritizing the current application if more resources are necessary. Active applications run and use memory until the user stops them, or the system needs more resources for other applications. At this point, any application could be stopped by the system. Low-priority applications are the first to be stopped. Priority is an essential factor because it is the property that Android analyzes when more resources are needed. Priority analysis of an application is not a straightforward process considering that it needs to know the dependencies of the application [22]. Therefore, an application's finalization order is determined by its own priority level. So, our application must be well structured with an adequate priority due to its realized function, and if it is not like this, there is a risk of a forced stop of the application. To understand this mechanism is helpful to know the application's states described in [20]. Real-time applications for gait analysis have higher priorities than other non-real-time applications.

### 3.1.5 *Life cycle*

The Android operating system controls all resources to provide a good response time for the application and to offer a good experience for the user. Android decides to stop or not a process. To make this decision, Android calculates the priority level of the application using the activity states. For this reason, it is helpful to know the states of the activities and their life cycle [20]. Therefore, an application and its activities have to coexist inside Android's system, where other applications and services are running. In this scenario, the knowledge about the application's life cycle and every state and every change that occurred during the process while the user uses the device are very important.

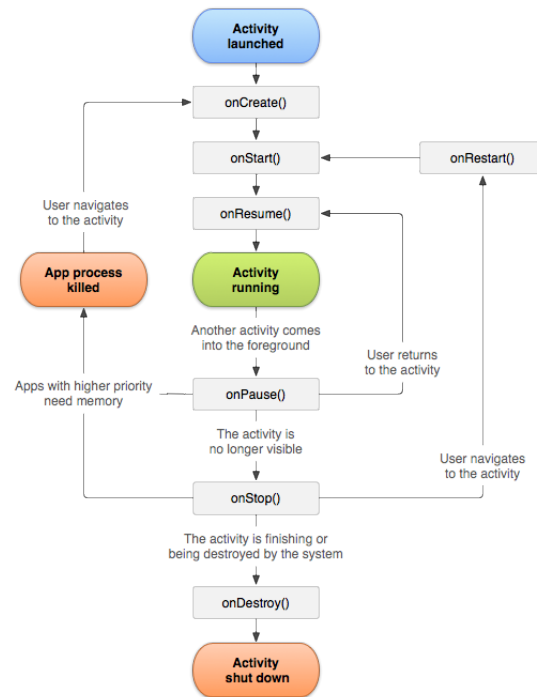


Figure 3.2: Illustration of activity life cycle

### 3.1.6 Services

An application's subprocess must often run in the background without interaction with the user. In these cases, it is common to use a service [22]. A service can perform extended operations, have an indefinite time to work, be called at the start of the application, and be switched off or controlled by activity. In general, applications are connected with other applications and interact with the user through the user interface [20]. If it is necessary to perform a long-time action without a UI, it is helpful to use a service. For example, a background function preprocesses the data while the signal processing application is running. In this case, the preprocessing step can be a service.

#### 3.1.6.1 Service life cycle

Services are designed to stay active more time than an application and to perform computing actions (processor or memory). Services are initialized, stopped, and controlled by other components, for instance: activities, other services, broadcast receivers, etc. [22]. A service should be created if the application offers functionality without the user's supervision or is a large task. Like an activity, a service has life cycle callback methods that can be implemented to monitor changes in the service's state and perform work at the appropriate times. From the point of view priority of the resources, an active service has higher priority than other inactive or invisible



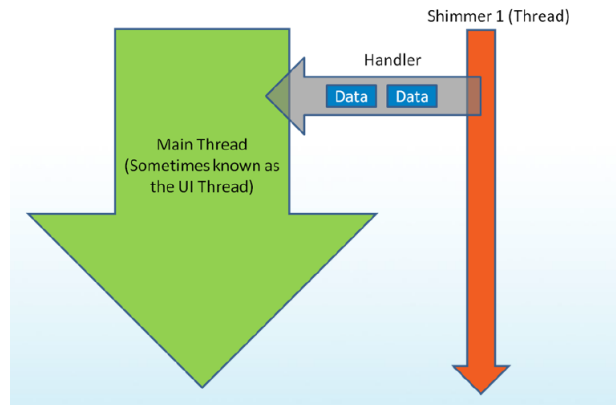


Figure 3.3: Illustration of separate thread and handler

activities. For this reason, it is less probable that Android finishes a service when a low resource state occurs. The easiest way to create a service is to call `startService()`. These services are in the background and are active for a long period. Services created with `startService()` can be stopped with `stopService()` or `stopSelf()` [20].

### 3.1.7 Threads

For the execution of an application, the system starts the main thread or also called UI thread [22, 23]. The main thread controls all the important events within the application, such as widgets, drawing, or dispatching other application-related events. It is also the thread in which the application communicates with components from the Android UI. The system does not create other threads for each instance of a component. Thus, performing intense processing tasks such as network access, data processing, or database queries in the main thread of the application will probably block the whole UI and can be the source of application not responding (ANR) dialogs [22]. Additionally, the Android UI is not threadsafe. There are two rules [22] to avoid the above mentioned possible problems:

- Do not block the UI thread.
- Perform intense tasks with a worker thread.

#### 3.1.7.1 Worker threads

Because of the single thread model described above, it is important not to block the UI thread. If the calculations to perform are not instantaneous, then the optimal approach is to make them in separate threads [24] as shown in Figure 3.3 (“background” or “worker” threads). In the gait application prototype developed in this work, the

worker threads are used for gathering the kinematic gait data from the IMUs, the preprocessing and processing steps.

### 3.1.8 *Bluetooth*

Android provides a Bluetooth application programming interface (API) to allow the connectivity of the application with other devices such as IMUs. The API [22] can manage and control the device Bluetooth setup to adjust the discovery parameters and to use a Bluetooth link to transfer data. These links are created through radiofrequency in industrial, scientific and medical (ISM) band at 2,4GHz to make communications between fixed and mobile devices easier. Bluetooth devices can create connections within range, depending on the transmission power. The typical range for smartphones is up to 10 meters. The Bluetooth API in Android allows us to discover new Bluetooth devices, consult our local adapter to detect pair devices, create radio frequency communication (RFCOMM) channels, and connect with other devices, data transfer, and manage multiple connections. In general, there are main classes to control and manage Bluetooth. Some of them are listed below [22]:

- **BluetoothAdapter:** Represents the Bluetooth adapter of our local device. The adapter allows us to do basic Bluetooth tasks: start Bluetooth scan, consult pair devices, and create sockets to listen to incoming connections from other devices.
- **BluetoothDevice:** Represents a remote Bluetooth device that lets us create a connection with the device or see related information (name, address, class, and state). This class is a wrapper of Bluetooth hardware.
- **BluetoothSocket:** is a Bluetooth connector, and RFCOMM is the most common connector.
- **BluetoothServerSocket:** Bluetooth server connector that is listening to incoming requests.
- **BluetoothClass:** This class describes, in general, a Bluetooth device.

The connection between the application and the IMU is based on the client-server implementation process [24]. Typically, the application opens a server Bluetooth socket, and the IMU starts the connection. This connection takes place on the same RFCOMM channel connected to the Bluetooth socket [22]. Once the connection is established, the input and output stream can be obtained, and the data transmission can start. The detailed description can be found in [22]

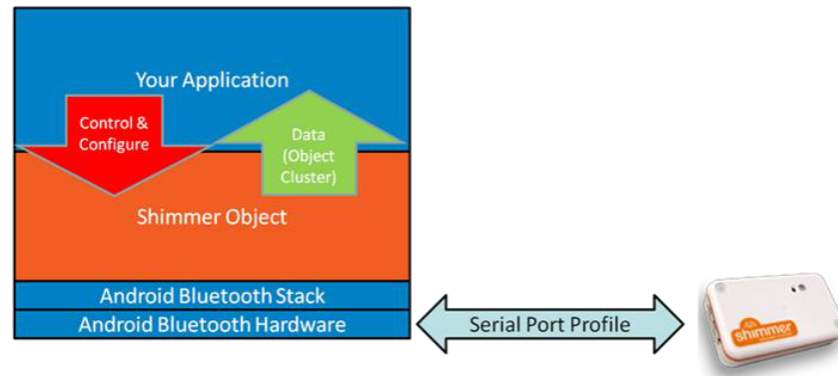


Figure 3.4: Illustration of Shimmer class for communications management.

### 3.1.9 Application implementation

The prototype application uses the concepts explained in previous sections to perform the desired actions:

- Graphical representation of processed and raw data.
- Sensor specification and selection.
- Feature specification.
- Save data in CSV format.
- Real-time kinematic data processing

The application uses the class “Shimmer” [24] to manage the Bluetooth communications with the IMUs as shown in Figure 3.4. This class uses threads to manage the connections. In addition, the application needs to perform long time processing operations with the data that comes from the IMUs. For that reason, it is helpful to create a service to manage the data [24]. The service will process, save and plot the processed and raw data. Until the buffer or window is not full, the service will add samples to the buffer. Once the buffer is complete, the service starts to process it (see Figure 3.6). The sensor data is encapsulated in a structure called *ObjectCluster* [24], and it is the way to manage the sensor data in the application. An overview of the structure can be observed in Figure 3.5. This structure uses *Multimap* [25] to organize the data from each axis. The way to dispatch the data is using *Handlers* [24] as shown in Figure 3.3. The shimmer class and the service use threads, and with the handler, they pass *ObjectCluster* to the main thread. In the shimmer class, the data is processed to transform the incoming bits from the sensor to raw/calibrated data to use in the application. After that, this data is sent to the service through the handler. Once the data is in the service, the service will process it as described above and send the data to the graph, and the *Logger* [24], as shown in Figure 3.6. In case

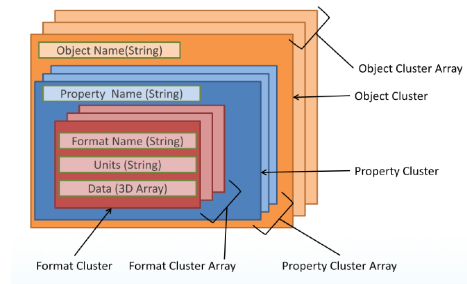


Figure 3.5: Illustration of ObjectCluster

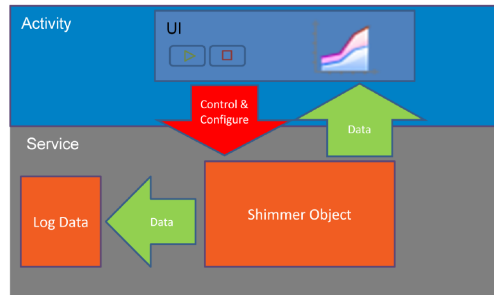


Figure 3.6: Illustration of application overview

of multiple wearable sensors (WSs), the UI thread manage the data from different threads as depicted in Figure 3.7. For real-time acoustic feedback scenarios, an extra thread is implemented to manage the sound parameters, as shown in Figure 3.8.

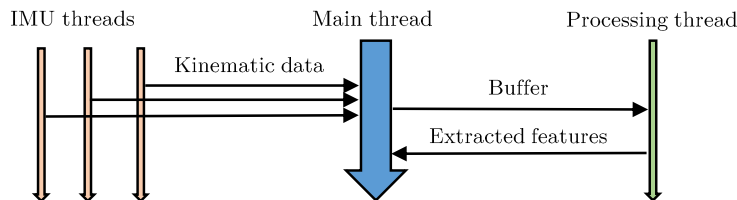


Figure 3.7: Illustration of the data flow between threads.

### 3.2 DATA MEASUREMENTS

This section describes the process of acquiring the kinematic data for the gait analysis. The kinematic data used in this work correspond to two different gait measurements: the free walking measurements and the measurements in the rehabilitation clinic with patients that underwent a hip endoprosthesis operation. The first one was used to extract essential cues from the kinematic data and develop the grading system for tracking the rehabilitation process. The second one was used to verify the results.

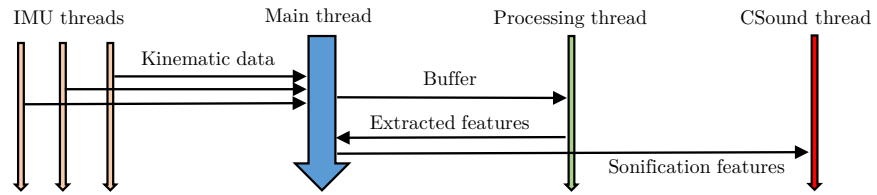


Figure 3.8: Data flow between the UI thread and the CSound thread

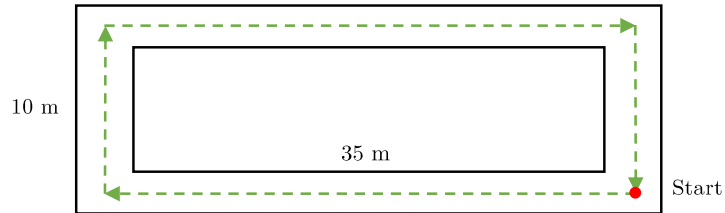


Figure 3.9: Walking route for the measurements.

### 3.2.1 Healthy participant measurements

The gait kinematic data from 20 healthy participants were acquired to analyze and extract essential cues for developing the grading system. For biomechanical and therapeutic reasons, the participants performed the walking route at their preferred gait speed so that participants could not think about their individual body movements. The purpose is that the body movements on the walking route are more natural and less forced. The participants started the measurements at the "Start" point (see Figure 3.9), performed one round, and finished at the same point as they started. All gait measurements consisted of two tests:

- Normal (without simulated walking impediment)
- Stressed (simulated walking impediment depicted in Figure 3.10)

The walking length of 90 m is mandatory for all measurements. Figure 3.9 depicted the walking route for the measurements. Directly after the first measurement, the second measurement was started. During the second measurement, a stone was placed under the heel and the participants had to perform the same walking route again. In general, the foot has three support points which form the shape of a triangle as shown in Figure 3.10. These three points are the Tuber calcanei (C), the Caput des Os metatarsae I (A) and the Caput des Os metatarsae V (B). The body weight is distributed among these three points. Modifying the support point of the foot allows the gait tempo, step cadence, gait symmetry and length to be changed. The measurement data of the test persons with simulated walking disabilities allow on the one hand a preselection of the characteristic gait features and on the other hand a reliability improvement of the quality metrics to be developed. Based on the measured data, the movement parameters, such as the joint angle estimates of the



Figure 3.10: Knee brace and modification of the support point of the foot. Support points: (A) Caput des Os metatarsae I, (B) Caput des Os metatarsae V and (C) Tuber calcanei

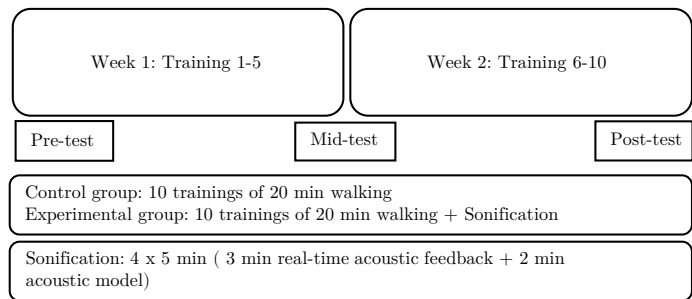


Figure 3.11: Sequence of measurements and intervention in the intervention study on patients for system assessment.

ankle, knee and hip joints, were determined from angular velocity and acceleration. The calculation of the joint angles is based on the method of sensor data fusion in signal level for signal error estimation reduction is explained in Chapter 4.

### 3.2.2 Rehabilitation clinic

In order to systematically investigate the effectiveness of the developed grading method (see Chapter 5), a study design was developed as shown in Figure 3.11. It provided a two-week intervention for a control group and an experimental group, each consisting of 10 patients after a hip endoprosthetic operation. The study participants of both groups received a 20 minute gait training five days per week, during which the kinematic gait data were recorded using the wearable sensor system (WSS) explained in Section 2.4. Only the experimental group received a real-time acoustic feedback (RTAF) during each training session, which consisted of four units of five minutes each, which included a 3-minute real-time sonification and a 2 minutes

acoustic gait model sequence. Both the control and experimental groups received feedback after each gait training session regarding the steps taken, the distance covered, and the average gait speed. Prior to the intervention, a pretest was performed, consisting of a timed-up-and-go test, a functional strength test (repeated standing up of chair within 30 seconds), and a gait analysis. This test sequence was repeated during the mid-test, after the fifth training session, during the post-test, after the tenth training session, and during the retest, on the second day after the end of the intervention.

### 3.3 CONCLUDING REMARKS

Mobile data acquisition is an essential part of the development of reliable and robust algorithms for gait analysis and rehabilitation monitoring. Therefore, in the first part of this chapter, the basic concepts for the creation of a gait processing application for Android devices have been described, and a brief introduction to the multi-thread implementation for kinematic signal processing have been discussed. The designed prototype application provides the facility of flexible and real-time measurement of the locomotion function in individuals, specifically those with gait disorders. For testing and specifying, visual feedback, experiments with healthy participants, emulated stressed walks and patients were performed. Seven IMUs were attached to the lower limbs of the body to obtain gait kinematic data. The prototype application delivers the representative features to distinguish gait abnormalities. Using the statistical signal analysis methods and machine learning (ML) model from Chapters 5 and 6, the significant feature set and the related range were obtained for detection of the normal and stressed walk. It is possible to reconfigure the visual feedback for different cases of gait disorders caused by injuries or endoprosthetic surgeries. The proposed mobile solution has a great potential to be deployed as a commercial product in support of digital healthcare and therapy. The last section of the chapter describes the two different campaign measurements performed for the acquisition of kinematic data for the development of the grading system. The first measurements were important in order to extract essential cues from the kinematic data and develop the grading system for tracking the rehabilitation process. The second measurement campaign took place at a rehabilitation clinic with the purpose of verifying the results with patients.





---

## SIGNAL PREPROCESSING

---

The preprocessing methods are applied to signals to prepare them in a suitable form for processing. Formatting, cleaning, sampling, and normalization are common methods performed on raw data to display the data in a useable format, generate smoothed and noise-removed data, resample data at regular or adaptive intervals without losing essential information, and normalize the data from different dimensions into the same scale [26]. In this Chapter, the three-dimensional gait kinematic signals obtained from the WSS are preprocessed. Prior to the feature extraction, the raw kinematic signals have to be preprocessed using sensor fusion methods such as the Kalman filter (KF), segmentation algorithms, and filtering.

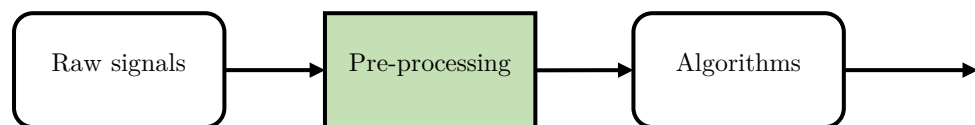


Figure 4.1: Gait analysis process.

### 4.1 SENSOR FUSION

A KF is an algorithm for optimal estimation of the system error from noisy measurements [27]. This algorithm is sequential and recursive and provides an optimal least mean variance estimation of the error states. The KF provides real-time statistical data associated with the estimation accuracy of the error states. The KF applies all of the measurement information to estimate the current state value of the system through appropriate weighting of these measurements. To achieve this, the KF uses the following information [28]:

- Information about the model of the system and its measurements.
- Knowledge about the statistical characteristics of the system errors, noise, and uncertainty.

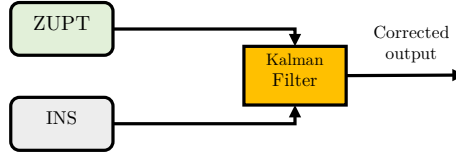


Figure 4.2: PDR diagram applying KF.

- The apriori information related to the initial conditions of the system states.

For gait applications, the KF is applied in a complementary configuration in which redundant measurements of the same signal with different noise characteristics are combined to minimize the error [27, 29]. Thus, the algorithm provides information at high rates, but its errors grow progressively over time because of the implicit mathematical integration in the algorithm, which causes the bias errors of both accelerometers and gyroscopes to increase at the output. The bias errors of the IMU usually appear at the low frequencies and are known as long-term errors. Thus, the KF limits the long-term errors of an inertial navigation system (INS) utilizing accurate low-frequency data from an external source. For the purpose of the thesis, the zero velocity update (ZUPT) is considered the external support source due to its accuracy, practical use, and low cost. Figure 4.2 depicts a typical use of KF for pedestrian dead recognition (PDR), where data from external ZUPT with good long term accuracy is combined with INS data with good short term accuracy in order to provide the best overall estimate of position and velocity.

#### 4.1.1 Discrete-time system representation

A discrete-time linear system can be described as [27]

$$\mathbf{x}_k = \Phi_{k,k-1}\mathbf{x}_{k-1} + \mathbf{G}_{k-1}\mathbf{w}_{k-1}, \quad (4.1)$$

where  $\mathbf{x}_k$  is the state vector,  $\Phi_{k,k-1}$  is the state transition matrix (STM),  $\mathbf{G}_{k-1}$  is the noise distribution matrix,  $\mathbf{w}_{k-1}$  is the process noise vector and  $k$  is the measurement iteration. Since the noise can affect more than one component of the state vector of a dynamic system, the introduction of a noise distribution vector  $\mathbf{G}$  takes into account the coupling of common noise disturbances into various components of the state dynamics [27]. The discrete-time linear measurement equation of the system is [27]

$$\mathbf{z}_k = \mathbf{H}_k\mathbf{x}_k + \boldsymbol{\eta}_k, \quad (4.2)$$

where  $\mathbf{z}_k$  is the measurement vector of the system,  $\mathbf{H}_k$  is the observation matrix and  $\boldsymbol{\eta}_k$  is the noise in the measurement. Figure 4.3 shows the discrete-time system

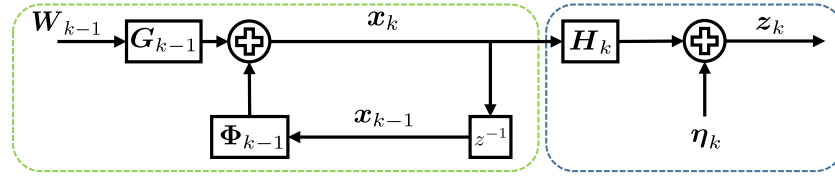


Figure 4.3: Processing and measurement models.

corresponding to Eq. 4.1 and 4.2. The STM represents the known dynamic behavior of the system which relates the state vector from iteration  $k - 1$  to  $k$ .

#### 4.1.2 Assumptions in Kalman filtering

Kalman filtering relies on the following assumptions [28, 30]. With this assumptions, the KF estimations are optimal [27].

- The system (both process and measurements) has to be described by linear models.
- The system noise  $w_k$  and the measurement noise  $\eta_k$  are uncorrelated zero-mean white noise processes with known autocovariance functions, hence

$$\mathbf{E}[w_k] = 0, \mathbf{E}[\eta_k] = 0 \quad \forall k, \quad (4.3)$$

$$\mathbf{E}[w_k \eta_j^T] = 0 \quad \forall k, j, \quad (4.4)$$

$$\mathbf{E}[w_k w_j^T] = \begin{cases} \mathbf{Q}_k & \text{for } k = j \\ 0 & k \neq j \end{cases}, \quad (4.5)$$

$$\mathbf{E}[\eta_k \eta_j^T] = \begin{cases} \mathbf{R}_k & \text{for } k = j \\ 0 & k \neq j \end{cases}, \quad (4.6)$$

where  $\mathbf{Q}_k$  and  $\mathbf{R}_k$  are known positive definitive matrices. In INS integration,  $\Phi_k$  represents the covariance matrix of the system noise associated with the INS errors, and  $\mathbf{R}_k$  represents the covariance matrix of the measurement noise associated with the position and velocity updates.

- The initial system state vector  $x_0$  is a random vector uncorrelated to both the process and measurement noises, thus

$$\mathbf{E}[x_0 w_j^T] = 0, \quad \mathbf{E}[x_0 \eta_j^T] = 0 \quad \forall k. \quad (4.7)$$

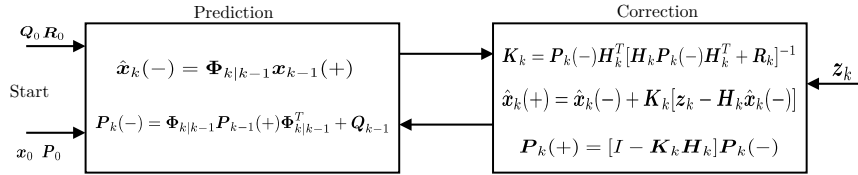


Figure 4.4: KF recursive processes.

- The mean value of the initial  $\bar{\mathbf{x}}_0$  and its covariance matrix  $\mathbf{P}_0$  are known, and can be expressed as

$$\bar{\mathbf{x}}_0 = \mathbf{E}[\mathbf{x}_0], \quad (4.8)$$

$$\mathbf{P}_0 = \mathbf{E}[(\mathbf{x}_0 - \bar{\mathbf{x}}_0)(\mathbf{x}_0 - \bar{\mathbf{x}}_0)^T]. \quad (4.9)$$

### 4.1.3 Estimation procedure

The states of a system are recursively estimated based on the KF algorithm with a feedback loop [27]. Using the a priori information of the system, the algorithm estimates the system's state at an iteration, and then it is compared with the feedback measurements, which are contaminated by noise [31]. As shown in Fig. 4.4 the operation of a KF has two phases: prediction and correction [27].

In the prediction phase, the system model is applied to propagate both the system's current state and its covariance estimates from iteration  $k - 1$  to  $k$  [27]. After that, in the correction phase, the measurements are used to update the previous estimations.

#### 4.1.3.1 Prediction

The estimate of the system state  $\mathbf{x}$  at time  $k$  given only the information up to time  $k - 1$ , is called prediction  $\hat{\mathbf{x}}_k(-)$ . It is also the *a priori* estimate because it applies 'prior' to a measurement. Since the system noise is zero-mean, the best prediction of the state at time  $k$  is [27]

$$\hat{\mathbf{x}}_k(-) = \Phi_{k|k-1} \mathbf{x}_{k-1}(+), \quad (4.10)$$

where  $\mathbf{x}_{k-1}(+)$  is the best estimate of state during the last iteration and is called the *a posteriori* estimate [27]. This is solely based on the process model, which is represented by the STM  $\Phi_{k|k-1}$ . KF also propagates the uncertainty about its estimate from epoch  $k - 1$  to  $k$ . This is called error covariance and is the expected value of the variance of the error in the states at time  $k$  given all the information up to time  $k - 1$  [27]. It is represented by the covariance matrix  $\mathbf{P}_k(-)$ , also known as the a priori covariance matrix [27]

$$\mathbf{P}_k(-) = \Phi_{k|k-1} \mathbf{P}_{k-1}(+) \Phi_{k|k-1}^T + \mathbf{G}_{k-1} \mathbf{Q}_{k-1} \mathbf{G}_{k-1}^T, \quad (4.11)$$

where  $\mathbf{P}_{k-1}(+)$  represents the best estimate of the covariance in the last epoch and is based upon the measurement at epoch  $k-1$  [27]. This is the *a posteriori* estimate of covariance. It should be noted that the *a priori* covariance matrix  $\mathbf{P}_k(-)$  depends on both the process noise and the *a posteriori* covariance  $\mathbf{P}_{k-1}(+)$ .

#### 4.1.3.2 Correction

Whenever a measurement from an external source becomes available, the KF corrects the predicted state [27]. Utilizing the information of the measurement covariance  $\mathbf{R}_k$ , the Kalman gain  $\mathbf{K}$  is computed to minimize the mean squared error of the estimate [27]

$$\mathbf{K}_k = \mathbf{P}_k(-)\mathbf{H}_k^T[\mathbf{H}_k\mathbf{P}_k(-)\mathbf{H}_k^T + \mathbf{R}_k]^{-1}. \quad (4.12)$$

The Kalman gain  $\mathbf{K}$  depends upon both the *a priori* covariance  $\mathbf{P}_k(-)$  and the measurement noise covariance  $\mathbf{R}_k$ . If the measurements are noisy (when  $\mathbf{R}_k$  increases) or the process noise is lower (when  $\mathbf{P}_k(-)$  reduces), then  $\mathbf{K}$  becomes relatively smaller [27]. When there is more noise in the process (when  $\mathbf{P}_k(-)$  increases), or the measurements are less noisy (when  $\mathbf{R}$  reduces), then  $\mathbf{K}$  becomes relatively larger. When  $\mathbf{K}$  is large, it assigns more weight to the measurements, and when it is small, it shows greater faith in the prediction [27]. In the context of PDR integration,  $\mathbf{K}$  takes relatively larger values when the ZUPT is more accurate and less noisy. In such a case, the measurement covariance matrix becomes relatively small. If eq. (4.12) is carefully examined, it is evident that small values of  $\mathbf{R}$  lead to relatively larger values of  $\mathbf{K}$ . When a new measurement  $\mathbf{z}_k$  is obtained at time  $t_k$ , it is compared with the predicted measurement  $\mathbf{H}_k\hat{\mathbf{x}}_k(-)$  based upon the *a priori* state estimate [27]. Their difference is weighted by  $\mathbf{K}$  and the prediction of the state vector is updated to generate the best estimate [27]. The estimate of the state at time  $t_k$  is therefore [27]

$$\hat{\mathbf{x}}_k(+) = \hat{\mathbf{x}}_k(-) + \mathbf{K}_k[\mathbf{z}_k - \mathbf{H}_k\hat{\mathbf{x}}_k(-)], \quad (4.13)$$

where  $\mathbf{H}_k\hat{\mathbf{x}}_k(-)$  is the predicted observation called  $\hat{\mathbf{z}}_k$ , and  $\mathbf{z}_k - \mathbf{H}_k\hat{\mathbf{x}}_k(-)$  is the innovation sequence, a vector of the difference between the actual observation  $\mathbf{z}_k$  and the predicted observation  $\hat{\mathbf{z}}_k$ . The innovation sequence is [27]

$$\mathbf{v}_k = \mathbf{z}_k - \hat{\mathbf{z}}_k = \mathbf{z}_k - \mathbf{H}_k\hat{\mathbf{x}}_k(-) \quad (4.14)$$

and represents the amount of useful information gathered from new measurements, whereas  $\mathbf{K}$  weights the useful information for the next update [27]. It can be seen that when  $\mathbf{K}$  is large due to the low noise in the measurements or high process noise is greater, the new information based on the measurements is given more weight. When  $\mathbf{K}$  is small due to the noisy measurements or the noise in the process, the innovation is small, and the new information is given less weight. Based on the value of  $\mathbf{K}$ , the

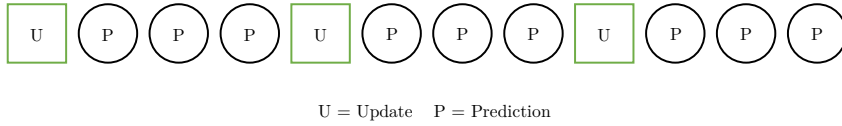


Figure 4.5: Prediction and update processes.

KF also updates the uncertainty of its new prediction  $\hat{\mathbf{x}}_k(+)$ , which is called the a posteriori covariance given by [27]

$$\mathbf{P}_k(+) = [\mathbf{I} - \mathbf{K}_k \mathbf{H}_k] \mathbf{P}_k(-). \quad (4.15)$$

Equation 4.15 is a bad simplification [32]. Small errors in the computation of  $\mathbf{K}$  in Eq. 4.12 could result in huge errors when using Eq. 4.15. This was a real problem in the 1960s and caused unstable behavior of the KF [27]. A numerically stable solution that uses an expanded form of the equation, known as the Joseph form [27]

$$\mathbf{P}_k(+) = [\mathbf{I} - \mathbf{K}_k \mathbf{H}_k] \mathbf{P}_k(-) [\mathbf{I} - \mathbf{K}_k \mathbf{H}_k]^T + \mathbf{K}_k \mathbf{R}_k \mathbf{K}_k^T \quad (4.16)$$

yields correct answers even when the computation of  $\mathbf{K}$  has an error (e.g., owing to rounding off). It is noteworthy that this form of the *a posteriori* error covariance  $\mathbf{P}_k(+)$  helps to avoid divergence by virtue of the assurance of positive semi-definiteness of  $\mathbf{P}_k(+)$ . In most PDR applications the KF update procedure is implemented at a lower rate than the predictions [27]. For example, in a typical application of integrating ZUPT and PDR through KF the prediction can be carried out at 50 Hz, whereas the update may occur at 1 Hz. Figure 4.5 shows the process for typical prediction and update rates.

#### 4.1.3.3 Algorithm steps

The KF algorithm consists of five sequential steps [27]:

- Filter initialization. This step provides the filter with the initial estimate for its states  $\hat{\mathbf{x}}_0$  and the uncertainty in the initial estimate  $\mathbf{P}_0$ . The estimate of  $\mathbf{P}_0$  is based upon knowledge of the approximate accuracy of the initial state estimates and is usually set to a relatively high value. The initial estimations of the system noise covariance matrix  $\mathbf{Q}$  and measurement noise covariance matrix  $\mathbf{R}$  also need to be provided to the filter. These are estimated on available data and optimized to obtain the best states.
- STM prediction. The matrix  $\Phi$  is computed and used to propagate the initial state to the next iteration, which is denoted by  $\hat{\mathbf{x}}_k(-)$ .

- In the second part of the prediction step, the covariance of the predicted state  $\mathbf{P}_k$  is calculated. This is based on the STM, the previous value of the state covariance  $\mathbf{P}_{k-1}$ , the last value of the process noise covariance  $\mathbf{Q}_{k-1}$ , and the noise distribution matrix  $\mathbf{G}_{k-1}$ .
- In the first step of the update stage, the Kalman gain  $\mathbf{K}_k$  is computed. This depends upon the a priori error covariance  $\mathbf{P}_k(-)$ , the process noise covariance  $\mathbf{R}_k$ , and the design matrix  $\mathbf{H}_k$ . When  $\mathbf{P}_k(-)$  is higher, the gain is higher, and when  $\mathbf{R}_k$  is higher, the gain is lower.
- In the second part of the prediction stage, the estimated (or the a priori) state  $\hat{\mathbf{x}}_k(-)$  is corrected whenever a measurement is received. This is based on the difference of the predicted measurement  $\mathbf{H}_k\hat{\mathbf{x}}_k(+)$  and the actual measurement  $\mathbf{z}_k$ . This difference contains the new information that forms the basis for the correction. When  $\mathbf{K}$  is higher, this difference is weighted more heavily and added to the a priori estimate in order to update this to the a posteriori estimate  $\hat{\mathbf{x}}_k(+)$ . Nevertheless, when  $\mathbf{K}$  is lower, the new information obtained from the measurement is given less weight, and the a priori estimate is considered to be relatively accurate.
- After correcting the state estimate, the KF goes a step further and also updates the a priori error covariance  $\mathbf{P}_k(-)$  to the a posteriori error covariance  $\mathbf{P}_k(+)$  to indicate the level of trust in the corrected estimate  $\hat{\mathbf{x}}_k(+)$ , which is proportional to gain  $\mathbf{K}_k$  and  $\mathbf{P}_k(-)$ .
- At this point, the KF has performed one iteration, and the information estimated in this loop will be used as a priori information in the following loop.

#### 4.1.4 Zero velocity update

Frequently in gait applications, there are no continuous update measurements available, and thus the estimation accuracy can suffer from velocity errors and their direct contributions to position errors. ZUPTs provide a relevant enhancement in the accuracy of the estimations compared to systems without ZUPT [27]. The procedure to carry out the ZUPT in gait applications is as follows

- Detecting the stand and swing phases from the kinematic gait signals
- Applying corrections during the stand phase.

The ZUPT method does not need any additional equipment, it applies to real and practical scenarios, and the cost is low. However, its major limitation is that the gait phases must be correctly detected. During the standing phase, the foot remains on

the ground, and the velocity during this period is set to 0, which corresponds to the correction process of the KF. In the swing phase, the KF performs the prediction process. Mathematically, this detection problem can be formulated as a binary hypothesis testing problem [33], where the detector chooses the hypothesis that IMU is stationary if [34]

$$T(\mathbf{z}_n^a, \mathbf{z}_n^\omega) < \gamma, \quad (4.17)$$

where  $\mathbf{z}_n^a = \mathbf{y}_k^a$  and  $\mathbf{z}_n^\omega = \mathbf{y}_k^\omega$  for  $k = n, \dots, n + W - 1$  denote the measured 3D acceleration signal and 3D angular rate signal at time instant  $n \in \mathbb{N}$ , respectively.  $T(\mathbf{z}_n^a, \mathbf{z}_n^\omega)$  is the test statistics of the detector and  $\gamma$  is the detector threshold. There are several methods to detect the different phases in a gait cycle. Methods such as, angular rate energy detector (ARED), stance optimal detector (SOD), acceleration moving variance detector (AMVD) and acceleration magnitude detection (AMD) are based on the energy of the kinematic signals [34].

#### ANGULAR RATE ENERGY DETECTOR (ARED)

$$T(\mathbf{z}_n^\omega) = \frac{1}{\sigma_\omega^2 W} \sum_{k=n}^{n+W-1} \|\mathbf{y}_k^\omega\|^2. \quad (4.18)$$

#### STANCE OPTIMAL DETECTOR (SOD)

$$T(\mathbf{z}_n^a, \mathbf{z}_n^\omega) = \frac{1}{W} \sum_{k=n}^{n+W-1} \frac{1}{\sigma_a^2} \left\| \mathbf{y}_k^a - g \frac{\bar{\mathbf{y}}_n^a}{\|\bar{\mathbf{y}}_n^a\|} \right\|^2 + \frac{1}{\sigma_\omega^2} \|\mathbf{y}_k^\omega\|^2. \quad (4.19)$$

#### ACCELERATION MAGNITUDE DETECTION (AMD)

$$T(\mathbf{z}_n^a) = \frac{1}{\sigma_a^2 W} \sum_{k=n}^{n+W-1} (\mathbf{y}_k^a - g)^2. \quad (4.20)$$

#### ACCELERATION MOVING VARIANCE DETECTOR (AMVD)

$$T(\mathbf{z}_n^a) = \frac{1}{\sigma_a^2 W} \sum_{k=n}^{n+W-1} \|\mathbf{y}_k^a - \bar{\mathbf{y}}_n^a\|^2, \quad (4.21)$$

where  $\sigma_a^2$  and  $\sigma_\omega^2$  are the variances of the acceleration and angular velocity rate signals.  $\bar{\mathbf{y}}_n^a$  describes the sample mean of the acceleration signal. The above mentioned detectors have been tested in [34] and the outcomes of the analysis reveals that the



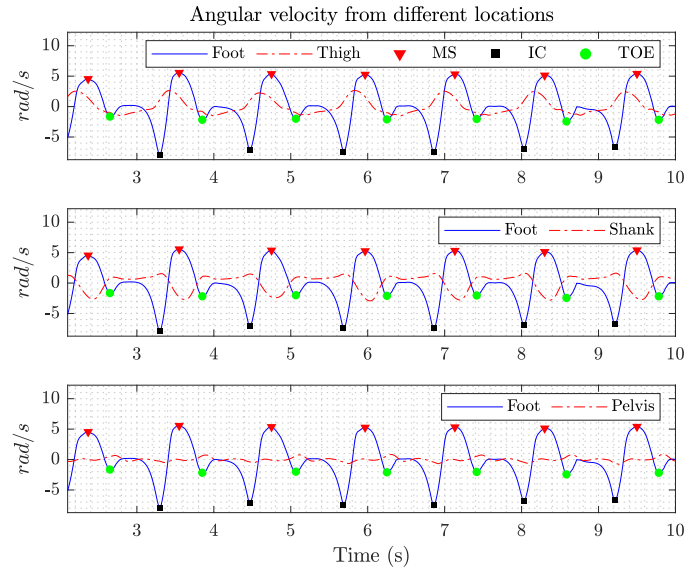


Figure 4.6: Illustration of the angular velocity in the sagittal plane from different locations. The IC and TOE events are obtained from the foot angular velocity. The red triangle, green circle and black square markers represent the MS, IC and TOE, respectively.

SOD detector performs similarly to the ARED [35, 36], which outperforms both the AMVD [37, 38] and the AMD [39, 40]. This indicates that the gyroscope signals hold the most reliable information for zero-velocity detection [41]. In this work, a gyroscope based method for gait segmentation is applied. It is possible to combine the physical knowledge of the human mechanics, and the information of the gyroscope signals [42, 43]. Human walking can be explained and described in the context of a gait cycle (GC). A stride is the distance between the IC of the first foot and the next IC of the same foot. In other words, a gait cycle is made up of two steps. Each stride contains a stance and a swing phase. The IC and toe off (TOE) events can be extracted from the gyroscope signal on the sagittal plane exploiting the feature in which, within each gait cycle, the foot alternatively rotates clockwise and counter-clockwise about the ankle joint [44]. The local maxima of the foot angular velocity are detected, and they are associated with the mid-swing (MS) phase [45]. As shown in Figure 4.6, within each pair of MS peaks, the first negative peak of the foot angular velocity is associated with the IC and the second one with the TOE. The optimal values for which the peaks comply with the actual/true IC and TOE are specified as follows: For the MS, the values of minimal peak distance and height were set to 50 samples and  $100^\circ/\text{s}$ , respectively. For the IC/TOE, the minimal peak distance and height were set to 30 samples and  $30^\circ/\text{s}$ , respectively. The value of the minimal peak distance for MS events was determined using the auto-correlation function of the foot angular velocity, due to the periodicity of the gait kinematic signals [46], and calculating the mean and variance of the distance (in samples) between MS peaks of

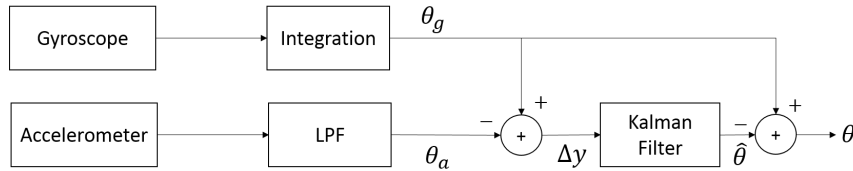


Figure 4.7: Block diagram of the indirect Kalman Filter.

the autocorrelation. From the knowledge of the ICs and TOEs, it is possible to define the duration of the stride, stance, and swing phases and, accordingly, other temporal parameters (cadence, step length, gait speed, etc.). The defined IC events were used to segment the kinematic gait data into gait cycles. Each gait cycle  $s(t)$  was resampled to the length of 100 samples so that all segments have the same length [47, 48].

#### 4.1.5 Lower body joint angle estimation

Joint angle estimation is known to be an important biomechanical parameter in learning the walking pattern of a person. For this, the sagittal plane information can be accomplished using the difference between the gyroscope and acceleration angles (Fig. 4.7). Even with very well-calibrated sensors, the joint angle obtained from the integration of angular velocity will drift after a short period. This drift is normally due to the temperature bias of the gyroscopes. To compensate the drift error, an indirect KF is applied. The state vector  $\mathbf{x}_n$  of the KF is defined as  $\mathbf{x}_n = [\hat{\theta} \ \beta]^T$ , where  $\hat{\theta}$  and  $\beta$  denote the error of the joint angle and the bias of the gyroscope measurement, respectively. The KF uses the angle of acceleration measurements  $\theta_a$  as a correction to the already estimated joint angle based on the integration of the gyroscope measurement  $\theta_g$  [49]. The KF estimates the joint angle error and subtracts it from the integrated angle to get the corrected estimation. The related state transition matrix  $\mathbf{F}$  and the measurement matrix  $\mathbf{H}$  of the KF are given by [49]

$$\mathbf{F} = \begin{bmatrix} 1 & T_s \\ 0 & 1 \end{bmatrix} \quad \text{and} \quad \mathbf{H} = \begin{bmatrix} 1 & 0 \end{bmatrix}, \quad (4.22)$$

where  $T_s$  is the sampling period of the IMU. Figure 4.8 presents the estimation of the lower body angles when a participant is walking in a straight line for a distance of 10 m. Figure 4.9 shows the sensor location for the measurements. Furthermore, the results from gait kinematic data collected from another sensor platform, denoted as a reference, are compared. It is clearly shown that both results have a good matching, which means that the proposed angle estimation algorithm is independent of the hardware platform used for data collection.

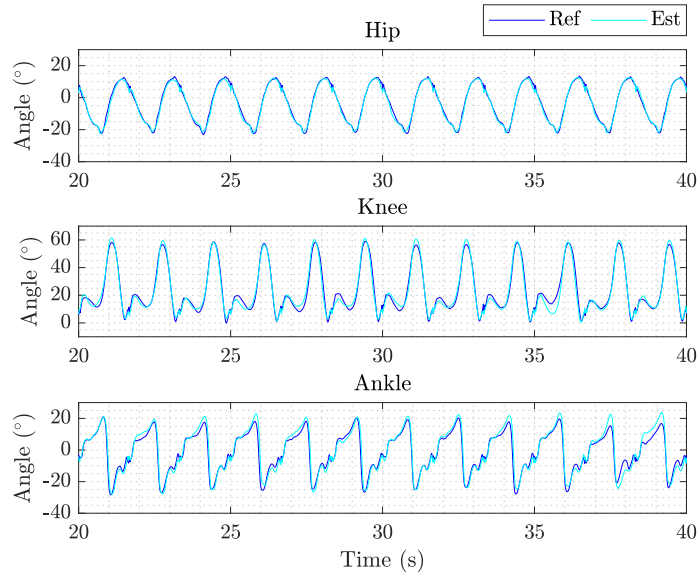


Figure 4.8: Lower body joint angles in the sagittal plane compared to the reference system.



Figure 4.9: Shimmer (white) and reference (orange) sensor system platform.

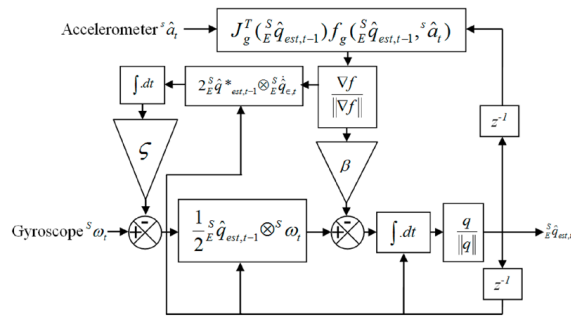


Figure 4.10: IMU Block diagram of the orientation filter.

#### 4.1.6 Quaternions and reference system

Quaternions are a concept related to the foundations of algebra and number theory [50, 51]. Quaternions are a mathematical representation consisting of four individual numeric, complex number components that can be used to represent the orien-

tation of a rigid body in a three-dimensional space [52]. The data measurements are essential for the accurate estimation of the IMU's orientation. Different types of sensors build in a IMU such as accelerometers and gyroscopes are susceptible to different factors. Accelerometers are susceptible to altitude and impact forces, while gyroscopes are susceptible to temperature changes and suffer from drift [53]. Consequently, accelerometers have poor dynamic characteristics, and gyroscopes have poor static characteristics. There are two coordinate systems in this work, the sensor frame (S) describing the sensor rotation and the global or earth frame (E). The approach rotates the sensor frame to the global frame and removes the gravitational component. The high gravitational force of the global frame is downwards toward earth. There are different methods to estimate the orientation of an IMU from IMU kinematic data such as rotation matrices, Euler angles, etc. [50]. In this work, the Madgwick method [54] which fuses accelerometer, gyroscope, and magnetometer data for quaternion estimation, is used.

$${}^S_E \hat{q} = [q_1, q_2, q_3, q_4] = \left[ \cos\left(\frac{\theta}{2}\right), -S_x \sin\left(\frac{\theta}{2}\right), -S_y \sin\left(\frac{\theta}{2}\right), -S_z \sin\left(\frac{\theta}{2}\right) \right]. \quad (4.23)$$

To denote the relative frame orientation between S and E,  ${}^S_E \hat{q}$  in equation 5.32 represents the orientation of frame E relative to frame S is a vector described in [54].

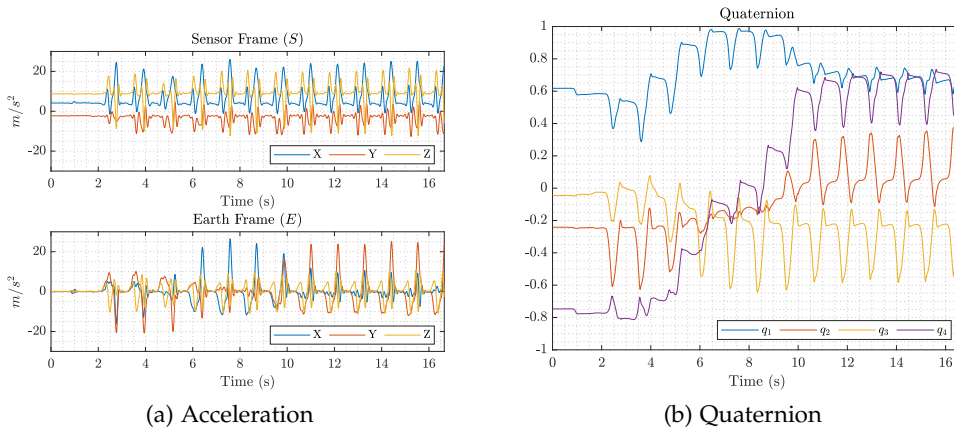


Figure 4.11: (a) Comparison between the acceleration in the sensor frame (S) and the earth frame E. (b) Quaternion used to rotate the signal from the sensor frame (S).

Figure 4.10 illustrates the above-mentioned method. With this method, the kinematic gait data is collected from the IMUs and transformed to the earth frame with a sampling frequency of 60 Hz,  $\beta$  gain of 0.1, and  $\sigma$  of 0.5. The compensated gyroscope measurement  ${}^S w_c$  is used in place of the gyroscope measurements  ${}^S w$ , where the magnitude of the angular error in each axis  ${}^S w$  is equal to a quaternion derivative of unit length, and then the integral gain  $\sigma$  directly defines the rate of convergence of the estimated gyroscope bias  ${}^S w_b$ , expressed as the magnitude of a quaternion deriva-

tive [51]. Figure 4.10 shows the block diagram for the quaternion estimation  ${}^S_E \hat{q}_{est,t}$  [54]. The gravity components are removed. Figure 4.11 shows the acceleration in the sensor frame  $S$  and global frame  $E$ . To provide a robust absolute orientation vector in the form of quaternion, the android prototype application combines the measurements from the 3-Axis accelerometer and 3-axis gyroscope and intelligently fuses the raw data to improve the output of each sensor, including offset calibration of each sensor.

#### 4.2 CONCLUDING REMARKS

In this chapter, the kinematic gait data of different sensors placed at the lower limbs of the body were collected and processed with the Android prototype application explained in Chapter 3. The quaternion method is first applied to raw data for estimating actual sensor orientation. The sensor fusion method estimates the lower body joint angles in the sagittal plane from the kinematic data applying a KF designed for this purpose. Our method was validated with the Xsens motion capture system. The presented signal preprocessing methods were applied to ten young and ten older subjects. The results show that it is possible to precisely estimate the lower body joint angles in the sagittal plane in a clinical setting outside of a gait laboratory. Thus, there is a great potential to extend the practice of rehabilitation monitoring to open spaces rather than limited gait laboratories.



---

## OBJECTIVE GAIT ASSESSMENT

---

This chapter introduces how signal processing methods and domain knowledge about gait are formulated and used to extract essential features from gait kinematic data to develop a robust metric that can monitor changes in the subject's movement patterns. Automatic recognition and assessment of human movement patterns are key features for an autonomous evaluation of motor activity in sports and rehabilitation. Feature extraction is a valuable method to derive the most representative characteristics of original data. Thus, the features exhibit important cues of original data to distinguish different activities and can be applied as a measure for the performance evaluation and classification purposes [55, 56]. Many different methods are available for extracting features specified for various applications. In [57–59] time-domain features such as mean, variance, and root mean square (RMS), being in direct relation to data and including the fundamental properties of the data waveform, were presented. Frequency-domain features such as spectral energy and spectral entropy, which are based mainly on the periodic structure of the data and obtained from Fourier transform (FT) of the original data [60, 61]. In order to obtain both time and frequency cues of the data, time-frequency features using wavelet transformation (WT) are proposed in [62, 63]. The WT enables simultaneous localization of the data signal in both time and frequency domains and thus is a popular technique for activity detection applications. Heuristic features and domain-specific features are other widely used features and investigated in [64] and [65]. Accordingly, time, frequency, and time-frequency features are extracted from gait kinematic signals. The last section of this chapter shows why traditionally used metrics such as cadence, step period, and stride period are not sufficient and shows how the metric evaluation can be used to complement the traditional methods by providing an overview of the accuracy and progress of the rehabilitation. A comprehensive diagram of the signal processing methods applied to the feature extraction in this chapter is depicted in Figure 5.1.

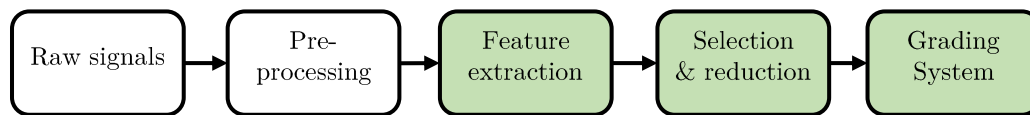


Figure 5.1: Overview of the objective gait assessment process

## 5.1 FEATURE EXTRACTION

Feature extraction is an essential procedure for classification and estimation in gait applications. For gait signals, such as IMU signals collected for human motion, it is necessary to analyze the properties of the signals with statistical methods to investigate peaks or correlations in the time domain or transform the signals into the frequency domain to evaluate the spectral characteristics. Several signal processing methods extract essential information from human motion-related signals, e.g., kinematic signals, and can be divided into two categories: statistical and transforming methods. The statistical methods measure the statistical distribution or aspects that could be evidence of the temporal characteristic of the signal. These methods are typically applied for feature extraction approaches for classifications tasks [66–69]. Transforming methods, such as fast Fourier transform (FFT) and WT, convert the information of the signal into other domains, and analyze the characteristics of the signals over the frequency and time [70, 71].

This section explains the signal processing methods to extract essential features from three-dimensional kinematic gait data in time, frequency, and time-frequency domains. The information on gait features allows to process and obtain values that can be useful to detect disorders in a person’s gait.

### 5.1.1 Time domain

Gait kinematic signals are a type of time series, and their time-analysis is performed generally at first due to that they are easier to interpret, and the related information can be directly understood from the signals. In gait analysis, time-series features are usually used to detect the amplitudes and timings of key events during the gait cycle. Multiple statistical parameters are applied as features, such as the mean, standard deviation, local maxima and minima, and zero crossings.

#### 5.1.1.1 Motion intensity

The RMS value indicates the motion intensity (MI) [72]. It is a statistical measure of the magnitude of a varying quantity and especially useful when the values are



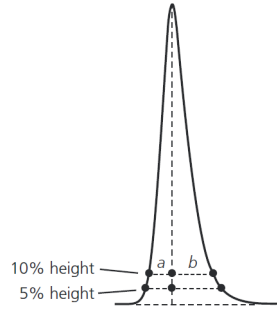


Figure 5.2: Illustration of peak asymmetric factor

positive and negative, e.g., gait kinematic signals. It can be calculated for a series of discrete values or for a continuously varying function. In the case of a signal with  $N$  samples  $\{x_1, x_2, x_3, \dots, x_N\}$ , the RMS value is

$$\text{RMS} = \sqrt{\frac{1}{N} \sum_{i=1}^N x_i^2}. \quad (5.1)$$

The RMS overall time of a periodic function is equal to the RMS of one period of the function. The RMS values of the three-dimensional kinematic gait data were extracted respectively using the equation above, and  $x_i$  is the acceleration in either vertical, Anterior-Posterior, or Medio-Lateral axis.

#### 5.1.1.2 Asymmetry factor

The measure of the peak tails within a signal is related to symmetry. In real-life scenarios, the peaks in gait data are not symmetric. It would be useful to add a feature to measure this characteristic. In this work, each peak in the data window will be processed to find a difference between normal and abnormal gait [73]. Figure 5.2 illustrates the calculation of the asymmetry factor.

$$\text{AsF} = \frac{b}{a} \quad (5.2)$$

#### 5.1.2 Regularity and symmetric features

Gait-related kinematic signals are semi-periodic due to the semi-periodic behavior of human walking. These signals may change from one period to another. The regularity and symmetric features quantify these changes.

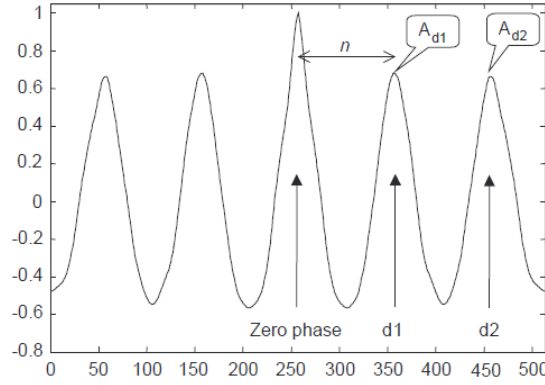


Figure 5.3: Autocorrelation function of acceleration data during normal walking.

#### 5.1.2.1 Unbiased correlation and autocorrelation coefficients

A mathematical operation that closely resembles convolution is correlation [74]. Two signal sequences are involved in correlation. Our objective in computing the correlation between two signals is to measure the degree to which the two signals are similar and thus extract some information. An autocorrelation coefficient ( $A$ ) is the sum of the products of the same signal  $x_i$  ( $i = 1, 2, 3, \dots, N$ ) multiplied by shifted version of itself ( $x_{i+m}$ ) and it is defined as [75]:

$$A(m) = \sum_{i=1}^{N-|m|} x_i x_{i+m}, \quad (5.3)$$

where  $m$  represents the phase shift in the number of samples. A cyclic signal will produce autocorrelation coefficients with peak values at  $m$  samples equivalent to the periodicity of the signal. Observing the autocorrelation function can be used to analyze the periodic characteristics within a signal. The autocorrelation function is usually plotted symmetrically, with the zeroth shift in the middle. For a kinematic gait signal such as accelerations during walking, the autocorrelation function can be computed to quantify the peak values at the first and second dominant period, representing phase shifts equal to one step and one stride, respectively [76]. Either biased or unbiased estimates of the autocorrelation coefficient can be computed [74].

Figure 5.3 illustrates two major peaks of the autocorrelation function of acceleration data during normal walking. Considering that the first shifted peak  $A_{d1}$  is related to one step at  $d_1$ , then it is possible to express the regularity of the acceleration signal between neighboring steps using the autocorrelation function. Thus, the values of the first and second peaks of the autocorrelation function  $A_{d1}$  and  $A_{d2}$  reflect step and stride regularity, respectively. The similarity of  $A_{d1} = A_{d2}$  reflects symmetry [77]. The peak value  $A_{d1} = A_{\text{coeff}}(d_1)$ , is the step period found at the lag time  $d_1$ , indicated the step regularity [77]. The peak value  $A_{d2} = A_{\text{coeff}}(d_2)$ , is the stride

period found at the  $d_2$  lag time, indicated the stride regularity (see Figure 5.3). The feature  $D$  in Eq. 5.4 can be used as an indicator to measure gait symmetry as [77].

$$D = |A_{d1} - A_{d2}|. \quad (5.4)$$

Low values of  $D$  indicate a more symmetric gait. A higher value of  $D$  indicates a more asymmetric gait.

### 5.1.3 Frequency domain

Frequency domain features are extracted from gait kinematic signals by transforming them from the time to the frequency domain using statistical and signal processing algorithms such as the Fourier transform and the Wavelet transform. In this section, three frequency domain features are considered for analysis.

#### 5.1.3.1 Fourier transform

Frequency analysis of time-discrete signals is usually and most conveniently performed on a digital signal processor, which may be a general-purpose digital computer or specially designed digital hardware. It is known that this type of representation is calculated through the Fourier transform  $X(\omega)$  of the sequence  $x(n)$  [78]. However,  $X(\omega)$  is a continuous function of frequency, and thus, it is not a computationally convenient representation of the sequence  $x(n)$ . The discrete Fourier transform (DFT) is a powerful computational tool for performing frequency analysis of time-discrete signals. FFT is an efficient algorithm to calculate the DFT and the inverse discrete Fourier transform (IDFT). FFT used in many applications, such as signal processing and digital filtering. In general, a finite-duration sequence  $x(n)$  of length  $L$  has a Fourier Transform [74]

$$X(\omega) = \sum_{n=0}^{L-1} x(n)e^{-j\omega n} \quad 0 \leq \omega \leq 2\pi, \quad (5.5)$$

where  $x(n)$  is 0 outside the range  $0 \leq n \leq L - 1$ . If  $X(\omega)$  is sampled equally at frequencies  $\omega = \frac{2\pi}{N}k, k = 0, 1, 2, \dots, N - 1$ , where  $N \geq L$  [74] then,

$$X(k) = \sum_{n=0}^{N-1} x(n)e^{-j2\pi kn/N} \quad k=0,1,2,\dots,N-1, \quad (5.6)$$

where  $x(n) = 0$  for  $n \leq L$ . The equation 5.6 is a formula to transform a  $L \leq N$  sequence into a sequence of samples  $X(k)$  of length  $N$ . The new sequence is obtained evaluating  $X(\omega)$  with  $N$  equally spaced discrete frequencies. Thus, Eq. 5.6 is called

DFT of  $x(n)$ . Also exists a relation to calculate the sequence  $x(n)$  from frequency domain [74]

$$x(n) = \frac{1}{N} \sum_{k=0}^{N-1} X(k) e^{-j2\pi kn/N} \quad n=0,1,2,\dots,N-1, \quad (5.7)$$

and is called IDFT. There are some alternatives to calculate DFT using less processor time. They are explained in detail in [74, 79, 80].

### 5.1.3.2 Power spectral density

Many phenomena in nature are best characterized statistically in terms of average. Due to the random fluctuations in these signals, a statistical viewpoint must be adopted, which deals with the average characteristics of random signals. In particular, the autocorrelation function of a random process is the appropriate statistical average that will be used for characterizing random signals in the time domain. The Fourier transform of the autocorrelation function, which yields the power density spectrum, provides the transformation from the time domain to the frequency domain [74]. The problem to deal with in this section is the estimation of the power spectral density (PSD) of a signal from the observation of the signal over a finite time interval. The finite record length of the data sequences is a significant problem for the quality of the power spectrum estimate. When treating with statistically stationary signals, more extended data is better to obtain an estimation from [74].

### 5.1.3.3 The periodogram

The finite-energy signals possess a Fourier transform and are characterized in the spectral domain by their energy spectral density [81]. On the other hand, there are some signals which do not have finite energy and therefore do not possess a Fourier transform. This type of signal has a finite average power and hence is characterized by a power density spectrum. If  $x(t)$  is a stationary random process, its correlation is [74]

$$\gamma_{xx}(\tau) = E[x^*(t)x(t+\tau)]. \quad (5.8)$$

The power spectrum density of the stationary random process, via the Wiener-Khinchine theorem, is the Fourier transform of the autocorrelation function

$$\Gamma_{xx}(f) = \int_{-\infty}^{\infty} \gamma_{xx}(\tau) e^{-j2\pi f\tau} d\tau. \quad (5.9)$$

Normally there is only one realization of the random process and only one estimation the power spectrum, but the true autocorrelation function is not known and also

the calculation of the fourier transform is not possible. On the other hand, from a single realization of the process it is possible to calculate [74]

$$R_{xx}(\tau) = \frac{1}{2T_0} \int_{-T_0}^{T_0} x^*(t)x(t+\tau) dt, \quad (5.10)$$

where  $2T_0$  is the observation interval. If the stationary random process is ergodic in the first and second moments (mean and autocorrelation), then [74]

$$\gamma_{xx}(\tau) = \lim_{T_0 \rightarrow \infty} R_{xx}(\tau) = \lim_{T_0 \rightarrow \infty} \frac{1}{2T_0} \int_{-T_0}^{T_0} x^*(t)x(t+\tau) dt. \quad (5.11)$$

This relation explains the use of the time average autocorrelation  $R_{xx}(\tau)$  as an estimate of the autocorrelation function  $\gamma_{xx}(\tau)$ . The Fourier transform of  $R_{xx}(\tau)$  supplies an estimate  $P_{xx}(f)$  of the power density spectrum [74]

$$\begin{aligned} P_{xx}(f) &= \int_{-T_0}^{T_0} R_{xx}(\tau) e^{-j2\pi f\tau} d\tau \\ &= \frac{1}{2T_0} \int_{-T_0}^{T_0} \left[ \int_{-T_0}^{T_0} x^*(t)x(t+\tau) dt \right] e^{-j2\pi f\tau} d\tau \\ &= \frac{1}{2T_0} \left| \int_{-T_0}^{T_0} x(t) e^{-j2\pi ft} dt \right|^2. \end{aligned} \quad (5.12)$$

for discrete signals, this relation can be expressed as

$$P_{xx}(f) = \frac{1}{N} \left| \sum_{n=0}^{N-1} x(n) e^{-j2\pi fn} \right|^2 = \frac{1}{N} |X(f)|^2, \quad (5.13)$$

where  $X(F)$  is the Fourier transform of the sample sequence  $x(n)$ . This well known form of the power spectrum density estimate is called *periodogram* [74].

#### 5.1.3.4 Spectral entropy

The concept of entropy in information theory is related to the uncertainty that exists in every random signal [81]. It is a magnitude of “noise” and “disorder” within a system. Two characteristics of entropy are as follows:

- The measurement of the information should be proportional. A little change in the probabilities of one element of the signal should make a little change in entropy.
- If all elements of the signal have the same probability, then entropy is maximized.

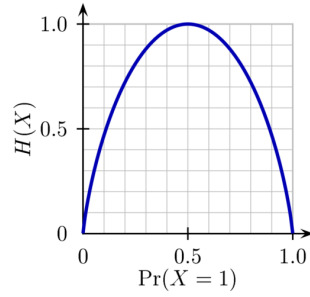


Figure 5.4: Example of the entropy function for an event with two equiprobable states

Suppose there is an event (random variable) with  $k$  - possible states, and these states have the same probability. Then the probability of one state will be  $\rho = \frac{1}{k}$ , and it can be expressed as

$$\begin{aligned} c &= \log_2(k) = \log_2\left(\frac{1}{\rho}\right) = \log_2\left(\frac{1}{\rho}\right) \\ &= \log_2(1) - \log_2(\rho) = 0 - \log_2(\rho) = -\log_2(\rho). \end{aligned} \quad (5.14)$$

Now, if each  $k$  state has  $\rho_i$  probability, then the entropy will be written as a weighted sum of the information amount

$$\begin{aligned} H &= -\rho_1 \log_2(\rho_1) - \rho_2 \log_2(\rho_2) - \dots - \rho_k \log_2(\rho_k) \\ &= -\sum_{i=1}^k \rho_i \log_2(\rho_i). \end{aligned} \quad (5.15)$$

If  $X$  is a message, the entropy for this message is  $H(X)$ , and is the weight value of the amount of information

$$H(X) = -\sum_{i=1} \rho(x_i) \log_2(\rho(x_i)), \quad (5.16)$$

which represents a measurement of the mean of the uncertainty of one random variable and, therefore, the amount of information [81]. Eq. 5.16 defines the Entropy [79]. As an example, if an event is taken with two equiprobable states, the entropy will be maximal, as shown in Figure 5.4. Supposing an input signal  $x(n)$  and its DFT  $X(f)$ . After computing PSD of the signal, it can be normalized and seen like a probability density function (PDF). After that, apply the entropy equation and the spectral entropy (SE) is obtained [79].

#### 5.1.3.5 Signal to modulation noise ratio

The randomly modulated periodicity (RMP) of the gait kinematic signals and lower body joint angles can also be used for the feature extraction. The kinematic signals

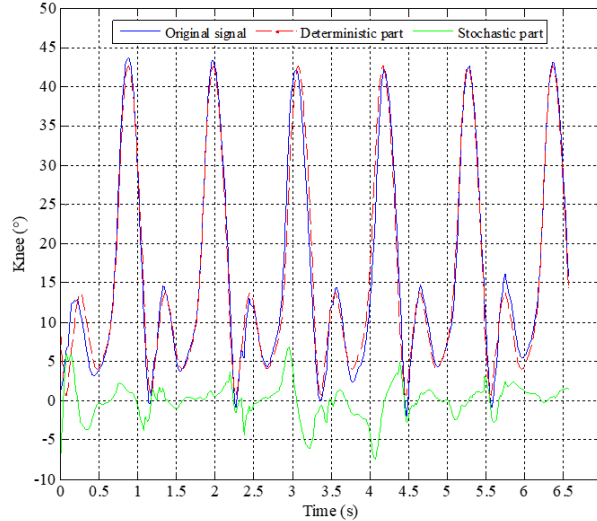


Figure 5.5: Example of the periodic and stochastic parts for the knee joint angle.

are generated by a non-linear physical mechanism and have inherent periodicity. In other words, the kinematic gait data is a deterministic signal with some unpredictable variations and thus belongs to a special class of signals called randomly modulated periodic signals. This RMP property provides valuable cues about the behavior of signals. A randomly modulated periodic signal  $x(t)$  of period  $T$  and  $K$  harmonic frequencies  $f_k = \frac{k}{T}$  is mathematically defined by [82, 83]

$$x(t) = s_0 + \frac{1}{K} \sum_{k=1}^K [(s_{1k} + u_{1k}(t))\cos(2\pi f_k t) + (s_{2k} + u_{2k}(t))\sin(2\pi f_k t)], \quad (5.17)$$

where  $s_0$  is the direct current (DC) part,  $s_{1k}$  and  $s_{2k}$  are constant. The modulation vector  $u(t) = u_{1k}(t), u_{2k}(t); k = 1, \dots, K$  is a zero mean random process with periodic block stationary and finite dependence. In other words,  $x(t)$  includes a deterministic part  $s(t)$  and a zero mean non-stationary stochastic part  $u(t)$  as

$$x(t) = s(t) + u(t). \quad (5.18)$$

Figure. 5.5 illustrates the periodic and stochastic parts of the lower body knee joint angle of a healthy participant. In connection with RMP signals, the sum signal-to-noise-modulation-ratio (SMNR) has been provided to quantify the amount of random variation relative to the underlying pure periodicity. In order to obtain the SMNR, the observed gait kinematic signal is segmented into  $M$  frames, each frame being of length  $T$ . If the sampling interval  $T_s = \frac{1}{2f_k}$ ,  $T = NT_s$  has  $N$  discrete samples  $x(t_n)$ , the

observed signal at time  $t_n$  in the  $m$ -th frame is  $x((m-1)T + t_n), n = 0, \dots, N-1$  and the DFT of this signal is given in [82, 83] as

$$X_m(k) = s_k + U_m(k), \quad (5.19)$$

with

$$s(t_n) = \frac{1}{M} \sum_{m=1}^M x((m-1)T + t_n), \quad (5.20)$$

$$s_k = \sum_{n=0}^{N-1} s(t_n) \exp(-j2\pi f_k t_n), \quad (5.21)$$

and

$$U_m(k) = \sum_{n=0}^{N-1} u((m-1)T + t_n) \exp(-j2\pi f_k t_n). \quad (5.22)$$

By assuming the weakly stationary stochastic part of the observed signal the variance of  $U_m(k)$  can be obtained as [82]

$$\sigma^2(k) = \frac{1}{M} \sum_{m=1}^M |U_m(k)|^2. \quad (5.23)$$

The estimation of sum SMNR given by

$$S = \sum_{k=1}^K \frac{M}{N} \rho_x(k) \quad (5.24)$$

with

$$\rho_x(k) = \frac{|s_k|^2}{\sigma_u^2(k)} \quad (5.25)$$

Eq. 5.25 defines the SMNR. The sum SMNR quantifies the amount of random variation in the signal [83].

#### 5.1.4 Time-frequency domain

In order to exploit the spectral relationships present in gait and capture local variations in the temporal gait kinematic signal, a representation is needed that allows to analyze these frequencies localized in time.

##### 5.1.4.1 Wavelet entropy

SE is a complexity measurement of gait signals introduced by applying the concept of Shannon entropy to power spectrum [84, 85]. The value of SE represents the relative presence of peaks or flatness of the spectral distribution in the power spectrum of a



gait signal. When a SE calculated by using the WT, it is called wavelet entropy (WE) [86]. Because WT is able to localize the non-stationary signal both in the time domain and in the frequency domain simultaneously [87], the time evolution of WE can be obtained to reveal the dynamic complexities of gait signals. This work applies the WE algorithm three to dimensional kinematic gait data to explore the complexity changes during the rehabilitation process. The wavelet transform decomposes a signal into a set of basis functions that are formed from a single prototype wavelet, called the mother wavelet function, by expansions and contractions in scales as well as shifts in the time domain. The discrete wavelet transform can be calculated by a fast algorithm of multiresolution signal decomposition [87]. This algorithm repeatedly filters the sampled time sequence  $x(n)$  by a set of paired high-pass and low-pass filters to yield a detailed component and an approximate component on every scale level. Each of the two components occupies half of the total frequency band on the corresponding scale level, with the detail one in the higher half and the approximate one in the lower half [88]. Since an orthonormal wavelet family is used, for a given time window, the total power  $Power_{total}$  of the signal is equal to the sum of each component power  $Power_j$ . The normalized power is  $p_j = \frac{Power_j}{Power_{total}}$  and  $\sum p_j = 1$ . The wavelet entropy in a time windows is defined as  $WE = -\sum p_j \ln(p_j)$  [86]. Time evolution of WE values can be obtained by shifting the time window along with the gait signal.

#### 5.1.4.2 Hilbert-Huang transform

The outcomes from previous studies in the field of biomechanics have concluded that the human gait is nonlinear and non-stationary [89]. In [90–92], nonlinear and non-stationary methods are proposed to analyze the gait signals due to their potential to extract complex relationships in the gait signals, which cannot be found with linear methods. Therefore, the Hilbert-Huang transformation (HHT) is proposed in this work to decompose the kinematic signals and to take advantage of nonlinear relationships between the foot signals and the lower limb joint angles [93]. The HHT applies the empirical mode decomposition (EMD) and the Hilbert transform (HT) [91]. The most important part of the HHT is the EMD method, which allows the decomposition of any data into a finite small number of intrinsic mode functions (IMFs). The IMF fulfills two conditions: First, the number of maxima and zero-crossing values must be equal or differ at least by one; Second, the average value of the envelopes corresponding to those created by the local maxima and minima must be zero. The EMD offers a possibility to exploit the information hidden in the gait signals and can be calculated from each gait cycle  $s(t)$  using the following steps:

- Detection of all extrema (minima and maxima) of  $s(t)$ .
- Interpolation and Cubic Spline curve fitting of the maxima and minima to obtain the upper envelope  $u(t)$  and the lower envelope  $l(t)$ , respectively.

- Calculation of the mean  $m_1(t) = \frac{u(t)+l(t)}{2}$  and the mode  $g_1(t) = \frac{u(t)-l(t)}{2}$  function of the envelopes.
- Calculation of the first component by subtracting the mean envelope function from the segment  $c_1(t) = s(t) - m_1(t)$ .
- If  $c_1(t)$  satisfies the IMF conditions,  $\text{imf}_1(t) = c_1(t)$  and continuing with the next step, otherwise replacing  $s(t)$  with  $c_1(t)$  and iteration of the first four steps.
- Calculation of the residual  $r_1(t) = s(t) - c_1(t)$  and iteration of the previous steps until becoming a monotonic function as final residual (The final residual is the trend of the segment).

Once the algorithm ends, the gait cycle  $s(t)$  can be expressed as a linear superposition of IMFs by

$$s(t) = \sum_{i=1}^n \text{imf}_i(t) + r_n(t), \quad (5.26)$$

where  $i = 1, \dots, n$  is the number of IMFs. Figure 5.6 shows the first two IMFs of the foot angular velocity in the sagittal plane. Once the gait cycle representation is obtained as a superposition of zero mean oscillatory modes, the HT can be applied to each IMF as follows:

$$H[\text{imf}_i(t)] = \frac{1}{\pi} \text{PV} \int_{-\infty}^{\infty} \frac{\text{imf}_i(\tau)}{t - \tau} d\tau. \quad (5.27)$$

PV denotes the Cauchy Principal Value of the integral. The residue  $r_n(t)$  should be left out of the Hilbert spectral analysis, since it is a monotonic function or a constant. The analytic signal  $z_i(t)$  is defined by

$$z_i(t) = \text{imf}_i(t) + jH[\text{imf}_i(t)] = a_i(t)e^{j\theta_i(t)}, \quad (5.28)$$

where  $a_i(t) = \sqrt{\text{imf}_i(t)^2 + H[\text{imf}_i(t)]^2}$  is the instantaneous amplitude (IA). To extract the instantaneous frequency (IF) and the instantaneous energy (IE) of each IMF, the derivative of the phase  $\theta_i(t)$  and the squared magnitude of  $a_i(t)$  are computed as below:

$$f_i(t) = \frac{1}{\pi} \frac{d\theta_i(t)}{dt}, \quad (5.29)$$

$$e_i(t) = |a_i(t)|^2. \quad (5.30)$$

## 5.2 FEATURE SELECTION AND DIMENSION REDUCTION

Both feature selection and dimension reduction methods are used to minimize the number of features in the dataset. In contrast to dimension reduction methods, which

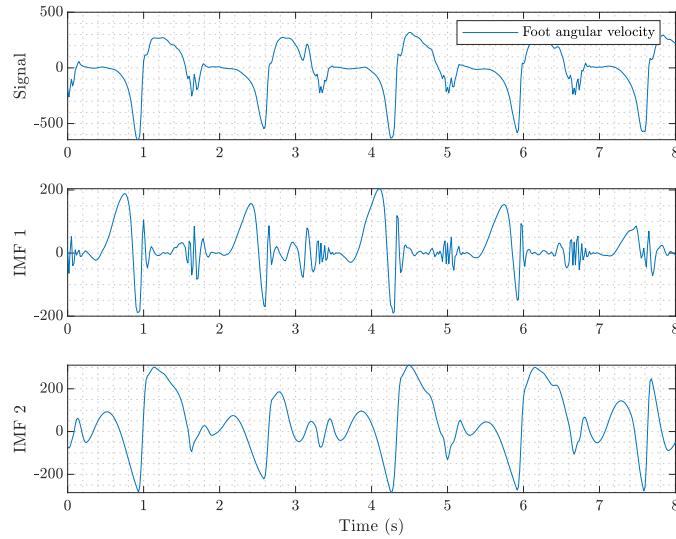


Figure 5.6: IMF signal decomposition for the foot angular velocity in the sagittal plane which, is used as input for the networks.

reduce the number of features by creating new combinations, feature selection methods include and exclude significant features present in the dataset without changing them. The feature selection methods automatically select the features in the dataset that are the most significant for generating a grading system. Feature selection methods usually filter out unneeded, irrelevant, and redundant features. Dimensionality reduction, or dimension reduction, reduces the number of random variables by eliminating the dimensions that are more likely to be noise. Dimension reduction methods normally transform the high dimensional space information to a lower space dimension. The main advantages of applying dimension reduction are as follows; First, the information needs less storage capacity and, therefore, the cost. Second, the information redundancy is removed; Third, the information visualization for low dimensions is easier to understand and analyze.

In order to develop a reliable grading system and an accurate classification, different feature extraction methods are considered in this thesis. The features are computed for each IMU, direction and joint angle, this procedure results in  $[7(\text{sensors}) * 3(\text{directions}) + 6(\text{jointangles})] * 9(\text{features per each signal}) = 243$  total features, where 'directions' refer to the  $(x, y, z)$  Cartesian coordinates of the global frame. Table 5.1 summarizes the extracted features from the kinematic data. The feature set can contain redundant information, which is not useful for the classification and modeling tasks. The next sections introduce the dimension reduction methods principal component analysis (PCA) and linear discriminant analysis (LDA). After reducing the dimension, the features mentioned can be treated as significant if they allow for a differentiation between normal and abnormal gait. The method paired t-test is described, and it allows to distinguish the relevance of the features [95]

### 5.2.1 Principal component analysis

This is one of the most popular techniques to reduce the dimension of the data and generate features in pattern recognition [96]. The vector  $\mathbf{x}$  contains the input information. In order to simplify the calculation presentation, the data samples are assumed to have zero mean  $E[\mathbf{x}] = 0$ . If not, the subtraction of the mean value from the can be performed. The original samples  $\mathbf{x}$  can be transformed into a new space using the following equation

$$\mathbf{y} = \mathbf{A}^T \mathbf{x}. \quad (5.31)$$

Since the input samples are expected to be zero mean, the output samples also have zero mean ( $E[\mathbf{y}] = 0$ ). Applying the definition of the correlation matrix to Eq. 5.31 it is obtained

$$\mathbf{R}_y = E[\mathbf{y}\mathbf{y}^T] = E[\mathbf{A}^T \mathbf{x} \mathbf{x}^T \mathbf{A}] = \mathbf{A}^T \mathbf{R}_x \mathbf{A}. \quad (5.32)$$

Typically, the estimation of the correlation matrix  $\mathbf{R}_x$  is the average over the training data. For example, if there are  $n$  data signals  $\mathbf{x}_k$ ,  $k = 1, 2, \dots, n$  then

$$\mathbf{R}_x \approx \frac{1}{n} \sum_{k=1}^n \mathbf{x}_k \mathbf{x}_k^T. \quad (5.33)$$

Due to the symmetry characteristic of  $\mathbf{R}_x$  its eigenvectors are mutually orthogonal [96]. Thus, if matrix  $\mathbf{A}$  is chosen so that its columns are the orthonormal eigenvectors  $\mathbf{a}_i$ ,  $i = 0, 1, \dots, N - 1$ , of  $\mathbf{R}_x$ , then  $\mathbf{R}_y$  is also diagonal

$$\mathbf{R}_y = \mathbf{A}^T \mathbf{R}_x \mathbf{A} = \Lambda, \quad (5.34)$$

where  $\Lambda$  is the diagonal matrix with the respective eigenvalues  $\lambda_i$ ,  $i = 0, 1, 2, \dots, N - 1$  of  $\mathbf{R}_x$ . The resulting transform is known as the Karhunen–Loève (KL) transform, and it achieves the original goal of generating mutually uncorrelated features [96, 97].

Table 5.1: Signal Features

Name	Type	Description
MI	Time analysis	Characterization of the movement intensity.
AsF	Time analysis	Measure of the signal symmetry.
Step period	Time analysis	Time between steps.
Stride period	Time analysis	Time between two steps of the same side.
Regularity	Time analysis	Characterizes the signal rhythmic and periodicity.
PSD	Frequency analysis	Mechanical power of the signal.
SE	Frequency analysis	Derived from information theory, a measure of the uncertainty of a signal [79].
SMNR	Frequency analysis	Characterizes the random variation relative to the periodicity [94].
WE	Time-Frequency analysis	Measure of the signal distortion and provide knowledge on the dynamic process.

### 5.2.2 Linear discriminant analysis

The method is based on the work of Fisher [98] on linear discrimination, and it is also known as LDA. Let the data samples,  $\mathbf{x}$ , be  $m$ -dimensional and from two classes. The objective is to create a linear combination of feature  $\mathbf{y}$  related to the components of  $\mathbf{x}$  [98]. In such a way, the idea is to condense the information in  $\mathbf{x}$  in a smaller number of features. This is achieved by looking for the direction  $\mathbf{w} \in \mathbb{R}^m$  which the two classes are best separated. Given  $\mathbf{x} \in \mathfrak{X}^m$  the scalar

$$\mathbf{y} = \frac{\mathbf{w}^T \mathbf{x}}{\|\mathbf{w}\|} \quad (5.35)$$

is the projection of  $\mathbf{x}$  along  $\mathbf{w}$ . Since scaling all our feature vectors by the same factor does not add any classification-related information, the scaling factor  $\|\mathbf{w}\|$  is ignored [98]. Applying the Fisher's discriminant ratio (FDR)

$$\text{FDR} = \frac{(\mu_1 - \mu_2)^2}{\sigma_1^2 + \sigma_2^2}, \quad (5.36)$$

where  $\mu_1, \mu_2$  are the mean values and  $\sigma_1^2, \sigma_2^2$  the variances of  $\mathbf{y}$  in the two classes  $w_1$  and  $w_2$ , respectively, after the projection along  $\mathbf{w}$ . Using Eq. 5.35 and omitting  $\|\mathbf{w}\|$ , it can be observed that

$$\mu_i = \mathbf{w}^T \boldsymbol{\mu}_i, i = 1, 2 \quad (5.37)$$

where  $\boldsymbol{\mu}_i, i = 1, 2$ , is the mean value of the data in  $w_i$  in the  $m$ -dimensional space. Assuming the classes to be equiprobable, it is easily shown that

$$(\mu_1 - \mu_2)^2 = \mathbf{w}^T (\boldsymbol{\mu}_1 - \boldsymbol{\mu}_2) (\boldsymbol{\mu}_1 - \boldsymbol{\mu}_2)^T \mathbf{w} \propto \mathbf{w}^T \mathbf{S}_b \mathbf{w} \quad (5.38)$$

with the between-class scatter matrix,  $\mathbf{S}_b$ , defined as

$$\mathbf{S}_b = \sum_{i=1}^M P_i (\boldsymbol{\mu}_i - \boldsymbol{\mu}_0) (\boldsymbol{\mu}_i - \boldsymbol{\mu}_0)^T, \quad (5.39)$$

$$\boldsymbol{\mu}_0 = \sum_i^M P_i \boldsymbol{\mu}_i, \quad (5.40)$$

where  $P_i$  is the a priori probability of class  $w_i$  and  $\boldsymbol{\mu}_0$  the global mean vector. That is  $P_i \approx \frac{n_i}{N}$ , where  $n_i$  is the number of samples in class  $w_i$ , out of a total  $N$  samples. The trace of  $\mathbf{S}_b$  is a measure of the average (over all classes) distance of the mean of each

individual class from the respective global value [96]. Analyzing the denominator of 5.36

$$\sigma_t^2 = E[(y - \mu_i)^2] = E[\mathbf{w}^T (\mathbf{x} - \boldsymbol{\mu}_i)(\mathbf{x} - \boldsymbol{\mu}_i)^T \mathbf{w}] = \mathbf{w}^T \mathbf{S}_w \mathbf{w}, \quad (5.41)$$

$$\mathbf{S}_w = \sum_{i=1}^M P_i E[(\mathbf{x} - \boldsymbol{\mu}_i)(\mathbf{x} - \boldsymbol{\mu}_i)^T], \quad (5.42)$$

where  $\sum_i$  is the covariance matrix corresponding to the data of class  $w_i$  in the  $m$ -dimensional space and  $\mathbf{S}_w$  is the within-class scatter matrix, which trace measure the average, overall classes, variance of the features [96]. Combining 5.41, 5.38 and 5.36 the optimal direction is obtained by maximizing Fisher's criterion

$$\text{FDR}(\mathbf{w}) = \frac{\mathbf{w}^T \mathbf{S}_b \mathbf{w}}{\mathbf{w}^T \mathbf{S}_w \mathbf{w}} \quad (5.43)$$

with respect to  $\mathbf{w}$ . This is the celebrated generalized Rayleigh quotient [99], which, is maximized if  $\mathbf{w}$  is chosen such that

$$\mathbf{S}_b \mathbf{w} = \lambda \mathbf{S}_w \mathbf{w}, \quad (5.44)$$

where  $\lambda$  is the largest eigenvalue of  $\mathbf{S}_w^{-1} \mathbf{S}_b$ . By the definition of  $\mathbf{S}_b$

$$\lambda \mathbf{S}_w \mathbf{w} = (\boldsymbol{\mu}_1 - \boldsymbol{\mu}_2)(\boldsymbol{\mu}_1 - \boldsymbol{\mu}_2)^T \mathbf{w} = \alpha(\boldsymbol{\mu}_1 - \boldsymbol{\mu}_2), \quad (5.45)$$

where  $\alpha$  is a scalar. The solution with respect to  $\mathbf{w}$  is

$$\mathbf{w} = \mathbf{S}_w^{-1} (\boldsymbol{\mu}_1 - \boldsymbol{\mu}_2) \quad (5.46)$$

assuming that  $\mathbf{S}_w$  is invertible.  $\mathbf{S}_w$  and  $\mathbf{S}_b$  are approximated by averaging using the data samples. As a consequence, the number of features has been reduced from  $m$  to  $1$  in an optimal way. Classification can now be performed based on  $y$ . Optimality assures that the class separability, with respect to  $y$ , is as high as possible, as this is measured by the FDR criterion.

### 5.2.3 Student's *t*-test

In this statistical hypothesis test, the data follow a Student's *t*-distribution [7, 100]. This test is commonly applied to data sets with a normal distribution to determine if the data sets are significantly different. The two-sample *t*-test is one of the most frequently used *t*-tests, which hypothesizes that the means of the two populations are equal. Different from the one-sample *t*-test, by which the statistical difference between a sample mean and a known or hypothesized value of the mean in the

population, the two-sample t-test tries to compare the means of two different samples [7]. The kinematic data in this work were obtained from two different groups of participants, normal and patients. Thus, the two-sample t-test is more suitable for the analysis and investigations in this work. The statistic of the two-sample t-test is defined as follows:

$$t = \frac{\bar{\mu}_x - \bar{\mu}_y}{\sqrt{\frac{\sigma_x}{n} + \frac{\sigma_y}{m}}}, \quad (5.47)$$

where  $\bar{\mu}_x$  and  $\bar{\mu}_y$  are the means of the two classes,  $\sigma_x$  and  $\sigma_y$  are their standard deviations, and  $n$  and  $m$  are their size. The two main test outputs are the hypothesis test results  $h$  and the  $\rho$ -value. The  $h$  is a logical value: if  $h = 1$ , this indicates the rejection of the null hypothesis at the alpha significance level; if  $h = 0$ , this indicates a failure to reject the null hypothesis at the alpha significance level. The  $\rho$ -value generated by the test is returned as a scalar value between 0 and 1. The table of values from the Student's t-distribution can be used to find this value. If the obtained  $\rho$ -value is smaller the threshold chosen for statistical significance, then the null hypothesis is rejected in favor of the alternative hypothesis. The significance level is usually chosen as 0.10, 0.05, 0.01, or 0.001.

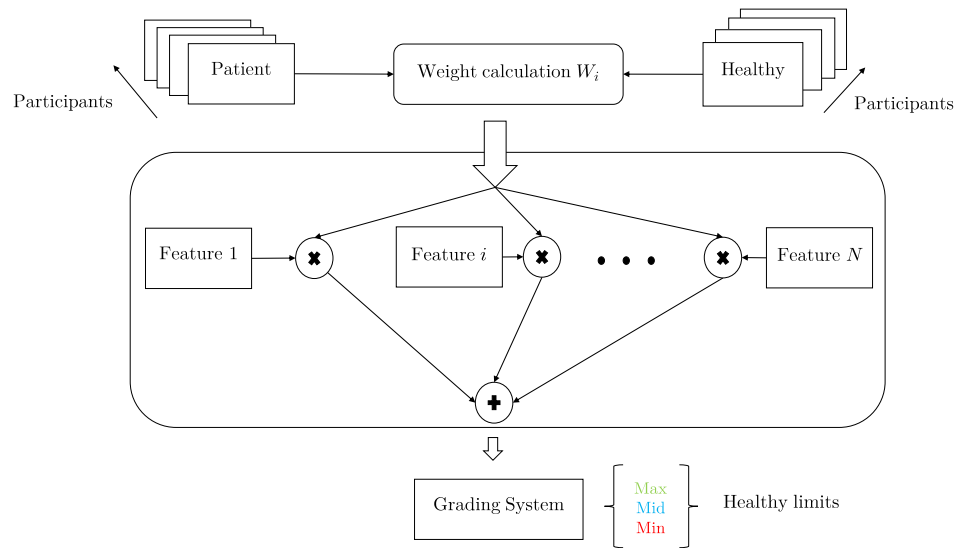


Figure 5.7: Grading system block diagram.

#### 5.2.4 SNR ranking

The signal to noise ratio (SNR) ranking for each feature can be obtained from [77]:

$$\text{SNR} = \frac{\mu_1 - \mu_2}{\sigma_1 + \sigma_2}, \quad (5.48)$$

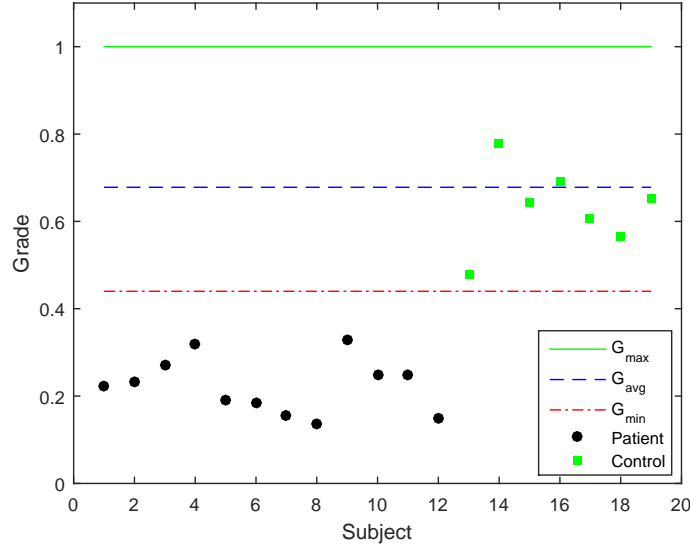


Figure 5.8: Efficiency of the grading system based on SNR

where  $\mu_1$  and  $\mu_2$  are the means of features for subjects with the normal and abnormal walk, respectively.  $\sigma_1$  and  $\sigma_2$  are the corresponding standard deviations. Intuitively, a more efficient classification is expected to be achieved using features of higher SNR values. The higher the SNR, the bigger the distance between the two groups. Subsequently, after several trails, a total of 26 features with high SNRs were selected.

### 5.3 GRADING SYSTEM

In this section, a novel grading system is proposed to quantify the gait characteristics of a subject (healthy or patient). Figure 5.7 shows the block diagram of the system. The novel grading system can be used to track the rehabilitation progress of patients. The concept of the grading system is based on maximum ratio combining (MRC), performed by

$$G = \sum_i^N F_i W_i, \quad (5.49)$$

where  $N$  is the number of the selected features,  $F_i$  is the feature value, and  $W_i$  is the weight of the contribution of each feature [101]. The grading system is trained using the information of healthy participants to set the boundaries of the healthy region. This region is based on the maximal, average and minimum values of the training data as shown in Figure 5.8.



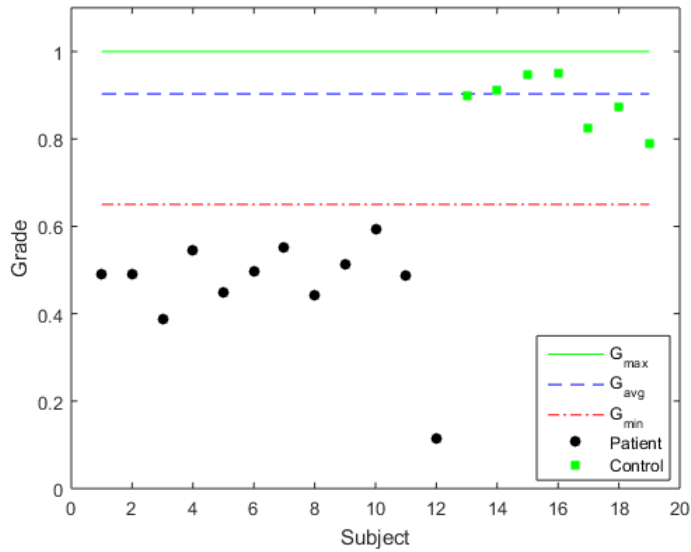


Figure 5.9: Efficiency of the grading system based on LDA

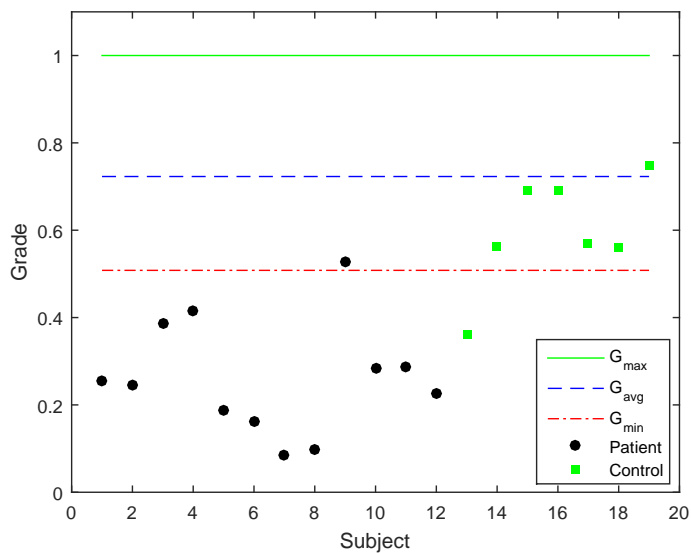


Figure 5.10: Efficiency of the grading system based on PCA

### 5.3.1 Results

In this section, the performance validation of the proposed grading systems is analyzed two-fold: First is the rehabilitation tracking; Second is the classification. The features mentioned in Section 5.1 can be treated as significant if they allow for a differentiation between normal and abnormal gait. In this part of the study, two groups, each consisting of eight subjects, are involved. The first group includes subjects with normal gait patterns, while the second group includes subjects with knee and hip operations. The above-mentioned features are calculated for all the subjects, and those

features with  $\rho$ -values less than 0.05 are considered significant [95]. Subsequently, the optimal feature set is obtained using SNR ranking bigger than 1. The first grading system utilizes the SNR values as the weight vector.

$$G_{SNR} = \sum_i^N F_i W_{SNR,i}, \quad (5.50)$$

The two other grading systems are based on the separation principle used by LDA and PCA.

$$G_{LDA} = \sum_i^N F_i W_{LDA,i}, \quad (5.51)$$

$$G_{PCA} = \sum_i^N F_i W_{PCA,i}. \quad (5.52)$$

Here, the grading value  $G$  is calculated using the Eigenvectors of the LDA/PCA as the weight values instead of the SNR values. LDA and PCA mainly differ in the related orthogonal basis used for. LDA looks for a feature space on which to project all data, such that the samples are maximally separated. PCA finds a feature space based on the features deviation from the global mean in the primary directions of variation in feature space [96]. The grading system has a training phase in which the grading boundaries are defined in terms of maximum, minimum and average values, i.e.,  $G_{max}$ ,  $G_{min}$ , and  $G_{avg}$  as shown in Fig. 5.8 to 5.10. Next, a test phase takes place in which the evaluation of performance of the classification and the grading systems. Based on the final feature set, a classification approach is also applied such that the goal is to classify each participant as either a normal or an abnormal gait pattern. In this context, supervised and unsupervised classification schemes are considered. As a result of the theorem of “No Free Lunch” [97], there is no optimal classifier. Alternatively, three different classifiers are evaluated in this study: LDA, PCA and naive Bayes (NB). The final feature set is used for the classification of eight patients and eight control subjects in the training phase to define the decision boundaries for the group separation. Once the decision boundaries are specified, the test data from eight patients and eight control subjects are used to verify the classification efficiency. Table 5.2 compares the three considered classifiers in terms of accuracy, sensitivity, and specificity. These results are also reflected in Fig. 5.8 to 5.10, where the participants with grades between  $G_{max}$  and  $G_{min}$  are considered as healthy (control) ones. Finally, Fig. 5.11 depicts the time correlation between the grades and the days after the operation. It is clearly seen that the grades increase with the days after the operation with all considered grading systems. This means that the proposed grading systems are able to objectively quantify the gait performance and the rehabilitation progress based on the final features set derived from the gait

Table 5.2: Classification results

Classifier	Accuracy	Sensitivity	Specificity
PCA	85.7%	85.7%	85.7%
LDA	90%	90%	90%
NB	88%	88%	88%

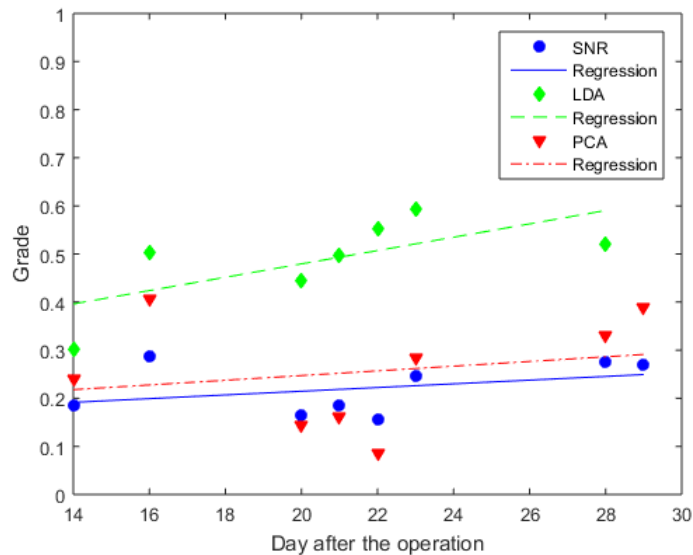


Figure 5.11: Assessment of the rehabilitation training.

analysis. Moreover, it is possible to provide a numerical performance comparison of patients. From Fig. 5.8 to 5.11, it can be concluded that the LDA-based grading system is preferred for two reasons: First, it has a high classification accuracy, and second, it has the highest grading-time correlation, and hence it has a better tracking capability. Additionally, it is possible to obtain an individual profile by calculating the grade of each feature separately.

### 5.3.2 Acoustic feedback for rehabilitation

The direct mapping of sound based on data and interactions is defined as sonification [102]. In this work, gait sonification means the direct rendering of biomechanical parameters to electronic sound to make it audible for subjects via headphones. Using the lower body joint angles calculated in Chapter 4 and the Csound interface for Android, it is possible to map an increasing pitch change utilizing the knee joint speed during the stretching phase and the IC events. The IC and the TOE walking events from gait were emphasized with low frequencies for easy detection of the stance phase. During the first four minutes of all rehabilitation sessions, the sub-

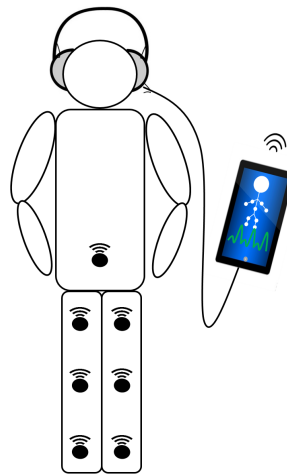


Figure 5.12: Wearable system setup consisting of seven IMUs, an Android tablet and headphones.

jects receive RTAF based on their own gait parameters followed by acoustic model sequences (AMS). This RTAF sequence structure was followed until the completion of the rehabilitation session. The acoustic models were created and developed based on the extracted features and the speed, weight, height, and step cadence using the software MATLAB. The acoustic model sequences were exported to the Android application to perform real-time feedback. Prior to the first rehabilitation session of each experimental subject, a gait test was performed to determine the gait cadence and initial settings to be used in the acoustic model sequence.

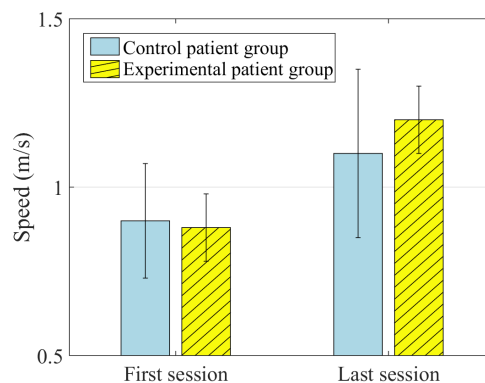


Figure 5.13: Gait speed comparison between the experimental and the control patient group with and without RTAF during the rehabilitation sessions. Striped bars represent the experimental patient group with real-time acoustic feedback.

### 5.3.2.1 Results

Evaluation and verification of the RTAF rehabilitation approach are performed using the grading system based on LDA. Figure 5.17 shows the comparison of the grades

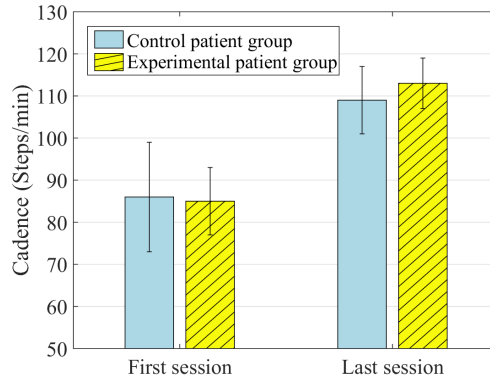


Figure 5.14: Gait cadence comparison between the experimental and the control patient group with and without RTAF during the rehabilitation sessions. Striped bars represent the experimental patient group with real-time acoustic feedback.

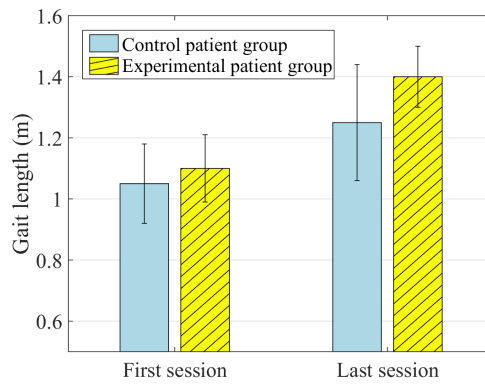


Figure 5.15: Gait length comparison between the experimental and the control patient group with and without RTAF during the rehabilitation sessions. Striped bars represent the experimental patient group with real-time acoustic feedback.

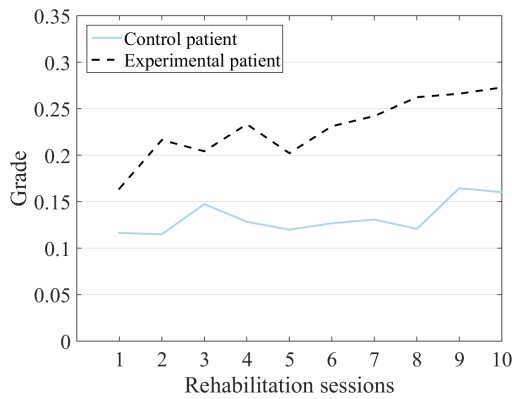


Figure 5.16: Individual performance comparison between an experimental and a control patient during the two weeks study

between the experimental and the control patient group using the proposed RTAF. In both cases, there is a positive correlation with the rehabilitation sessions, but the

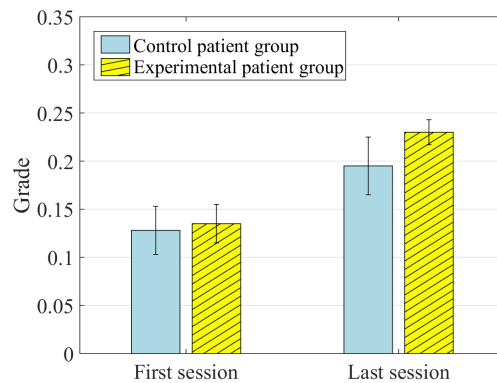


Figure 5.17: Individual performance comparison between an experimental and a control patient during the two weeks study

grade of the experimental subjects increases faster, very likely due to the positive effect of the acoustic feedback. It is possible to observe an improvement in the grade in the experimental group. In Figures 5.13 to 5.15, a notable improvement in the gait parameters is observed in the experimental group using the real-time acoustic feedback for the gait speed, the gait cadence, and the gait length. The acoustic feedback makes it easier for the experimental subjects to identify the cadence tempos and movement patterns and adapt themselves more precisely [103].

The grading system is not only able to objectively quantify the gait performance and the rehabilitation progress but also can provide a numerical performance, monitoring, and tracking. Figure 5.16 shows the individual performance of one experimental subject and one control subject. Hereby, it is also possible to create an individual profile and use the grading system to adjust the RTAF corresponding to the individual performance and specific impairment. The outcomes from this study evidence positive effects of the real-time acoustic feedback. The results regarding the first rehabilitation training sessions are similar for both groups due to the adaptation phase to the feedback. After the adaptation phase, it is possible to see that the variance in the experimental group is lower than in the control group. These results agree with previous studies pointing to strong associations between the auditory and motor areas of the brain [104, 105].

#### 5.4 CONCLUDING REMARKS

The main goals investigated in this work are twofold: First, the use of signal processing methods for individualization and quantification of rehabilitation or therapy methods. Second, reduction of the rehabilitation duration. Hereby, the most significant features are extracted in real-time from gait signals belonging to healthy participants without any pathological background and patients who underwent hip

surgery. Based on these features, the RTAF is created utilizing the individual gait patterns of each subject. According to the results, the grading system is able to track and objectively quantify the rehabilitation course for each subject. The RTAF supports the subjects when they are performing the tasks during the rehabilitation session so that they are able to adjust their motion pattern to the acoustic feedback. Therefore, the proposed application for wearable IMU platforms which is able to precisely quantify the rehabilitation progress associated with hip surgery, create and sonify the most important gait cues, and classify the experimental and control group objectively. Our proposed approach allows mobile and comfortable therapy. Further signal processing schemes and an extension of the sonification will be the subject of future investigations. The final goal is to develop a medically approved system with an individualized and adjustable solution that can be applied to daily clinical practice.





---

DIGITAL TWINS OF GAIT KINEMATICS

---

The main goal of new wearable sensor systems (WSSs) is to provide a variety of practical applications for gait assessment to anybody, anywhere, any time. Therefore, the next generation of WSSs exhibit reduce number of physical sensors, easily interpretable and reliable data. To achieve this, WSS have to overcome different types of impairments in the gait signals and sensors. This chapter focuses on the concept of “digital twin (DT)”, which allows reducing of number of physical sensors by including a “virtual” sensors. The DT investigated in this thesis is based on memory polynomial model (MPM) and deep learning (DL) methods.

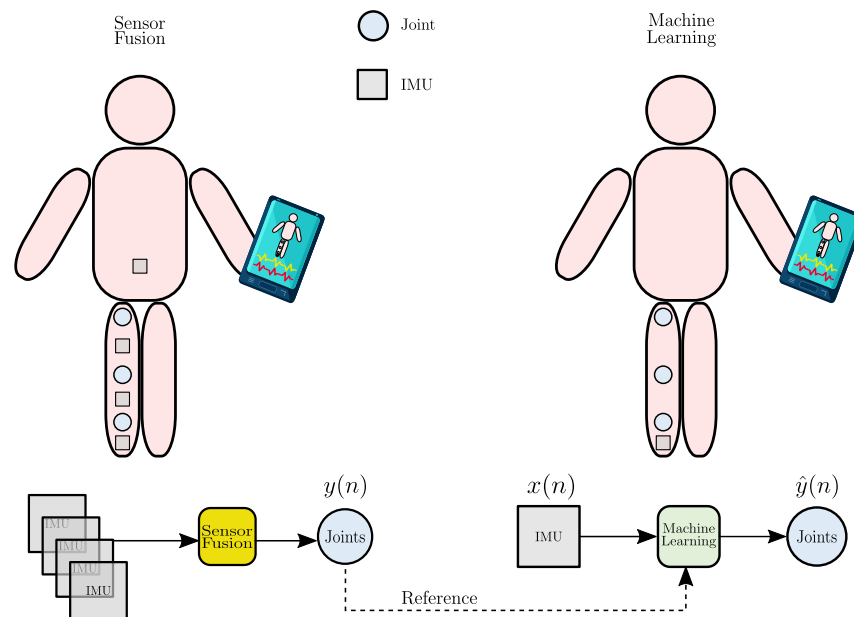


Figure 6.1: Overall system concept: The gait kinematic data  $x(n)$  are collected and processed with ML methods in the Android application for digital and biomedical healthcare systems. On the left side, the traditional sensor fusion algorithm based on KF estimates the lower limb joint signals using the information from several IMUs. On the right side, the novel ML approach estimates the lower limb joint angles based on the information of only one IMU placed on the foot. The dashed line represents the reference data  $y(n)$  for the training and test phases of the ML approaches.

## 6.1 RELATED WORK

WSSs allow extensive data acquisition in a simple and convenient way regarding their portability and flexible attachment to any part of the body (e.g., lower limbs, upper limbs, torso, Etc.) [106–109]. Among them, IMUs are of particular interest to scientists and engineers in diverse application fields due to their small size, low cost, lightweight, good precision, and non-invasive characteristics [47, 54, 110, 111]. An inertial sensor performs multi-parameter sensing, such as 3D linear acceleration, 3D angular velocity, and 3D magnetic field, and thus allows to capture of a wide range of locomotor activities and patterns [51, 112]. The main challenge here is to analyze, extract and translate the relevant information on normal and pathological gait behavior into practical and affordable interventions. The high dimensionality poses this and great diversity of the gait data, as well as the time and effort involved in the sensor placing and configuration [44, 48, 113–115]. The issue concerning the high dimensionality of the gait data has been solved by applying conventional dimension reduction techniques such as PCA and LDA [116]. In [117], PCA is applied to get a smaller set of features for the classification of gait data recorded by a multi-sensor wearable system. A similar approach was used in [118] to classify subjects using one IMU placed at different body locations.

To keep the system complexity as low as possible, one solution approach is to reduce the number of sensors in the WSS via sensor virtualization or “digital twins” [46, 119]. The digital equivalent can replace the physical counterpart (see Figure 6.1) and requires no special knowledge of the physical structure of the human biomechanics, which in the case of the human movement is complex [120]. In other words, by applying signal and statistical processing methods to data from a smaller number of sensors, the remaining sensor signals can be estimated rather than being directly measured. The authors in [119] proposed a novel MPM for the estimation of the lower limb joint angles based only on the magnitude of the acceleration signal of one IMU located at the ankle. In [46], an extended Kalman filter (EKF) was used to estimate the vertical hip acceleration and sagittal trunk posture by applying a heuristically modified Fourier series model based on the vertical acceleration and sagittal angular velocity from one IMU placed at the ankle. A novel double-pendulum model was proposed in [121], in which a small number of sensors attached on both sides of the shank were used to estimate the movements of the thighs. The feasibility of the estimation of gait kinematics with a reduced number of sensors has been demonstrated in previous studies. This serves as the basis for the realization of high-precision, robust, and customizable digital twins capable of replacing hardware sensors, which is an excellent advantage for diverse digital healthcare and bioinformatics applications.

Nevertheless, the most promising way to utilize the vast amount of gait data generated by modern wearable sensors is the use of ML [122] due to its capability of integrating both stochastic and computer science for identifying patterns in large data sets [123]. In the field of gait analysis, healthcare, and bioinformatics, ML is applied in general to either the task of classification or estimation. Regarding the first, multiple studies have been conducted in the field of gait analysis, such as activity or gait phases recognition [124–127]. In [128], the authors trained a convolutional neural network (CNN) based on linear acceleration and angular velocities from inertial sensors to automatically classify human activities. A similar approach was proposed in [92], where the data from five different sensors placed on the body were collected, and a CNN was trained for subject identification.

Regarding estimation, many studies apply ML and deep learning to simulated gait data obtained from the markers of camera systems to assess lower limb kinematics [129–131]. In [132, 133], a generalized regression neural network (GRNN) was trained to estimate foot, lower leg, and thigh kinematics in the sagittal plane from emulated 2D foot acceleration signals from a complex camera system and four IMUs during walking. In [130], a multilayer perceptron (MLP) was used to simulate the complexities of lower limb motions together with a camera system as input data for the neural network (NN). Few studies have applied deep learning techniques for estimation tasks with real kinematic data. A deep CNN was proposed in [134] for gait parameter extraction based on one IMU attached to the shoe. The authors in [135] obtained a value of  $7^\circ$  root mean square error (RMSE) in the estimation of the knee joint angle with mechanomyography signals and a CNN.

The potential of NNs and deep learning for modeling the nonlinear relationship of lower body joint angles from foot movement and its applicability as a “digital twin” for gait kinematic analysis has not yet been explored. Therefore, unlike the aforementioned studies, this work evaluates the performance of different approaches in modeling lower body joint angles using nonlinear methods and the gait kinematics records of a single IMU attached to the foot. The capability to monitor the subject’s rehabilitation is also evaluated.

## 6.2 MODELING APPROACHES

The representation of real objects or events applying mathematical statements is defined as modeling. Modeling is divided into two classes, physical and behavioral modeling [136].

### 6.2.1 *Physical models*

For this class of models, the theoretical rules describing the interactions between elements in the system, their constitutive relations, and the knowledge about the real system are required. This modeling class is appropriate for muscle level simulation and can be very accurate, and complex [136, 137].

### 6.2.2 *Behavioral models*

A black box or behavioral model does not require prior knowledge of the physical systems. Its structure consists of the relation between input and out measurements [136]. The model parameters are identified from the input and output measurement data. As a result, the characteristics of data obtained from the measurement, such as the method applied, the execution of the measurement, and the quality of data, affect the model accuracy [138]. This model is appropriate for gait data analysis due to the vast amount of available data. Therefore, all the models investigated in this thesis are behavioral.

## 6.3 POLYNOMIAL MODELS FOR JOINT ESTIMATION

The human gait is a complex process that includes acting and synchronizing many different muscles. In reality, the lower body joint angle estimation depends on previous gait kinematic data and the current gait kinematic data of the sensor. This phenomenon is called the memory effect, or simply temporal dynamics. These memory effects are due to continuous activations of the muscles and the transitions from one gait phase to the next one. It can be observed as asymmetries in the lower body joint angles  $y(n)$  from the left and right sides and dependent variations in the magnitude of the gait kinematic signals  $x(n)$ . For higher accuracy applications, e.g., rehabilitation, the memory effects become severe and cannot be ignored. Hence, memory-less models are not accurate enough [136]. Therefore, a model which considers memory effects should be used for such applications. Different nonlinear models with memory are presented and compared to the memory polynomial model in the following sections.

### 6.3.1 *Volterra model and special cases*

The Volterra model can be used to describe any nonlinear stable signal with fading memory, with an arbitrary small error [139]. However, its main disadvantages are the huge increase in the number of parameters with respect to nonlinear and memory length, which causes a large increase of complexity in the identification of model

parameters [136]. This is the reason why it is highly unpractical to use the Volterra model for signals with high nonlinear orders and memory lengths. This Volterra model can be expressed mathematically as follows [140]

$$y(n) = \sum_k \sum_{l_1} \dots \sum_{l_{2k+1}} l_{2k+1} h_{2k+1}(l_1, l_2, \dots, l_{2k+1}) \prod_{i=1}^{k+1} (x(n-l_i)) \prod_{i=k+2}^{2k+1} x^*(n-l_i). \quad (6.1)$$

From the equation above it is clear that the number of coefficients of the Volterra model increases exponentially as the memory length and the nonlinear order increase [140]. As mentioned above, the Volterra model is unpractical for modeling lower body joint angles in real-time applications. This reason motivated researchers to look for simplifications of the Volterra model. The Wiener, the Hammerstein, and the Wiener-Hammerstein models and their parallel versions are included in the category of special cases of the Volterra model for modeling nonlinear signals [136]. The Wiener model consists of a linear time invariant (LTI) system followed by a memory-less nonlinearity. The Hammerstein model is a memory-less nonlinearity followed by an LTI. The Wiener-Hammerstein model consists of an LTI system followed by a memory-less nonlinearity, which is in turn followed by another LTI system. The parallel Hammerstein model is an extension of the standard Hammerstein model. The main difference between the parallel Hammerstein and the standard Hammerstein models is that in the parallel Hammerstein model, different static nonlinear orders are filtered with different LTI systems [136, 140].

### 6.3.2 Comparison to MPM

Comparing the MPM with the Hammerstein model, it can be observed that the Hammerstein model is a particular case of the MPM when only the odd polynomial terms are considered for the nonlinearity of the Hammerstein model [136]. When comparing the MPM with the parallel Hammerstein, it is observed that the MPM is equivalent to the parallel Hammerstein model. It can also be shown that the MPM is a special case of the parallel Wiener model [140]. In summary, when considering polynomial types of nonlinearities, both the Wiener and the Hammerstein models are special cases of the Volterra model [136]. In fact, it can be shown that the MPM is equivalent to the parallel Hammerstein model [136]. In [140], the author shows that a MPM is a special case of the parallel Wiener model. The parallel Hammerstein model includes the Hammerstein model as a special case, and the parallel Wiener model includes the Wiener model as a particular case. Hammerstein and Wiener models are the most specialized with the least number of coefficients but are by no means the easiest to identify. The MPM however, offers a good compromise between generality and ease of parameter estimation and implementation [136, 140, 141]. In this work, the MPM is investigated and applied to model the lower body joint angles.

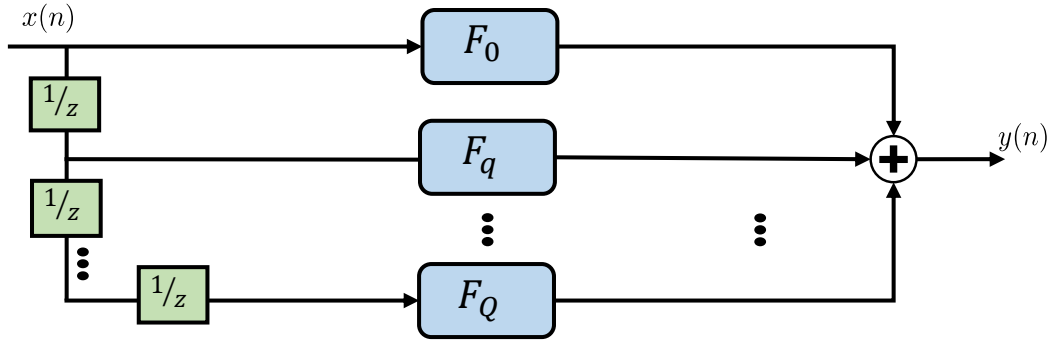


Figure 6.2: The memory polynomial model.

6.3.3 The memory-polynomial model for joint estimation

The memory polynomial model (MPM) consists of several delay taps and nonlinear static functions [141]. In this model, the amount of parameters is considerable low due to the truncation of the general Volterra model. The truncation consist only in the diagonal terms of the kernels [136]. The model is shown in Fig. 6.2 and 6.3. A MPM considering memory effects and nonlinearity is given by the following equation [136]

$$y(n) = \sum_{q=0}^Q \sum_{k=1}^K a_{k-1,q} |x(n-q)|^{(k-1)} x(n-q), \tag{6.2}$$

where  $x(n)$  is the gait kinematic signal,  $y(n)$  is the joint angle,  $a_{k,q}$  are the model parameters,  $Q$  is the memory depth and  $K$  is the order of the polynomial. Equation 6.2 can be rewritten as follows

$$y(n) = \sum_{q=0}^Q F_q(n-q) \tag{6.3}$$

$$= F_0(n) + F_1(n-1) + \dots + F_Q(n-Q), \tag{6.4}$$

where

$$F_q(n) = \sum_{k=1}^K a_{k,q} |x(n)|^{(k-1)} x(n) \tag{6.5}$$

$$= a_{1,q} |x(n)| + a_{2,q} |x(n)|^2 + a_{3,q} |x(n)|^3 + \dots + a_{K,q} |x(n)|^K. \tag{6.6}$$

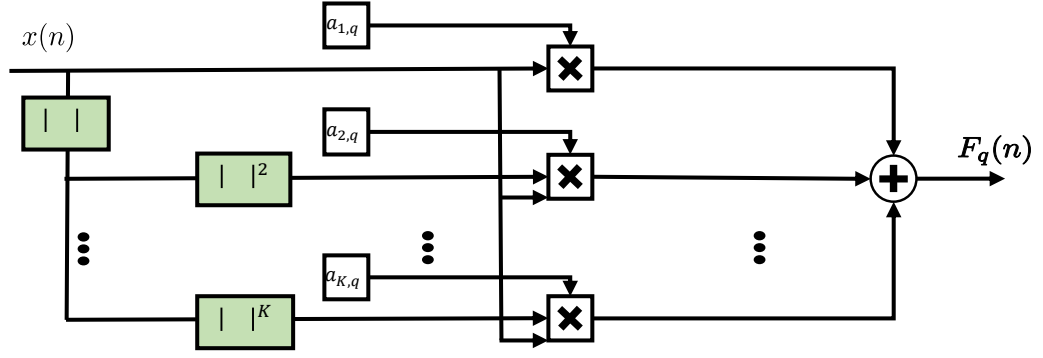


Figure 6.3: MPM implementation

### 6.3.4 Memory polynomial model identification

The parameter identification of the MPM is very easy compared to other models [136]. The coefficients are calculated from the training data using least squares (LS). The process can be explained as follows: The matrices  $\mathbf{Y}$  and  $\mathbf{H}$  are defined as [136]

$$\mathbf{Y} = [y(n) \ y(n+1) \ \dots \ y(n+N-1)]^T \quad (6.7)$$

$$\mathbf{H} = [\mathbf{H}_0 \ \mathbf{H}_q \ \mathbf{H}_Q] \quad (6.8)$$

$$\mathbf{H}_q = \begin{bmatrix} h_{1,0}(n) & h_{2,1}(0) & h_{3,1}(n) & \dots & h_{K,q}(n) \\ \vdots & \vdots & \ddots & \vdots & \\ h_{1,0}(n+N-1) & h_{2,1}(n+N-1) & h_{3,1}(n+N-1) & \dots & h_{K,q}(n+N-1) \end{bmatrix} \quad (6.9)$$

with

$$h_{k-1,q}(n) = |x(n-q)|^{k-1} x(n-q), \quad (6.10)$$

where  $y(n)$  are the lower body joint angles and  $N$  is the length of the data. The model parameters are defined by

$$\mathbf{a} = [\mathbf{a}_0 \ \dots \ \mathbf{a}_q \ \dots \ \mathbf{a}_Q]^T, \quad (6.11)$$

with

$$\mathbf{a}_q = [a_{1,q} \ a_{2,q} \ a_{3,q} \ \dots \ a_{K,q}]. \quad (6.12)$$

The following equation describes the relation of the model parameters and the gait kinematic signals

$$\mathbf{Y} = \mathbf{H}\mathbf{a}. \quad (6.13)$$

To achieve the minimum RMSE between the reference and the estimated joint angles, the estimated parameter matrix  $\hat{\mathbf{a}}$  can be calculated from the following equations

$$(\mathbf{H}\mathbf{H}^*)(\mathbf{H}^*\mathbf{H})^{-1} = \mathbf{I}, \quad (6.14)$$

where  $\mathbf{H}^*$  is the conjugate transpose of  $\mathbf{H}$ , also known as the Hermitian transpose of the matrix. The equation 6.13 can be rewritten as

$$(\mathbf{H}\mathbf{H}^*)(\mathbf{H}^*\mathbf{H})^{-1}\mathbf{Y} = \mathbf{H}\mathbf{a}. \quad (6.15)$$

The parameter matrix  $\mathbf{a}$  can be approximated according to the LS criterion by  $\hat{\mathbf{a}}$  as follows

$$\hat{\mathbf{a}} = \mathbf{H}^*(\mathbf{H}^*\mathbf{H})^{-1}\mathbf{Y}, \quad (6.16)$$

where

$$\hat{\mathbf{a}} = [\hat{\mathbf{a}}_0 \dots \hat{\mathbf{a}}_q \dots \hat{\mathbf{a}}_Q]^T \quad (6.17)$$

and

$$\mathbf{H}^+ = \mathbf{H}^*(\mathbf{H}^*\mathbf{H})^{-1}, \quad (6.18)$$

where  $\mathbf{H}^+$  is the pseudo inverse matrix of  $\mathbf{H}$  defined above. With 6.18 it is possible to rewrite 6.16 as

$$\hat{\mathbf{a}} = \mathbf{H}^+\mathbf{Y}. \quad (6.19)$$

The joint angles can be estimated from the gait kinematic input signals and the estimated parameters as follows:

$$\hat{\mathbf{Y}} = [\hat{y}(n) \hat{y}(n+1) \dots \hat{y}(n+N-1)]^T \quad (6.20)$$

$$= \mathbf{H}\hat{\mathbf{a}} = \sum_{q=0}^Q \mathbf{H}_q \hat{\mathbf{a}}_q, \quad (6.21)$$

The error between the reference and estimated joint angles can be defined as

$$\mathbf{E} = \mathbf{Y} - \hat{\mathbf{Y}} = [e(n) e(n+1) \dots e(n+N-1)]^T. \quad (6.22)$$

The least square estimate is defined to minimize the  $\|\mathbf{E}\|^2$ .

### 6.3.5 Results

The first attempt of realizing digital twins for gait rehabilitation is to determine kinematics (joint angles) of the lower limbs using only the accelerometer data of the IMUs placed at the feet. This includes also the following signal processing steps. The raw accelerometer data ( $\mathbf{S} \in \mathbb{R}^{N \times 3}$ ) of relevance for gait analysis is contaminated with various noise factors such as motion artifacts, step impacts, sensor orientation and location related noises. In order to overcome this problem, the norm of the accelerometer signal is calculated and used as input for the MPM. This step is calculated by

$$x(n) = \|\mathbf{S}(n)\|_2 = \sqrt{|\mathbf{S}_{n,1}|^2 + |\mathbf{S}_{n,2}|^2 + |\mathbf{S}_{n,3}|^2}, \quad \forall n \in \mathbb{N} \quad (6.23)$$



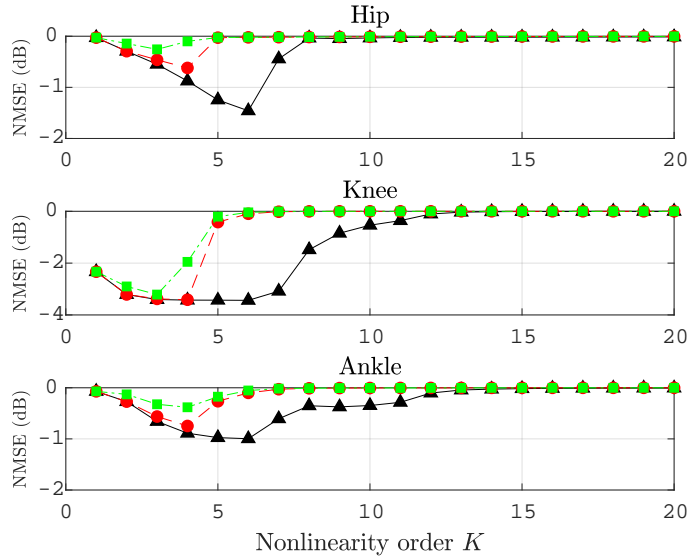


Figure 6.4: Performance comparison of MPM for different nonlinearity orders  $K$ . Triangle markers represent the all-order terms. Circle markers represent the even-order terms. Square markers represent the odd-order terms. The optimal values can be found, where the NMSE is minimized.

where  $\mathbf{S}(n)$  is a row vector of the matrix  $\mathbf{S}$ . The signal  $x(n)$  is then filtered using a Butterworth low-pass filter with a cutoff frequency of 7 Hz to reduce the high-frequency components. Due to the dynamic gait pattern, the length of each gait cycle differs from one cycle to another and from one participant to another. To remove the person-related features of walking speed and step period, we need to normalize the gait cycles. Therefore, the gait cycle is detected using the ZUPT detection algorithm from Section 4 to find the ICs [142–144]. Afterward, gait cycle normalization can be performed by resampling the data to a cyclic length of 100 samples [145]. The data recorded in this study were used to define the left and right gait cycle independently for each side. The total amount of cycles for each participant was set to 50. The biomechanical signals used as references for this study are the lower body joint angles (hip, knee, and ankle). To estimate above-mentioned joint angles, the sensor fusion technique based on a KF from Section 4 is applied [146]. To assess the efficiency of the MPM in simulating the lower body joint angles, the MPM is implemented in MATLAB, followed by the estimation of the model parameters  $K$  and  $Q$ . The performance of the MPM is evaluated twofold: First, the system concept is evaluated with the data from the 18 participants to prove the possibility of modeling the desired signals using the data from the accelerometer at the foot. Second, the generation of a model and its cross-validation using the normalized mean square error (NMSE) is carried out to evaluate the MPM performance. Hereto the data from different participants are used to estimate the desired lower limb joint angle signals. The nonlinearity order  $K$  and the memory depth  $Q$  have to be determined, respectively. The nonlinearity order delivering the minimum value of NMSE is used to determine

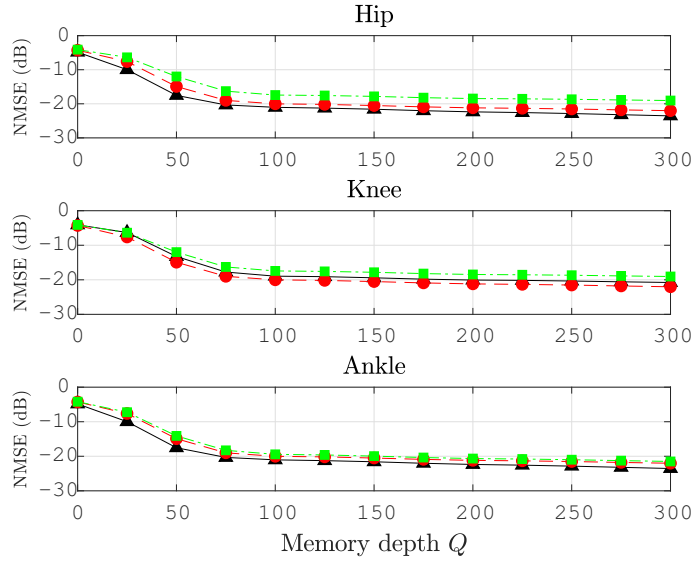


Figure 6.5: Performance comparison of MPM for different values of the memory depth parameter  $Q$  using the optimal values of  $K$ . Triangle markers represent the all-order terms. Circle markers represent the even-order terms. Square markers represent the odd-order terms.

the memory depth. Fig. 6.4 shows the MPM performance in terms of mean NMSE for all participants as a function of the nonlinearity order for hip, knee, and ankle angles for all the participants according to

$$\text{NMSE}_{\text{avg}}(\text{dB}) = 10 \log_{10} \left( \frac{1}{P} \sum_{p=1}^P \frac{\sum_{n=0}^{N-1} |y_p(n) - \hat{y}_p(n)|^2}{\sum_{n=0}^{N-1} |y_p(n)|^2} \right). \quad (6.24)$$

Here,  $y_p(n)$  is the joint angle signal of the  $p$ -th participant and  $\hat{y}_p(n)$  represents the modeled joint angle signal using the participant specific model.  $P$  is the number of investigated participants. This is achieved taking into account either all, even or odd-order terms. An optimal solution is given, where the NMSE is minimized. Having the nonlinearity order estimation, the memory depth of the MPM model is determined. Fig. 6.5 shows the results of mean NMSE vs. memory depth for hip, knee and ankle angles. The NMSE results for the evaluation of the required memory depth  $Q$  show no minimum as for the estimation of the nonlinearity order  $K$ . Therefore, we select  $Q$  such that an NMSE of at least -20 dB is reached, which for the investigated signals relates to an absolute error of approximately  $5^\circ$  ( $4^\circ$ ,  $6^\circ$  and  $4^\circ$  for the joint hip, knee and ankle angles, respectively).

Fig. 6.6 shows the estimation of the joint angles using the MPM and the optimal values for  $K$  and  $Q$ . It is seen that an NMSE of about -20 dB can be achieved for each joint angle at different values of order and memory depth. For ankle and hip angle modeling an order  $K = 6$  and memory depth  $Q = 75$  samples is sufficient to achieve

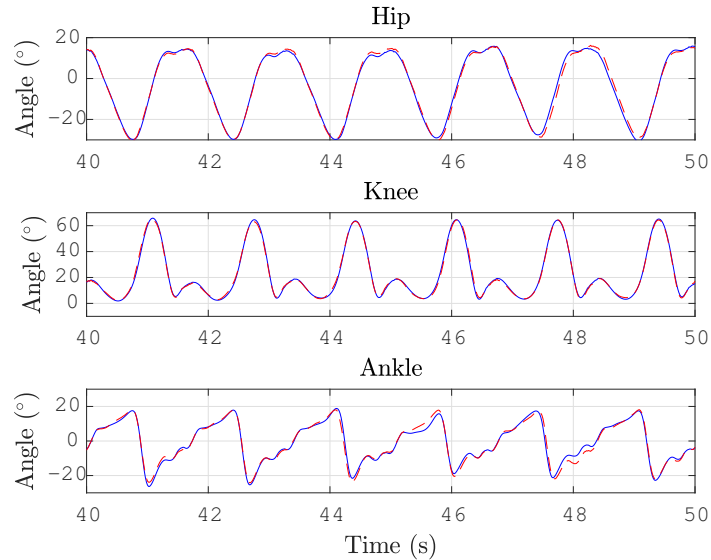


Figure 6.6: Estimation of the joint angles using the MPM and the optimal values for  $K$  and  $Q$ . The blue solid line represents the reference signal. The red dashed line represents the estimation.

the given accuracy, whereas this is achievable for the knee angle at  $K = 6$  and  $Q = 200$  as shown in Tab. 6.1. These results show the polynomial's capacity to model lower body joint signals.

To evaluate the MPM for the estimation of lower body joint angles, the cross-validation technique is applied. Cross-validation is normally used in machine learning to estimate the capability of a model on new data sets. For the cross-validation analysis the data is separated in subsets, namely, training and test. The procedure is often called  $\xi$ -fold cross-validation. In this part of the analysis, the value of  $\xi$  is set to 10 for the evaluation of the MPM. The training set is formed using the 70% of the data and the remaining 30% is allocated for the test set. The training and test sets contain data from different participants. Therefore, the test set is unseen data for the MPM. The results of the capability of MPM are depicted in Fig. 6.7. It can be seen, that the test set estimated and reference signals differ more significantly compared to the training set. The related estimation performance in terms of mean NMSE using the estimated coefficients  $\mathbf{a}$  from the training set amounts about -12 dB, -15 dB and

Table 6.1: Optimal parameters for the MPM of different joint angles based on an IMU located at one foot.

	K			Q		
	All	Even	Odd	All	Even	Odd
Hip	6	4	3	75	100	>300
Knee	6	4	3	200	100	>300
Ankle	6	4	4	75	100	150

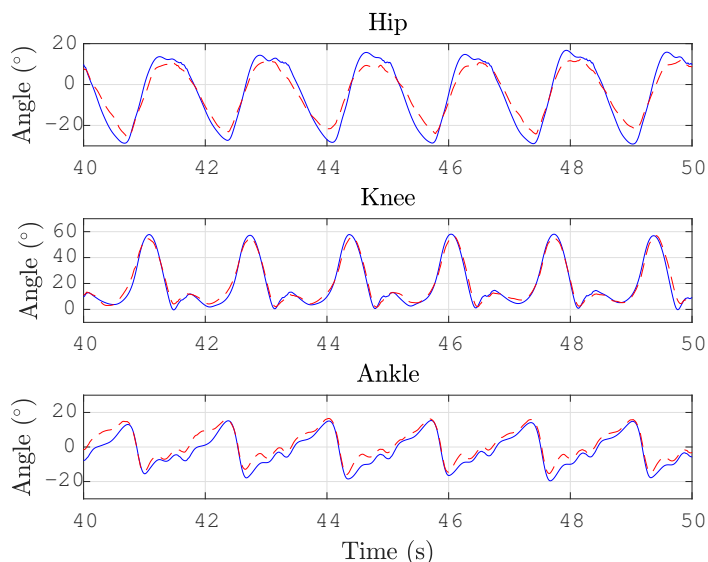


Figure 6.7: Cross-validation estimation results of the joint angles using the proposed MPM and the optimal values for  $K$  and  $Q$ . The blue solid line represents the reference signal. The red dashed line represents the estimation.

-7 dB for the hip, knee and ankle, respectively. The reason for the inferior NMSE results is the high dynamic nature of gait patterns on the one hand, and on the other, the limitations involved in data recording. On this basis, significant analysis on large data sets as well as different placements of IMU sensor to record accelerometer data is the subject of investigations in our future work.

#### 6.4 NEURONAL NETWORKS FOR JOINT ESTIMATION

A NN is a model whose layered structure is comparable to the networked structure of neurons in the brain, with layers of connected nodes [147]. NNs can be trained to recognize patterns, classify data, and estimate future events. A NN breaks down the input into different layers of abstraction. Its behavior is defined by the way in which individual neurons are connected and by the weights of those connections. These weights are automatically adapted during training following a specified optimization rule before the neural network achieves a desired level of performance. Regarding the sequential and nonlinear characteristics of the kinematic gait signals, in this work we considered GRNN, nonlinear autoregressive network with exogenous inputs (NARX) and LSTM networks for black box modeling between the kinematic gait data and the lower body joint angles in the sagittal plane. A brief introduction of the network architectures is provided in the following sections.

### 6.4.1 Generalized regression neural networks

Generalized regression neural networks (GRNNs) are used in different applications related to modeling, system identification, prediction, and control of dynamic systems [148]. It has been shown that GRNNs can also be applied for joint angle estimation using kinematic data, and it will be used in this work as a reference to compare the performance of the different networks [132]. The GRNN is a single-pass neural network that uses a Gaussian activation function in the hidden layer [149]. The model process is based on kernel density estimation from a set of inputs  $\mathbf{x}$  (kinematic data) and outputs  $\mathbf{y}$  (joint angles). The GRNN estimation applies the conditional expectation of output  $\hat{\mathbf{y}}(n)$  given the input  $\mathbf{x}$  [132]:

$$\hat{\mathbf{y}}(\mathbf{x}) = E[\mathbf{y}|\mathbf{x}] = \frac{\int \mathbf{y} p(\mathbf{y}, \mathbf{x}) d\mathbf{y}}{\int p(\mathbf{y}, \mathbf{x}) d\mathbf{y}}, \quad (6.25)$$

where  $p(\mathbf{y}|\mathbf{x})$  is the conditional probability density function [149]. It is possible to estimate the joint probability density  $\hat{p}(\mathbf{y}, \mathbf{x})$  given by [132, 148]:

$$\hat{p}(\mathbf{y}, \mathbf{x}) = \frac{1}{K} \sum_{i=1}^K \frac{1}{(2\pi)^{(D+1)/2} \epsilon^{(D+1)}} e^{-\left(\frac{(\mathbf{y}-\mathbf{y}_i)^2 + \|\mathbf{x}-\mathbf{x}_i\|^2}{2\epsilon^2}\right)}, \quad (6.26)$$

where  $D$  is the dimension of the input data. After simplifying the integrals in the numerator and denominator, the final expression of the estimator is given by [132, 148]

$$\hat{\mathbf{y}}(\mathbf{x}) = \frac{\sum_{i=1}^K \mathbf{y}_i e^{(-\|\mathbf{x}-\mathbf{x}_i\|^2/2\epsilon^2)}}{\sum_{i=1}^K e^{(-\|\mathbf{x}-\mathbf{x}_i\|^2/2\epsilon^2)}}, \quad (6.27)$$

where the parameter  $\epsilon$  is the bandwidth of the Gaussian kernel.

### 6.4.2 Recurrent neural networks

A feedforward neural network (FNN) or multilayer perceptron (MLP), is a network model in which the information is processed through interconnection of different nodes (units or neurons) and different activation functions  $\phi$ . The neurons are grouped into different layers  $l$ . The layers are interconnected using weighted connections  $W_{ij}^l$ , where  $W_{ij}^l$  is the weights matrix connecting the neurons in layer  $l$  with the neurons in layer  $l+1$ . The activation functions project the input information to a space in which it becomes separable. The relation between the input  $\mathbf{x}_t^l = (\mathbf{x}_1^l, \dots, \mathbf{x}_T^l) \in \mathbb{R}^{D \times T}$  and output  $\mathbf{y}_t^l = (\mathbf{y}_1^l, \dots, \mathbf{y}_T^l) \in \mathbb{R}^{3 \times T}$  sequences of a neuron is define as follows:

$$\mathbf{y}_t^{l+1} = \phi(W_{ij}^l \mathbf{x}_t^l + \mathbf{b}^l), \quad (6.28)$$

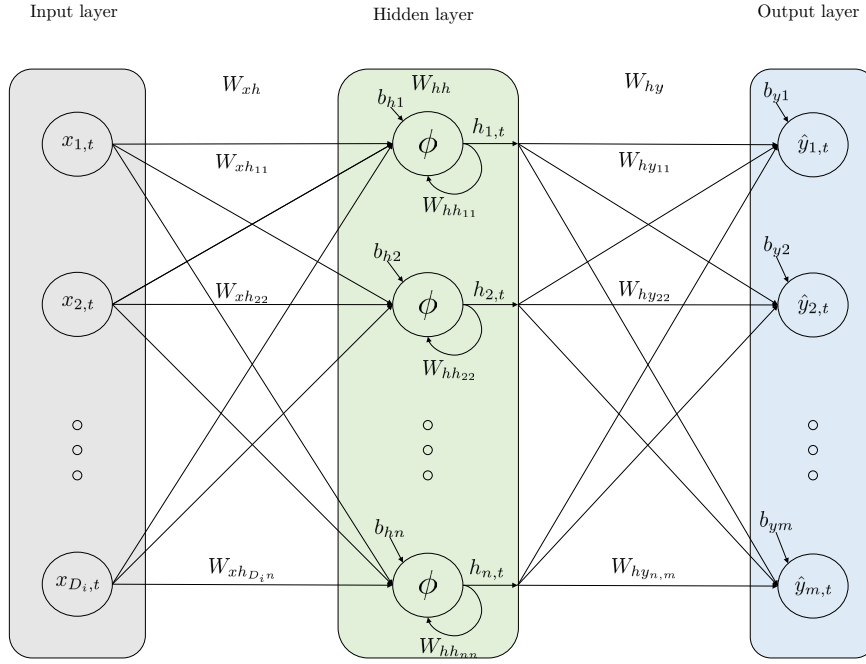


Figure 6.8: Architecture of a RNN with an input, a hidden and an output layer. The network maps the input sequence  $\mathbf{x}_{D_i,t}$  to a hidden sequence  $\mathbf{h}_{n,t}$  and to a sequence of outputs  $\mathbf{y}_{m,t}$ . The parameters  $D_i$ ,  $n$  and  $m$  are the number of signals, the number of hidden units and the number of outputs, respectively.  $W_{xh}$ ,  $W_{hh}$  and  $W_{hy}$  are the input to hidden, hidden to hidden and hidden to output matrices, respectively. The bias vectors of the network are represented by  $\mathbf{b}_h$  for the hidden layer and by  $\mathbf{b}_y$  for the output layer.

where  $\mathbf{b}^l$  is the bias associated to the neurons in layer  $l$ . The last layer of a MLP is defined as the output. Typically, MLPs use fully-connected layers, in which each neuron of layer  $l$  is connected to the all neurons of the layer  $l+1$ . The principal limitation of MLP, is the assumption that the inputs and outputs are independent from each other. In the case of gait kinematic data, it is important to include temporal information in the network. Recurrent neural networks (RNNs) can model time series, audio, video, anything that is presented by means of data sequences. In the sequence data, the present values depend on their past values, as it is the case for the joint angles. RNNs are able to learn arbitrary nonlinear dynamical mappings, such as those commonly found in nonlinear time series prediction [150]. They are not only of interest for the prediction of time series but also generally for the control of the dynamical systems. In [151, 152], the authors explored the possibilities of knee and ankle angle prediction using the surface electromyography signal by applying NARX and LSTM networks. They proved the efficient applicability of recurrent neural network based nonlinear models for predicting human lower limb joint angles. Compared with FNN, where the data flow occurs only in one direction, RNNs apply a back-coupling which results in an asynchronous data flow between nodes. The

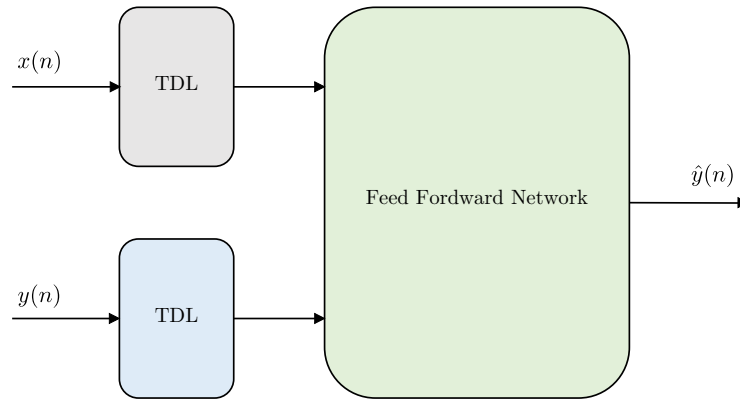


Figure 6.9: A NARX network with series to parallel architecture. The TDL blocks introduce past values (memory effect) of the input and output signals to the network

architecture of a simple RNN is similar to that of a MLP, except that the output of the neuron in hidden layer is fed back to itself with a weight and a time delay as depicted in Figure 6.8. The feedback of previous hidden values (memory effect) allows the network to learn the temporal dynamics of sequential data. A RNN maps a input sequence  $\mathbf{x}_t^l$  to a sequence of hidden values  $\mathbf{h}_t^l = (\mathbf{h}_1^l, \dots, \mathbf{h}_T^l)$  and outputs a sequence  $\mathbf{y}_t^l$  iteratively using the following equations:

$$\mathbf{h}_t^l = \phi(W_{xh}^l \mathbf{x}_t + W_{hh}^l \mathbf{h}_{t-1}^l + \mathbf{b}_h^l), \quad (6.29)$$

$$\hat{\mathbf{y}}_t^{l+1} = W_{hy}^l \mathbf{h}_t^l + \mathbf{b}_y^l, \quad t = 1, 2, \dots, T \quad (6.30)$$

where  $\phi(\cdot)$  is the hidden layer activation function,  $W$  the weight matrices ( $W_{xh}^l$  is the input to hidden weight matrix,  $W_{hh}^l$  is the hidden to hidden weight matrix and  $W_{hy}^l$  is the hidden to output weight matrix),  $\mathbf{b}_h^l$  is the hidden bias vector and  $\mathbf{b}_y^l$  is the bias vector of the output.

#### 6.4.2.1 Nonlinear autoregressive network with exogenous inputs

Nonlinear autoregressive network with exogenous inputs (NARXs) have been considered as a good predictor for time series problems and used to model various nonlinear dynamic systems [153]. They provide the ability to incorporate past values of estimated output  $y(t)$  and exogenous inputs  $x(t)$ . This property of the NARX network makes it more suitable for the modeling problem as the time history information of inputs (kinematic gait data) and past values of the output (estimated lower body joint angles) carries a significant amount of information. The general mathe-

mathematical relationship between inputs and outputs for a NARX neural network model is represented as

$$\hat{\mathbf{y}}(n) = \phi(\mathbf{x}(n), \dots, \mathbf{x}(n-p), \mathbf{y}(n-1), \dots, \mathbf{y}(n-q)), \quad (6.31)$$

where the value of the estimated output signal  $\hat{\mathbf{y}}(n)$  depends on  $q$  previous output values and  $p$  previous input values.  $\phi(\cdot)$  is the nonlinear mapping function and is approximated by the FNN. The tapped delay line (TDL) blocks introduce past values ( $q$  and  $p$ ) of the input and output signals to the network. Due to the advantages over the parallel architecture, such as higher accuracy of the feedforward network input, pure feedforward architecture and use of static backpropagation for training, the serial to parallel architecture shown in Figure 6.9 is considered in this work. The hyperparameters used for the training are explained in Section 6.5.1.2.

## 6.5 DEEP NEURONAL NETWORKS FOR JOINT ESTIMATION AND REHABILITATION MONITORING

Deep structured learning or hierarchical learning is inspired by the biological neural networks' structure and function [154]. It is based initially on the concept of multi-layer artificial neural network (ANN) with the aim to learn data representations automatically; thus, deep learning becomes the method of choice where the classification features, if known at all, are complex, with no straight forward quantitative relation to the raw data [154]. Typically, the term "deep" refers to the number of layers in the variety of possible networks structures such as: FNN, GRNN, CNN, RNN and LSTM a special kind of RNN. This thesis focus on models for gait applications such as CNN and LSTM.

### 6.5.1 Long short-term memory network for joint estimation

Long short-term memory (LSTM) networks are a special type of RNN. The LSTM cell reads the input time series sequentially and transforms the input data into a hidden state at each time step, whereby the current hidden state is a nonlinear function of the current input and the previous hidden state. The advantage of LSTM networks over other types of RNN is that the dependency of the current on the previous hidden state is designed in such a way that the LSTM obtains the ability to keep parts of its hidden state over a larger number of time steps in comparison with other RNN architectures, such as NARX. In [131], this type of network was used to estimate the lower body joint angles with simulated kinematic data obtained from the markers of a camera system. The main cell of a LSTM shown in Figure 6.10 is made of input, output and forget gates. The concept of *gate* was introduced to avoid the problems



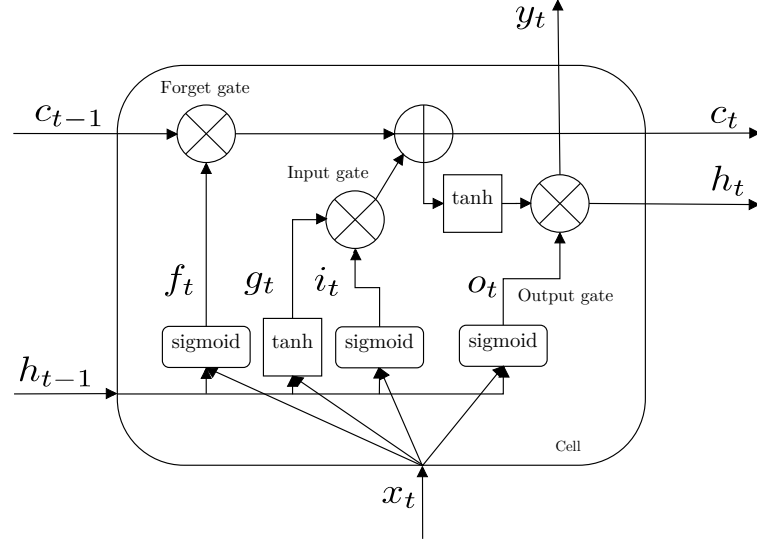


Figure 6.10: LSTM cell. The cell can process data sequentially and keeps its hidden state  $\mathbf{h}$  over the time.

with vanishing or exploding gradients [155]. The LSTM cell remembers the values over an arbitrary interval of time and the other gates can be seen as neurons with an activation function based on the current data  $\mathbf{x}_t$ , a hidden state  $\mathbf{h}_{t-1}$  from the previous iteration, the weight matrices  $W_{ij}$  and bias  $\mathbf{b}_i$  associated to the gates  $i$  and  $j$ . The activation functions are sigmoid ( $\sigma$ ) or tanh. The gates can be seen as the flow regulator of values through the LSTM connections, and control which operation is performed by the cell at each iteration. For the sake of clarity, the super index  $l$  has been omitted. For a LSTM cell (see Figure 6.10), the evolution of its parameters are determined at each iteration by

$$\mathbf{i}_t = \phi_i(W_{xi}\mathbf{x}_t + W_{hi}\mathbf{h}_{t-1} + \mathbf{b}_i) \quad (6.32)$$

$$\mathbf{f}_t = \phi(W_{xf}\mathbf{x}_t + W_{hf}\mathbf{h}_{t-1} + \mathbf{b}_f) \quad (6.33)$$

$$\mathbf{o}_t = \phi(W_{xo}\mathbf{x}_t + W_{ho}\mathbf{h}_{t-1} + \mathbf{b}_o) \quad (6.34)$$

$$\mathbf{g}_t = \phi(W_{xg}\mathbf{x}_t + W_{hg}\mathbf{h}_{t-1} + \mathbf{b}_g) \quad (6.35)$$

$$\mathbf{c}_t = \mathbf{f}_t\mathbf{c}_{t-1} + \mathbf{i}_t\tilde{\mathbf{g}}_t \quad (6.36)$$

$$\mathbf{y}_t = \mathbf{h}_t = \mathbf{o}_t\phi(\mathbf{c}_t), \quad (6.37)$$

where  $\mathbf{i}_t$ ,  $\mathbf{f}_t$ ,  $\mathbf{o}_t$  and  $\mathbf{c}_t$  are the input, forget, output and cell activation gates, respectively. The weights  $W_{ij}$  and biases  $\mathbf{b}_i$  of the gate connections are learned or updated during the network training.

Table 6.2: Input sets of the neural networks.

Signals	3D Acc	A	3D Gyr	G	IMFs	IF	IE	Total signals (D)
Set 1	x		x					6
Set 2	x	x	x	x				8
Set 3	x	x	x	x	x			24
Set 4	x	x	x	x	x	x		40
Set 5	x	x	x	x	x	x	x	56
Number of signals	3	1	3	1	16	16	16	

#### 6.5.1.1 Dataset

For this work, 20 healthy subjects (mean age:  $28 \pm 4$  years, height:  $181 \pm 3.5$  cm) were considered. The medical history of all participants showed no pathological findings or surgical intervention in the lower limbs. The data recording was performed via wearable wireless IMUs as described in Chapter 3. Only the three-dimensional linear acceleration and three-dimensional angular velocity signals were recorded for the investigations using the WSS and an Android tablet. The lower limb joint angles in the sagittal plane were calculated using the information from four IMUs and a KF. The IMUs were placed on the right side at the foot, lower leg, upper leg and the pelvis of the participants as shown in Figure 6.1. They were secured with tight tape to reduce motion artifacts. Each participant performed a walk test in forward direction of around 20 m at a preferred velocity, and subsequently five walking trials. The kinematic gait data of the subjects were recorded and segmented in gait cycles. In order to extend the information of the kinematic gait signals, for each gait cycle, the norm of the acceleration and the gyroscope and the HHT were calculated. The number of IMFs used in this work is two. Table 6.2 shows the different input sets used to train the different networks. The input sets have the dimensions  $D_i \times 124400$ , where  $D_i$  is the total number of signals of each input set ( $i = 1, \dots, 5$ ) and the length of the kinematic signals is 124400 samples. The first input set comprised 3D linear acceleration and angular velocity signals from the IMU on the foot. The second set extends the information of the kinematic signals using the norm of the acceleration and angular velocity. The third set includes the IMFs of the kinematic signals. The fourth and the fifth sets additionally include the IFs and the IEs information, respectively. The output of the networks are the lower body joint angles in the sagittal plane with dimensions  $3 \times 124400$ .

6.5.1.2 *Network Training*

The networks analyzed in this study were implemented in Matlab. They were trained to model the relation between the kinematic gait data from one IMU placed on the foot and the lower body joint angles in the sagittal plane. Five different sets of kinematic signals (see Table 6.2) were used as input and reference lower body joint angles in the sagittal plane as output. The input sets were divided in 80%/20% for the training and test phases, respectively. The performance metric used to compare the different networks is the RMSE, which is calculated according to

$$\text{RMSE} = \sqrt{\frac{1}{L} \sum_{n=1}^L (y(n) - \hat{y}(n))^2}, \quad (6.38)$$

where  $L$  is the length of the signals.  $y(n)$  and  $\hat{y}(n)$  are the reference and estimation signals respectively. The evaluation of the different networks is based on a 10-fold cross-validation scheme to reflect random influences of the data. Due to the different ranges of motion of the lower limbs and the amplitudes of input signals, a normalization of the signals (training and test) is carried out separately. For that reason, the signals are normalized to the range  $[-1,1]$  using the following equation

$$y' = 2 \frac{y - \min(y)}{\max(y) - \min(y)} - 1 \quad (6.39)$$

where  $y'$  is the normalized reference signal. After the training phase, the signals were scaled back to the original amplitudes.

Since  $\epsilon$  is the only free parameter in GRNN the network was trained using a grid search to find the optimal value for the  $\epsilon$  parameter. The optimal value for  $\epsilon$  was determined experimentally and amounts to 1.3.

The NARX network includes three layers (an input layer, a hidden layer and an output layer) and a feedback connection enclosing the input layer. In the input layer, a TDL of two samples was experimentally found to achieve the best performance for different number of neurons. A hyperbolic tangent function and a linear function were selected as the transfer functions of the hidden and output layers. After an iterative process to choose the number of neurons of the hidden layer, the optimal number of neurons were set to 100. The optimization function applied was the scaled conjugate gradient [156].

The structure of the LSTM network was built with three LSTM layers, a fully connected layer and a linear layer. To prevent overfitting, dropout layers were used after each LSTM layer. These type of layers drop nodes randomly on the hidden layers during the training phase. The dropout rate was fixed to 0.3. The LSTM network was trained using the state-of-the-art Adam optimization method [157], which solves an optimization problem viewed as an error function depending on the network param-

Table 6.3: Average RMSE performance comparison of the different neural networks and inputs sets.

		Set 1	Set 2	Set 3	Set 4	Set 5
<b>GRNN</b>	Hip (°)	3.64	3.38	3.74	<b>3.17</b>	3.64
	Knee (°)	5.36	5.14	5.31	<b>4.88</b>	5.35
	Ankle (°)	5.21	4.67	4.88	<b>4.53</b>	4.69
<b>NARX</b>	Hip (°)	2.64	2.53	2.71	<b>2.52</b>	2.86
	Knee (°)	3.25	2.92	3.28	<b>2.31</b>	3.62
	Ankle (°)	4.65	3.49	4.73	<b>3.28</b>	3.92
<b>LSTM</b>	Hip (°)	2.37	2.11	2.32	<b>1.91</b>	2.68
	Knee (°)	2.87	2.64	2.95	<b>2.12</b>	2.82
	Ankle (°)	3.54	2.76	2.86	<b>2.57</b>	3.21

eters. The error measures the difference between the reference and the estimation on the training input set. The backpropagation algorithm changes the weights and biased of all layers with the goal of minimizing the error. In practice only random subsets of the training data called mini-batches are given to the optimization algorithm in one iteration of the training phase to improve the speed of the learning phase [158]. Different mini-batch sizes were analyzed and the best tradeoff between speed and performance was found to be 100. The weight initialization was performed using Xavier [155]. The aim of weight initialization is to prevent layer activation outputs from exploding or vanishing during the course of a forward pass through the deep neural network. The learning rate were set to 0.01. The training epochs were set to 50, which was found to achieve a good trade-off between generalization and classification accuracy, and at the same time avoids overfitting. A stop loss criterion was applied to the training progress by evaluating the validation loss over the validation steps. The training was stopped if there was no improvement in the validation loss during the last 3 validation checks. The configuration of the computer used for training the networks consisted of an Intel® Core 10980XE™, 128 GB RAM and an two NVIDIA GeForce RTX 2070 Super.

### 6.5.2 Results

In this section, the results achieved with the neural networks are presented. Table 6.3 shows the performance of different input sets in the nonlinear estimation of the lower body joint angles in the sagittal plane using the proposed networks. Figure 6.11 shows the joint angle estimation using the GRNN. Figure 6.12 presents the joint angle estimation using the proposed NARX network. Figure 6.13 shows the joint angle estimation using the proposed LSTM network. The blue lines represent the reference

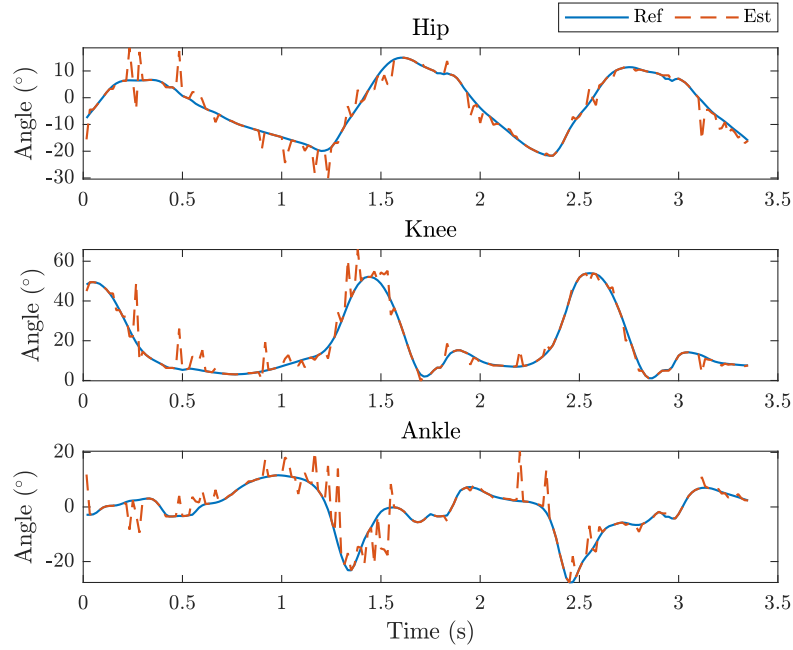


Figure 6.11: Estimated lower limb joint angles in the sagittal plane using the GRNN with the input set 4 and the reference lower limb joint angles from the wearable system. Blue solid lines and red dashed lines are the reference and the estimated joints angles, respectively.

joint angles and the red dashed lines represents the estimated joint angles. As seen in Table 6.3, the LSTM outperforms the other NNs and achieves up to  $1.85^\circ$  and  $0.63^\circ$  better results for the estimation of the lower limb joint angles compared to GRNN and NARX, respectively. According to previous studies [159, 160], the extension of the information from kinematic signals through transformations and using signals from accelerometer and gyroscopes improves the performance of the networks. In this study, the best results in terms of RMSE, were found with the input set 4 and an average RMSE of  $1.91^\circ$ ,  $2.12^\circ$  and  $2.57^\circ$  for the hip, knee and ankle joints angles was achieved. The aim of this study was to evaluate the efficiency of nonlinear techniques in predicting lower limb joint angles from one IMU placed on the foot and provide an easy-to-use wearable system. Therefore, different neural network structures were investigated and the analysis framework was introduced. The first part of the analysis was the segmentation of the gait signals using the gyroscope information to find the IC and TOE events. Afterward, the gait information of each gait cycle was extended by including the norm and the HHT. Five different input sets were fed successively to train the NNs. The lower limb joint angles prediction improved using the input sets 2 and 4 and the best results were achieved with input set 4. Due to extension of information, the NNs were capable to learn the nonlinear relationship between the foot movement and the joint angles and to reduce the estimation error. The LSTM performed better than NARX and GRNN in terms of RMSE, respectively.

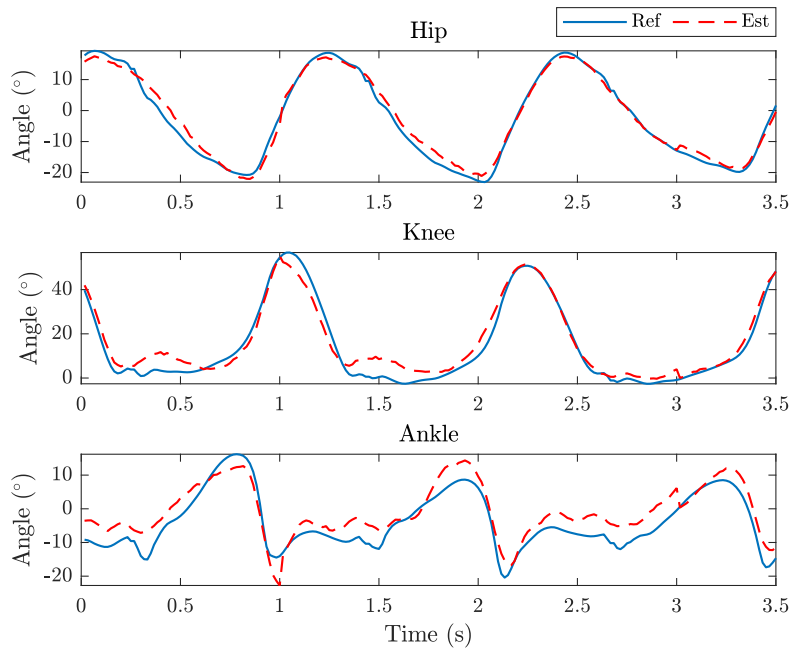


Figure 6.12: Estimated lower limb joint angles in the sagittal plane using the NARX with the input set 4 and the reference lower limb joint angles from the wearable system. Blue solid lines and red dashed lines are the reference and the estimated joints angles, respectively.

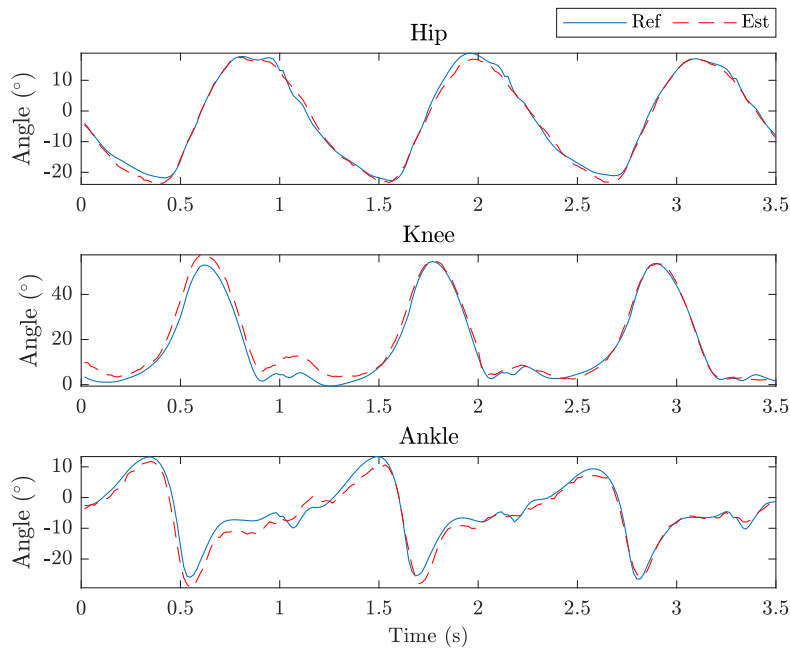


Figure 6.13: Estimated lower limb joint angles in the sagittal plane using the LSTM with the input set 4 and the reference lower limb joint angles from the wearable system. Blue solid lines and red dashed lines are the reference and the estimated joints angles, respectively.

One possible reason for the better performance of RNN compared to GRNN is that GRNNs are single-pass neural networks with no back propagation. Another reason is that the GRNN do not incorporate the previous values for the estimation of the joint angles. The performance difference between LSTM and NARX can be explain due to the LSTM cell structure (see Figure 6.10). The cell has the ability to forget parts of its previously stored memory, as well as to add parts of the new information over a larger number of time steps.

Previous studies on the estimation of lower limb joint angles have been conducted in the recent years. Nevertheless, in our work in the NN structure, the type of applied sensors, the number of datasets and location of IMUs and the type of data (simulated/virtual kinematic) are different. In [130], an artificial NN is applied to simulate the progression of angle values in the lower limbs, where the angles extracted from a camera system are the inputs for the network, and the correlation coefficient between the input and output signals serves as the performance measure. In [129], the lower limb joint angles were estimated using a CNN with a camera system, 23 markers and 9 strain sensors. The RMSE results obtained in the sagittal plane for inter-participant were  $5.39^\circ$ ,  $6.38^\circ$  and  $3.92^\circ$  for hip, knee and ankle, respectively. The authors in [135] obtained a value of  $7^\circ$  RMSE in the estimation of the knee joint angle with mechanomyography signals and a CNN. The outcomes reported in [131],  $1.74^\circ$ ,  $1.92^\circ$  and  $1.80^\circ$  for the hip, knee and ankle joint angles in the sagittal plane are comparable with those in this work. However, the larger data set applied in their study and the simulated kinematic data obtained from the markers of the camera system, which do not include the soft tissue movements measured by IMUs, could explain the relatively better performance in the estimation of the lower limb joint angles. According to our studies, the pattern and range of motion of the lower limb joint angles varies from one subject to another, and in particular those for the ankle and knee are less consistent compared to those of the hip. A larger data set could further improve the estimation results. In addition, the anthropometric differences and various walking styles of the subjects can lead to individual biomechanical gait parameters, and thus estimation errors, which can be tolerated to a certain degree.

### 6.5.3 Convolutional neuronal networks for rehabilitation monitoring

It has been shown that CNNs are suitable for processing multidimensional data [158]. They have the ability to learn a high level of abstraction and features by applying a convolution operation to the raw input data. The CNN architecture used here is based on the following building layers: Convolutional (Conv), batch normalization (BN), rectified linear unit (ReLU), dropout (D), anterior posterior (AP), fully connected (FC) and Softmax (see Fig. 6.1). A convolutional connection between layers is defined by a set of  $K_l$  kernels  $h_1, \dots, h_{K_l}$  of length  $L_l$  and biases  $b_1, \dots, b_{N_l}$ . The

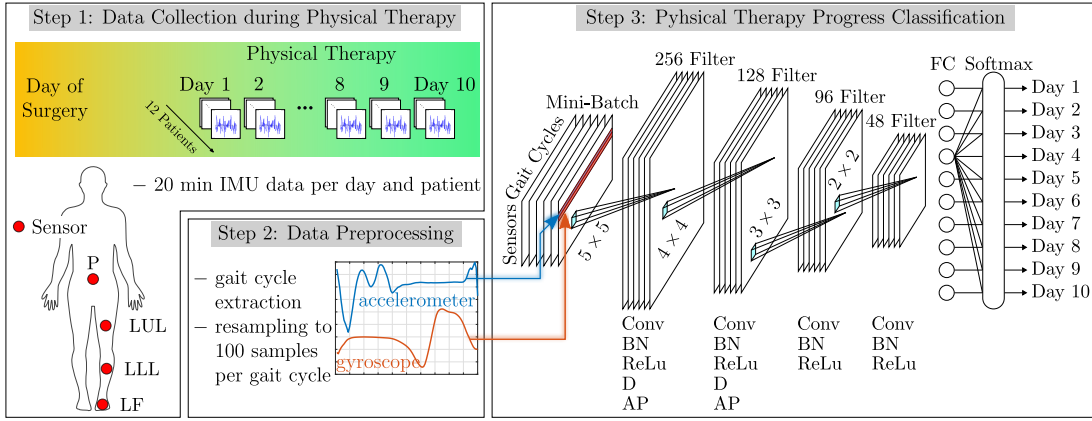


Figure 6.14: Wearable System Concept: the gait kinematic data are collected and processed with ML methods in an Android application for digital and biomedical health-care systems. First step, data collection from patients with hip unilateral arthroplasty surgery. Second step, segmentation of kinematic signals in GC. Third step, use of different IMUs and kinematic signals to train the proposed DCNN for rehabilitation progress monitoring.

index  $l$  hereby represents a label for the layer. Given a multidimensional input vector  $x_d$  with  $d = 1, \dots, K_{l-1}$ , the output of the convolutional connection is computed as [138]

$$o_n = \phi \left( \sum_d h_{n,d} * x_d + b_n \right), \tag{6.40}$$

with  $n = 1, \dots, K_l$ . To increase the stability of the CNN, BN normalizes the output of the previous activation layer by subtracting the batch mean and dividing by the batch standard deviation. The activation function  $\phi$  used for this type of connection is ReLU. Dropout layers work by probabilistically removing inputs from a previous layer to the next one. The dropout parameter is defined as  $r$ . It has the effect of making nodes in the network generally more robust to the inputs. The AP layers increase robustness of the extracted features. The feature maps obtained by the convolutional connection are downsampled by taking the average in temporal windows of length  $p$ . The fully connected layer connects all outputs from the previous layer to all the inputs on the next layer. This type of connection is defined by a set of weight vectors  $W_1, \dots, W_{K_l}$  and biases  $b_1, \dots, b_{N_l}$ . Given a single-channel input vector  $x$ , the activation of the densely connected layer is computed by matrix multiplication as [138]

$$a_k = \text{ReLu} \left( \sum_l W_{l,k} * x_l + b_k \right), \tag{6.41}$$

with  $k = 1, \dots, K_l$ . Following the dense layer, a Softmax layer is applied. The Softmax layer turns numeric output of the last linear layer of a multi-class classification net-



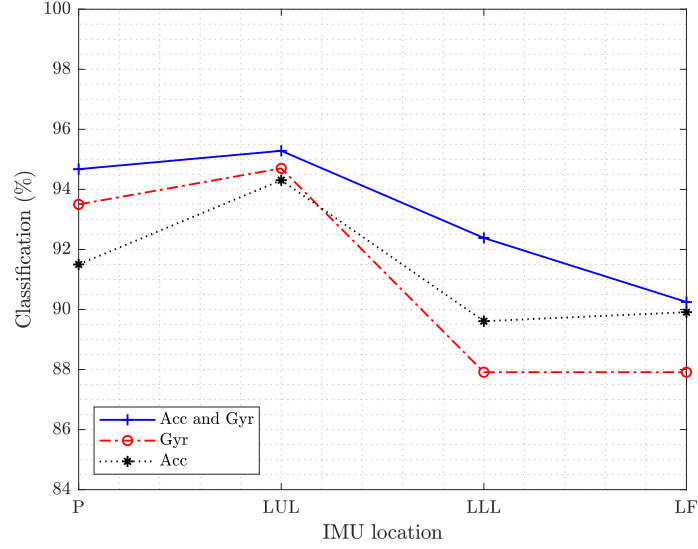


Figure 6.15: Classification accuracy of one IMU applying the proposed DCNN for Pelvis (P), Left Upper Leg (LUL), Left Lower Leg (LLL) and Left Foot (LF).

work into probabilities by taking the exponents of each output and then normalizing each number with the sum of the exponents. The Softmax output vector adds up to one. The last layer of the network is the classification layer. This layer uses the cross entropy loss function for multi-class classification. The cross entropy loss function is given by

$$c(y, m) = -\omega_m \log \left( \frac{e^{y_m}}{\sum_{u=0}^{M-1} e^{y_u}} \right), \quad (6.42)$$

where  $\omega_m$  is the loss weight of each class.  $y_m$  and  $y_u$  are the outputs to the different classes. The index  $m = 0, \dots, M - 1$  refers to the number of classes, which in this study is 10. Although there are numerous advantages regarding the depth structure of a DCNN, a drawback from a structure with several layers are the complicated hyper-parameters as well as the choice of architectures, which increases the difficulty to build an appropriate and efficient model. Despite there are several studies [161, 162] in the area of the parameter automatic optimization for deep architectures, this procedure is extremely time-consuming and the optimal solution easily tends to converge to a local minimum because of the considerable amount of parameters. Thus, the DCNN model was build initially based on a few general design principles [163]. Then, different network configurations are tested using the kinematic data to look for the best performance. The best architecture is set as final model.

Table 6.4: Proposed DCNN architecture and hyperparameters.

Layer	Parameters and functions
Input	$R \times C \times 1 \times 98116$
Convolutional	5x5, 256, 'same', BN, ReLu, D (r = 0.5) AP (2x2,Stride=1)
Convolutional	4x4, 128, 'same', BN, ReLu, D (r = 0.2) AP (2x2,Stride=2)
Convolutional	3x3, 96, 'same', BN, ReLu
Convolutional	2x2, 48, 'same', BN, ReLu
Fully connected	10 classes
SoftMax	
Classification	Cross Entropy

#### 6.5.4 Results

The lower body gait kinematic data from twelve patients with hip unilateral arthroplasty were used for this study. The study lasted for two weeks excluding weekends and the patients had to perform one rehabilitation session of 20 min per day after the operation. The gait kinematic data were separated in different rehabilitation days (1 to 10). The 3D linear acceleration and 3D angular velocity were segmented into GCs using the method described in Chapter 4. The kinematic data from each patient and day were mixed together using different signals (linear acceleration and/or angular velocity) and IMUs (pelvis, thigh, shank and foot) to build a larger dataset for training, validating and testing the DCNN network. The 4D input matrix dimensions ( $R \times C \times d \times S$ ) of the each dataset fed into the DCNN depended on the number of IMUs and gait kinematic signals. The total number of available input matrices  $S$ , after the segmentation of the gait kinematic data of all twelve patients, is 98116. The number of channels  $d$  is 1. The columns  $C$  of the input data matrix is set to 1 GC (100 samples). The rows  $R$  of the input data matrix depends on the number of IMUs (1 to 4) and kinematic signals (3 to 24). In case of applying only one type of kinematic signal (acceleration or angular velocity), the number of signals per IMU is 3. In case of applying both kinematic signals (acceleration and angular velocity), the number of signals per IMU is 6 (see Table 6.4).

To analyze the optimal placement of the IMUs and the impact of different kinematic signals on the rehabilitation progress monitoring, the CNN was implemented in Matlab and trained several times with different IMU combinations and signals. For all cases, the training, validation and test data were randomly split into 70% | 15% | 15%, respectively. For optimization, we used the adaptive moment estimation (ADAM) method [157]. The mini-batch size and learning rate were set to 32 and 0.01, re-

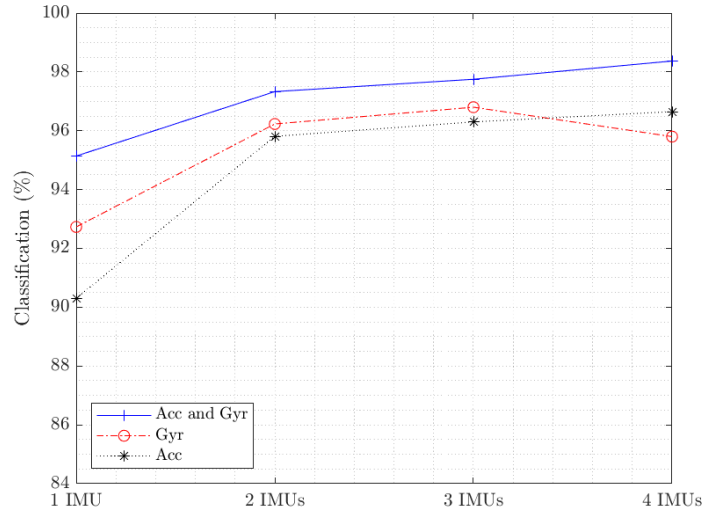


Figure 6.16: Classification accuracy of multiple IMUs applying the proposed DCNN.

spectively. The training epochs were set to 15, which was found to achieve a good trade-off between generalization and classification accuracy, and at the same time avoids overfitting. A stop loss criterion was applied to the training progress by evaluating the validation loss over the validation steps. The training was stopped if there was no improvement in the validation loss during the last 3 validation checks.

Fig. 6.15 shows the classification accuracy for different locations of the IMUs and the effect of combining different kinematic signals for the progress monitoring. It can be seen that the classification accuracy for different sensors decreases as in the following order: thigh (LUL), pelvis (P), shank (LLL) and foot (LF). The best results for one IMU are achieved at the thigh with 3D acceleration and 3D angular velocity, since the related sensor is directly located below the hip joint and therefore, the kinematic signals reflect the changes of the limb motion range during the rehabilitation progress. The shank and the foot locations are not directly affected after the operation and thus exhibit low classification accuracy. Figure 6.16 shows the classification accuracy for more than one sensor and the effect of different kinematic signals. It is seen that using more sensors for the rehabilitation monitoring progress leads to an improvement of the accuracy. For two IMUs, the thigh and the pelvis achieved the best results. For three IMUs, the thigh, pelvis and shank led to the highest classification accuracy. The effect of different kinematic signals (3D accelerometer and 3D angular velocity) of the IMUs regarding the classification accuracy are not consistent for gyroscopes and accelerometers. In the case of one IMU, the 3D angular velocity signals achieve better results than the 3D acceleration for the pelvis and thigh. However, the 3D acceleration signals achieve better results than the 3D angular velocity for the shank and foot. This effect may suggest that upper limb locations are convenient for gyroscopes and lower limb locations are more suitable for acceleration sensors. Therefore, the

combination of the complementary information from different sensors, signals and locations increases the classification accuracy.

## 6.6 CONCLUDING REMARKS

The main focus of this chapter is to investigate the efficiency of MPM, ML and deep neural networks applied in joint angle modeling of the lower limbs using the kinematic records of a single IMU placed on the foot and application of CNN for the rehabilitation monitoring using the kinematic data.

In the first part of this Chapter, the idea of memory polynomial modeling to simulate the physical mechanism of gait kinematics was presented. Therefore, the IMU sensors used recorded kinematic data at the feet in order to model the hip, ankle and knee joint angles in the sagittal plane. Using gait cycle normalization and the LS estimation approach the MPM is identified and the optimal solution is obtained using the normalized mean square error (NMSE). The performance of the MPM in modeling the desired signals is verified and an absolute error of approximately  $5^\circ$  ( $4^\circ$ ,  $6^\circ$  and  $4^\circ$  for the joint hip, knee and ankle angles, respectively) is achieved. The MPM capability to estimate the desired signal using data from other participants was examined. The NMSE differs from one joint angle estimation to another and the performance is lower than the given NMSE in modeling. The initial work shows that the MPM has potential in building digital twins for gait rehabilitation; however further investigations need to be performed to improve the model accuracy. Thus, the focus of our future work is the improvement of the model performance using different sensor placements, pre-processing and estimation approaches followed by significant analysis on a larger data set.

The second part of the chapter compared three different neural networks approaches with different input combinations was performed and the RMSE was used to assess the estimation accuracy of the lower limb joint angles in the sagittal plane. The LSTM outperforms the GRNN and NARX networks and achieves up to  $1.85^\circ$  and  $0.63^\circ$  better results for the estimation of the lower limb joint angles, respectively. The best results in terms of RMSE, were obtained with the input set 4 and an average RMSE of  $1.91^\circ$ ,  $2.12^\circ$  and  $2.57^\circ$  for the hip, knee and ankle joints angles was achieved. According to the evaluation results, LSTM networks are very accurate in the estimation of lower limb joint angles, and of great potential in building digital twins for gait rehabilitation. Future research activities could focus on the lower limb joint estimation using CNNs to reduce the estimation error, perform estimation more precisely and simplify the preprocessing steps on the kinematic data. The application of the proposed framework to bigger data set to achieve and establish a general applicable system could be the subject of future studies as well. Looking ahead, this work supports the use of wearable sensors in combination with machine learning techniques

for the estimation of lower limb joint angles in digital health and rehabilitation applications. Ultimately, the straightforward and easy use of the proposed wearable system in the form of digital twins has considerable practical implications, and opens new possibilities for in-field diagnosis and better prevention strategies.

The last part of this chapter investigated the application of the proposed DCNN for the rehabilitation monitoring using the kinematic data of patients with unilateral hip arthroplasty operation. The results show that the proposed DCNN is capable to monitor the progress of the rehabilitation in response to a physiotherapeutic training. Therefore, the integration of machine learning and wearable sensor technology provide an objective way to understand the changes on the human movement during the rehabilitation process. A comprehensive analysis of multiple locations of the wearable sensors for rehabilitation monitoring was performed with the gait kinematic data from four IMUs located at different positions on the body: pelvis, thigh, shank and foot, respectively. The effect of different type of signals (acceleration and angular velocity) was also analyzed. The gait kinematic signals were segmented into GCs and used as input for the proposed DCNN for rehabilitation progress classification. For one IMU, the best results were obtained from the sensor placed on the thigh due to the direct relation to the motion range of the hip. Future work will include the analysis of the number of GCs and kernel size used for the DCNN input data.



---

## CONCLUSIONS AND FUTURE WORK

---

This research project has investigated different signal processing methods and machine learning architectures for digital healthcare systems based on smartphones. This reliable and validated solution can be used in clinical and outdoor settings in supervised and unsupervised scenarios. Smartphone-based solutions, combined with wearable sensing units, can genuinely become a generalized and low-cost solution for providing appropriate resources for quantitative movement analysis with an excellent clinical value, providing enhanced practical and mobility support to an aging population.

While this thesis addresses many open issues described in the first chapter, such as the quantitative statement on healthy and patient gait, the rehabilitation evaluation, reduction of the number of sensors, increasing accuracy, development and optimization of the classification for rehabilitation monitoring, assessment of the quality of the rehabilitation and the problem of the amount of data generated by the systems among others, there are other use cases and application-based conditions which may come to light during the implementation the proposed framework in real-world scenarios. Moreover, some limitations may restrict its direct application in various scenarios and thus require future work. One such requirement may be that the framework should be fast enough to be executed in near real-time. Currently, the prototype application implementation is near real-time as it requires temporal windowing for the feature extraction values in order to extract relevant information from every window. One approach to improve the performance would be to parse the kinematic signal in small batches and run the algorithm over each such batch of data. The data batches or windowing is necessary to adjust the algorithm to different gait speeds. Also, currently, the machine and deep learning methods are implemented in MATLAB® R2019b (MathWorks, USA) with in-built functions and routines. The processing performance could be increased by moving the high-level language to the native language, such as C/C++, and using faster scripts and functions for high calculation operations. Another problem when monitoring a patient over long periods would generate sensor data containing activities other than just walking, such as other daily living activities. Integrating an activity recognition process could be a workable approach to select walking periods from the unprocessed kinematic data and use them

for the proposed method. Thus for other tasks other than walking, the data could be saved or neglected to save energy and increase battery life or even applied for walking detection tasks to obtain better detection accuracies. The presented algorithms have been tested and verified with a few patients with hip unilateral arthroplasty surgery. Therefore the number of participants is a current limitation. This was because of the absence of pathological gait databases. Extremely challenging gait patterns with undefined gait events would be the goal for further investigation and analysis. For further development of gait analysis, it is necessary to conduct measurements and studies in laboratory environments with fixed settings and perform more studies and measurement campaigns to collect the patients' daily activities and rehabilitation sessions. The comprehension of patients' actions and habits would yield functional specifications such as system requirements, adjust the battery consumption, data storage, feedback to patients, and develop reliable and robust algorithms. Furthermore, homes, offices, and public transport will soon be equipped with several sensors. Thus fusing the information from different sensing modalities would generate much deeper and contextual information about the patient's movements and activities and thus leading to newer solutions and improved support systems.



---

## BIBLIOGRAPHY

---

- [1] P. Larrañaga et al. "Machine learning in bioinformatics." In: *Briefings in Bioinformatics* 7.1 (Mar. 2006), pp. 86–112. ISSN: 1467-5463. DOI: 10.1093/bib/bbk007. URL: <https://doi.org/10.1093/bib/bbk007>.
- [2] Z. Abu-Faraj, G. Harris, P. Smith, and S. Hassani. "Human Gait and Clinical Movement Analysis." In: Dec. 2015, pp. 1–34.
- [3] M. Whittle. *Gait Analysis: An Introduction*. Butterworth-Heinemann, 2007. ISBN: 9780750688833.
- [4] J. Perry and J. Burnfield. *Gait Analysis: Normal and Pathological Function*. Feb. 2010. ISBN: 978-1556427664.
- [5] Ronny Kurniawan Ibrahim. "Novel Gait Models and Features for Gait Patterns Classification." In: (2011).
- [6] R. M. Guimarães and B. Isaacs. "Characteristics of the gait in old people who fall." In: *International rehabilitation medicine* 2 4 (1980), pp. 177–80.
- [7] Xingchen Wang. "Machine Learning for Gait Classification." In: (2017).
- [8] C. Frigo and P. Crenna. "Multichannel SEMG in clinical gait analysis: A review and state-of-the-art." In: *Clinical biomechanics (Bristol, Avon)* 24 (Dec. 2008), pp. 236–45. DOI: 10.1016/j.clinbiomech.2008.07.012.
- [9] *AMTI Force and Motion*. <https://www.amti.biz/>. Accessed: 2020-09-17.
- [10] *Optitrack*. <https://optitrack.com/>. Accessed: 2020-09-17.
- [11] Siddhartha K. "Gait Event Detection in the Real World." In: (2018).
- [12] A. Godfrey, R. Conway, D. Meagher, and G. O'Laighin. "Direct measurement of human movement by accelerometry." In: *Medical engineering & physics* 30.10 (Dec. 2008), pp. 1364–1386. ISSN: 1350-4533. DOI: 10.1016/j.medengphy.2008.09.005. URL: <http://dx.doi.org/10.1016/j.medengphy.2008.09.005>.
- [13] J. J. Kavanagh and H. B. Menz. "Accelerometry: A technique for quantifying movement patterns during walking." In: *Gait & Posture* 28.1 (2008), pp. 1 – 15. ISSN: 0966-6362. DOI: <http://dx.doi.org/10.1016/j.gaitpost.2007.10.010>. URL: <http://www.sciencedirect.com/science/article/pii/S0966636207002706>.
- [14] W. Jirattigalachote, M. Hunt, M. Cutkosky, and S. Delp. "Quantified self and human movement: A review on the clinical impact of wearable sensing and feedback for gait analysis and intervention." In: *Gait & Posture* 40 (May 2014). DOI: 10.1016/j.gaitpost.2014.03.189.
- [15] R. Caldas et al. "A systematic review of gait analysis methods based on inertial sensors and adaptive algorithms." In: *Gait & Posture* 57 (June 2017), pp. 204–210. DOI: 10.1016/j.gaitpost.2017.06.019.
- [16] A. Muro, B. Zapiain, and A. Mendez-Zorrilla. "Gait Analysis Methods: An Overview of Wearable and Non-Wearable Systems, Highlighting Clinical Applications." In: *Sensors (Basel, Switzerland)* 14 (Feb. 2014), pp. 3362–94. DOI: 10.3390/s140203362.

- [17] X. Yun and E. R. Bachmann. "Design, Implementation, and Experimental Results of a Quaternion-Based Kalman Filter for Human Body Motion Tracking." In: *IEEE Transactions on Robotics* 22.6 (2006), pp. 1216–1227.
- [18] *IMU User Guide Rev1.4*. [http://www.shimmersensing.com/images/uploads/docs/IMU\\_User\\_Guide\\_rev1.4.pdf](http://www.shimmersensing.com/images/uploads/docs/IMU_User_Guide_rev1.4.pdf). Accessed: 2021-06-13.
- [19] A. Burns et al. "SHIMMER: A Wireless Sensor Platform for Noninvasive Biomedical Research." In: *IEEE Sensors Journal* (Sept. 2010). DOI: 10.1109/JSEN.2010.2045498.
- [20] S. McCracken. *Android 4 Desarrollo Profesional de Aplicaciones*. De profesional a profesional. Inforbook's, 2013. ISBN: 978-84-15033-65-3. URL: <http://www.inforbooks.com/llibres.php?id=978-84-15033-65-3>.
- [21] J.T. Gironés. *El Gran Libro de Android*. EL GRAN LIBRO DE. Marcombo, 2013. ISBN: 9788426719973. URL: [http://books.google.de/books?id=K9hnCJ\\\_NGq4C](http://books.google.de/books?id=K9hnCJ\_NGq4C).
- [22] Google, ed. <http://developer.android.com/>. Google. 2020.
- [23] H.M. Deitel, P.J. Deitel, and A.V.R. Elizondo. *Cómo programar en Java*. 5th. Pearson Educación. Pearson Educación, 2004. ISBN: 9702605180. URL: <http://books.google.es/books?id=tR7k9ga5Cj0C>.
- [24] *Shimmer: Discovery in Motion*. URL: <http://www.shimmersensing.com/>.
- [25] Jared Levy, ed. *Multimaps*-<https://google-collections.googlecode.com/svn/trunk/javadoc/com/google/common/collect/Multimap.html>. Google.
- [26] X. Wang. "Machine Learning for Gait Classification." In: 2017.
- [27] A. Noureldin, T.B. Karamat, and J. Georgy. *Fundamentals of Inertial Navigation, Satellite-based Positioning and their Integration*. Springer Berlin Heidelberg, 2012. ISBN: 9783642304651. URL: <https://books.google.de/books?id=a-BqvoCd2RkC>.
- [28] Peter S Maybeck. *Stochastic models, estimation, and control*. Academic press, 1982.
- [29] Robert Grover Brown and Patrick Y C Hwang. *Introduction to random signals and applied kalman filtering: with MATLAB exercises and solutions; 3rd ed*. New York, NY: Wiley, 1997.
- [30] G. Minkler and J. Minkler. *Theory and Application of Kalman Filtering*. Magellan Book Company, 1993. ISBN: 9780962161827.
- [31] G. Welch and G. Bishop. "An Introduction to the Kalman Filter: SIGGRAPH 2001 Course 8." In: *Computer Graphics, Annual Conference on Computer Graphics & Interactive Techniques*. 2001, pp. 12–17.
- [32] R.S. Bucy, P.D. Joseph, Karreman Mathematics Research Collection, and University of Southern California los Angeles Dept. of Aerospace Engineering. *Filtering for Stochastic Processes with Applications to Guidance*. Interscience tracts in pure and applied mathematics. Interscience Publishers, 1968.
- [33] S.M. Kay. *Fundamentals of Statistical Signal Processing: Detection theory*. Fundamentals of Statistical Si. Prentice-Hall PTR, 1998. ISBN: 9780133457117. URL: <https://books.google.de/books?id=va9LAQAAIAAJ>.

- [34] I. Skog, J.-O Nilsson, and P. Händel. "Evaluation of zero-velocity detectors for foot-mounted inertial navigation systems." In: *International Conference on Indoor Positioning and Indoor Navigation (IPIN)*. IEEE. Oct. 2010, pp. 1–6.
- [35] R. Feliz Alonso, E. Zalama Casanova, and J. Gómez García-Bermejo. "Pedestrian tracking using inertial sensors." In: (2009).
- [36] L. Ojeda and J. Borenstein. "Non-GPS Navigation for Security Personnel and First Responders." In: *Journal of Navigation - J NAVIG* 60 (Sept. 2007).
- [37] S. Godha and G. Lachapelle. "Foot mounted inertial system for pedestrian navigation." In: *Measurement Science and Technology* 19.7 (May 2008), p. 075202.
- [38] S. Kwakkel, Gérard Lachapelle, and Elizabeth Cannon. "GNSS Aided In Situ Human Lower Limb Kinematics During Running." In: *21st International Technical Meeting of the Satellite Division of the Institute of Navigation, ION GNSS 2008* 4 (Jan. 2008).
- [39] S. Godha, G. Lachapelle, and E. Cannon. "Integrated GPS/INS System for Pedestrian Navigation in a Signal Degraded Environment." In: *ION GNSS* (Jan. 2006).
- [40] B. Krach and P. Robertson. "Integration of Foot-Mounted Inertial Sensors into a Bayesian Location Estimation Framework." In: Apr. 2008, pp. 55 –61. ISBN: 978-1-4244-1798-8. DOI: 10.1109/WPNC.2008.4510357.
- [41] J. Taborri, E. Palermo, S. Rossi, and P. Cappa. "Gait Partitioning Methods: A Systematic Review." In: *Sensors* 16.1 (2016). ISSN: 1424-8220. DOI: 10.3390/s16010066. URL: <http://www.mdpi.com/1424-8220/16/1/66>.
- [42] Kamiar Aminian et al. "Spatio-temporal Parameters of Gait Measured by an Ambulatory System Using Miniature Gyroscopes." In: *Journal of biomechanics* 35 (June 2002), pp. 689–99. DOI: 10.1016/S0021-9290(02)00008-8.
- [43] A. Salarian et al. "Gait assessment in Parkinson's disease: toward an ambulatory system for long-term monitoring." In: *IEEE Transactions on Biomedical Engineering* 51.8 (2004), pp. 1434–1443.
- [44] G.P. Panebianco, M.C. Bisi, R. Stagni, and S. Fantozzi. "Analysis of the performance of 17 algorithms from a systematic review: Influence of sensor position, analyzed variable and computational approach in gait timing estimation from IMU measurements." In: *Gait & Posture* 66 (2018), pp. 76 –82. ISSN: 0966-6362.
- [45] A.M. Sabatini, C. Martelloni, S. Scapellato, and F. Cavallo. "Assessment of walking features from foot inertial sensing." In: *IEEE Transactions on Biomedical Engineering* 52.3 (Mar. 2005), pp. 486–494. ISSN: 1558-2531. DOI: 10.1109/TBME.2004.840727.
- [46] A. Baghdadi, L.A. Cavuoto, and J.L. Crassidis. "Hip and Trunk Kinematics Estimation in Gait Through Kalman Filter Using IMU Data at the Ankle." In: *IEEE Sensors Journal* 18.10 (May 2018), pp. 4253–4260. ISSN: 2379-9153.
- [47] S.K.A. Kork et al. "Biometric database for human gait recognition using wearable sensors and a smartphone." In: *2017 2nd International Conference on Bioengineering for Smart Technologies (BioSMART)*. Aug. 2017, pp. 1–4.

- [48] N.H. Ghassemi et al. "Segmentation of Gait Sequences in Sensor-Based Movement Analysis: A Comparison of Methods in Parkinson's Disease." In: *Sensors* 18.1 (2018). ISSN: 1424-8220. DOI: 10.3390/s18010145. URL: <https://www.mdpi.com/1424-8220/18/1/145>.
- [49] Hiroki Saito and Takashi Watanabe. "Kalman-Filtering-Based Joint Angle Measurement with Wireless Wearable Sensor System for Simplified Gait Analysis." In: *IEICE Transactions on Information and Systems* E94.D.8 (2011), pp. 1716–1720. DOI: 10.1587/transinf.E94.D.1716.
- [50] R.M. Rogers. *Applied Mathematics in Integrated Navigation Systems*. AIAA education series Bd. 1. American Institute of Aeronautics and Astronautics, 2003. ISBN: 9781563476563. URL: <https://books.google.de/books?id=dfS2WcYba9wC>.
- [51] M.A. Anwary, H. Yu, and M. Vassallo. "An Automatic Gait Feature Extraction Method for Identifying Gait Asymmetry Using Wearable Sensors." In: *Sensors* 18 (Feb. 2018), p. 676. DOI: 10.3390/s18020676.
- [52] J.B. Kuipers. *Quaternions and Rotation Sequences: A Primer with Applications to Orbits, Aerospace, and Virtual Reality*. Princeton paperbacks. Princeton University Press, 2002. ISBN: 9780691102986.
- [53] R. A. Arif, Y. Hongnian, and M. Vassallo. "An Automatic Gait Feature Extraction Method for Identifying Gait Asymmetry Using Wearable Sensors." In: *Sensors*. 2018.
- [54] S. O. H. Madgwick, A. J. L. Harrison, and R. Vaidyanathan. "Estimation of IMU and MARG orientation using a gradient descent algorithm." In: *2011 IEEE International Conference on Rehabilitation Robotics*. 2011, pp. 1–7. DOI: 10.1109/ICORR.2011.5975346.
- [55] N. Krishnan, C. Juillard, D. Colbry, and S. Panchanathan. "Recognition of hand movements using wearable accelerometers." In: *JAISE* 1 (Jan. 2009), pp. 143–155. DOI: 10.3233/AIS-2009-0019.
- [56] A. Avci et al. "Activity Recognition Using Inertial Sensing for Healthcare, Well-being and Sports Applications: A Survey." In: *Architecture of Computing Systems (ARCS), 2010 23rd International Conference on*. Feb. 2010, pp. 1–10.
- [57] Nishkam Ravi, Nikhil Dandekar, Preetham Mysore, and Michael L. Littman. "Activity Recognition from Accelerometer Data." In: *AAAI*. 2005.
- [58] T. Huynh and B. Schiele. "Analyzing Features for Activity Recognition." In: New York, NY, USA: Association for Computing Machinery, 2005, 159–163. DOI: 10.1145/1107548.1107591. URL: <https://doi.org/10.1145/1107548.1107591>.
- [59] U. Maurer, A. Smailagic, D. P. Siewiorek, and M. Deisher. "Activity recognition and monitoring using multiple sensors on different body positions." In: *International Workshop on Wearable and Implantable Body Sensor Networks (BSN'06)*. 2006, 4 pp.–116.
- [60] I.A. Rezek and S.J. Roberts. *Stochastic Complexity Measures for Physiological Signal Analysis*. 1996.

- [61] T. Inouye et al. "Quantification of EEG irregularity by use of the entropy of the power spectrum." In: *Electroencephalography and Clinical Neurophysiology* 79.3 (1991), pp. 204–210. ISSN: 0013-4694. DOI: [https://doi.org/10.1016/0013-4694\(91\)90138-T](https://doi.org/10.1016/0013-4694(91)90138-T). URL: <http://www.sciencedirect.com/science/article/pii/001346949190138T>.
- [62] Z. Feng and H. Chen. "Analyze the Dynamic Features of Rat EEG Using Wavelet Entropy." In: *Conference proceedings : ... Annual International Conference of the IEEE Engineering in Medicine and Biology Society. IEEE Engineering in Medicine and Biology Society. Conference 1* (Feb. 2005), pp. 833–6. DOI: 10.1109/IEMBS.2005.1616544.
- [63] M Sekine et al. "Analysis of Acceleration Signals using Wavelet Transform." In: *Methods of information in medicine* 39 (July 2000), pp. 183–5. DOI: 10.1055/s-0038-1634267.
- [64] D. Karantonis et al. "Implementation of a Real-Time Human Movement Classifier Using a Triaxial Accelerometer for Ambulatory Monitoring." In: *Information Technology in Biomedicine, IEEE Transactions on* 10 (Feb. 2006), pp. 156–167. DOI: 10.1109/TITB.2005.856864.
- [65] J. Wu et al. "Gesture Recognition with a 3-D Accelerometer." In: vol. 5585. July 2009, pp. 25–38. ISBN: 978-3-642-02829-8. DOI: 10.1007/978-3-642-02830-4\_4.
- [66] Y. Xia, Q. Gao, and Q. Ye. "Classification of gait rhythm signals between patients with neuro-degenerative diseases and normal subjects: Experiments with statistical features and different classification models." In: *Biomedical Signal Processing and Control* 18 (Apr. 2015). DOI: 10.1016/j.bspc.2015.02.002.
- [67] D. Lai, R. Begg, and M. Palaniswami. "Computational Intelligence in Gait Research: A Perspective on Current Applications and Future Challenges." In: *IEEE Transactions on Information Technology in Biomedicine* 13 (Sept. 2009), pp. 687–702. DOI: 10.1109/TITB.2009.2022913.
- [68] S. Dutta, D. Ghosh, and S. Samanta. "Non linear approach to study the dynamics of neurodegenerative diseases by Multifractal Detrended Cross-correlation Analysis—A quantitative assessment on gait disease." In: *Physica A: Statistical Mechanics and its Applications* 448 (2016), pp. 181–195. ISSN: 0378-4371. DOI: <https://doi.org/10.1016/j.physa.2015.12.074>. URL: <http://www.sciencedirect.com/science/article/pii/S0378437115011024>.
- [69] M. D. Djurić-Jovičić et al. "Automatic Identification and Classification of Freezing of Gait Episodes in Parkinson's Disease Patients." In: *IEEE Transactions on Neural Systems and Rehabilitation Engineering* 22.3 (2014), pp. 685–694.
- [70] E. Baratin et al. "Wavelet-Based Characterization of Gait Signal For Neurological Abnormalities." In: *Gait & Posture* 41 (Jan. 2015). DOI: 10.1016/j.gaitpost.2015.01.012.
- [71] S.H. Lee and J. S. Lim. "Parkinson's disease classification using gait characteristics and wavelet-based feature extraction." In: *Expert Systems with Applications* 39.8 (2012), pp. 7338–7344. ISSN: 0957-4174. DOI: <https://doi.org/10.1016/j.eswa.2012.01.084>. URL: <http://www.sciencedirect.com/science/article/pii/S0957417412000978>.

- [72] R. Moe-Nilssen. "A new method for evaluating motor control in gait under real life environmental conditions. Part 2: Gait analysis." In: *Clinical Biomechanics* 13.4-5 (1998), pp. 328–335. ISSN: 0268-0033. URL: <http://www.sciencedirect.com/science/article/pii/S0268003398000904>".
- [73] E. Cusó, X. Guardino, J.M. Riera, and M. Gassiot. "Non-linear fitting method for recorded chromatographic peaks." In: *Journal of Chromatography A* 95.2 (1974), pp. 147–157. ISSN: 0021-9673. DOI: [http://dx.doi.org/10.1016/S0021-9673\(00\)84073-X](http://dx.doi.org/10.1016/S0021-9673(00)84073-X). URL: <http://www.sciencedirect.com/science/article/pii/S002196730084073X>.
- [74] J. G. Proakis and D. G. Manolakis. *Digital Signal Processing (3rd Ed.): Principles, Algorithms, and Applications*. Upper Saddle River, NJ, USA: Prentice-Hall, Inc., 1996. ISBN: 0-13-373762-4.
- [75] R. Moe-Nilssen and J. L. Helbostad. "Estimation of gait cycle characteristics by trunk accelerometry." In: *Journal of biomechanics* 37.1 (2004), pp. 121–126.
- [76] D.T.H. Lai, R.K. Begg, and M. Palaniswami. "Computational Intelligence in Gait Research: A Perspective on Current Applications and Future Challenges." In: *Information Technology in Biomedicine, IEEE Transactions on* 13.5 (Sept. 2009), pp. 687–702. ISSN: 1089-7771. DOI: 10.1109/TITB.2009.2022913.
- [77] M. Yang et al. "Assessing Accelerometer Based Gait Features to Support Gait Analysis for People with Complex Regional Pain Syndrome." In: *PETRA '10* (2010), 48:1–48:7. DOI: 10.1145/1839294.1839352.
- [78] A. V. Oppenheim, A. S. Willsky, and S. H. Nawab. *Signals & systems / Alan V. Oppenheim, Alan S. Willsky, with S. Hamad Nawab*. English. 2nd ed. Previous ed.: 1983. Upper Saddle River, N.J. : Prentice Hall ; London : Prentice-Hall International, 1997. ISBN: 0138147574.
- [79] S. Haykin. *Communication systems*. English. New York : Wiley, 1978. ISBN: 0471029777.
- [80] Alan V. Oppenheim, Ronald W. Schaffer, and John R. Buck. *Discrete-time Signal Processing (2Nd Ed.)* Upper Saddle River, NJ, USA: Prentice-Hall, Inc., 1999. ISBN: 0-13-754920-2.
- [81] A. B. Carlson, P. Crilly, and P. B. Crilly. *Communication Systems*. McGraw-Hill Education, 2009. ISBN: 9780073380407. URL: <http://books.google.de/books?id=-hRGAQAIAAJ>.
- [82] M. J. Hinich. "A statistical theory of signal coherence." In: *IEEE Journal of Oceanic Engineering* 25.2 (2000), pp. 256–261. DOI: 10.1109/48.838988.
- [83] Melvin J. Hinich and Phillip Wild. "Detecting finite bandwidth periodic signals in stationary noise using the signal coherence spectrum." In: *Signal Processing* 85.8 (2005), pp. 1557–1562. ISSN: 0165-1684. DOI: <https://doi.org/10.1016/j.sigpro.2005.02.008>. URL: <http://www.sciencedirect.com/science/article/pii/S0165168405000770>.
- [84] I. A. Rezek and S. J. Roberts. "Stochastic complexity measures for physiological signal analysis." In: *IEEE Transactions on Biomedical Engineering* 45.9 (1998), pp. 1186–1191. DOI: 10.1109/10.709563.

- [85] T Inouye et al. "Quantification of EEG irregularity by use of the entropy of the power spectrum." In: *Electroencephalography and clinical neurophysiology* 79.3 (1991), 204–210. ISSN: 0013-4694. DOI: 10.1016/0013-4694(91)90138-t.
- [86] O. Rosso et al. "Wavelet entropy: A new tool for analysis of short duration brain electrical signals." In: *Journal of Neuroscience Methods* 105 (Jan. 2001), pp. 65–75.
- [87] S. G. Mallat. "A theory for multiresolution signal decomposition: the wavelet representation." In: *IEEE Transactions on Pattern Analysis and Machine Intelligence* 11.7 (1989), pp. 674–693. DOI: 10.1109/34.192463.
- [88] D. Li, D.S.K. Magnuson, and R. Jung. "Non-stationary analysis of extracellular neural activity." In: *Neurocomputing* 32-33 (2000), pp. 1083–1093. ISSN: 0925-2312. DOI: [https://doi.org/10.1016/S0925-2312\(00\)00282-4](https://doi.org/10.1016/S0925-2312(00)00282-4). URL: <http://www.sciencedirect.com/science/article/pii/S0925231200002824>.
- [89] J. Walleczek. "Self-Organized Biological Dynamics and Nonlinear Control: Toward Understanding Complexity, Chaos and Emergent Function in Living Systems." In: Aug. 2009. ISBN: 9780521624367. DOI: 10.1017/CB09780511535338.016.
- [90] Atefeh Goshvarpour and Ateke Goshvarpour. "Nonlinear Analysis of Human Gait Signals." In: *International Journal of Information Engineering and Electronic Business* 4 (Apr. 2012). DOI: 10.5815/ijieeb.2012.02.03.
- [91] N. Huang et al. "The empirical mode decomposition and the Hilbert spectrum for nonlinear and non-stationary time series analysis." In: *Proceedings of the Royal Society of London. Series A: Mathematical, Physical and Engineering Sciences* 454 (Mar. 1998), pp. 903–995. DOI: 10.1098/rspa.1998.0193.
- [92] O. Dehzangi, M. Taherisadr, and R. ChangaVala. "IMU-Based Gait Recognition Using Convolutional Neural Networks and Multi-Sensor Fusion." In: *Sensors* 17 (Nov. 2017), p. 2735. DOI: 10.3390/s17122735.
- [93] G. Huang, C. Wu, and J. Lin. "Gait analysis by using tri-axial accelerometer of smart phones." In: *2012 International Conference on Computerized Healthcare (ICCH)*. Dec. 2012, pp. 29–34. DOI: 10.1109/ICCH.2012.6724466.
- [94] S. Moghaddamnia, J. Peissig, G. Schmitz, and A. O. Effenberg. "A simplified approach for autonomous quality assessment of cyclic movements." In: *2013 18th International Conference on Digital Signal Processing (DSP)*. 2013, pp. 1–5. DOI: 10.1109/ICDSP.2013.6622672.
- [95] D. C. Montgomery and G. C. Runger. *Applied Statistics and Probability for Engineers*. John Wiley & Sons, 2010.
- [96] S. Theodoridis and K. Koutroumbas. *Pattern Recognition, Fourth Edition*. 4th. Academic Press, 2008. ISBN: 1597492728, 9781597492720.
- [97] R.O. Duda, P.E. Hart, and D.G. Stork. *Pattern Classification (2Nd Edition)*. Wiley-Interscience, 2000. ISBN: 0471056693.
- [98] R. A. Fisher. "The use of Multiple Measurement in Taxonomic Problems." In: *Annals of Eugenics* 7.2 (1936), pp. 179–188. DOI: 10.1111/j.1469-1809.1936.tb02137.x.
- [99] G. Engeln-Müllges, K. Niederdrenk, and R. Wodicka. *Numerik-Algorithmen*. Xpert. press Series. Springer Berlin Heidelberg, 2010. ISBN: 9783642134739.

- [100] Damir Kalpić, Nikica Hlupić, and Miodrag Lovrić. "Student's t-Tests." In: *International Encyclopedia of Statistical Science*. Ed. by Miodrag Lovric. Berlin, Heidelberg: Springer Berlin Heidelberg, 2011, pp. 1559–1563. DOI: 10.1007/978-3-642-04898-2\_641.
- [101] S. Moghaddamnia, J. Peissig, G. Schmitz, and A.O. Effenberg. "On the efficiency of an autonomous cyclic motion grading system." In: *Statistical Signal Processing (SSP), 2014 IEEE Workshop on*. June 2014, pp. 512–515. DOI: 10.1109/SSP.2014.6884688.
- [102] T. Hermann, A. Hunt, and J.G. Neuhoff. *The Sonification Handbook*. Logos Verlag Berlin, Germany, 2011.
- [103] A. O. Effenberg et al. "Movement sonification: effects on motor learning beyond rhythmic adjustments." In: *Frontiers in neuroscience* 10 (2016), p. 219.
- [104] R. Sigrist et al. "Sonification and haptic feedback in addition to visual feedback enhances complex motor task learning." In: *Experimental brain research* 233.3 (2015), pp. 909–925.
- [105] D. Schol et al. "Moving with music for stroke rehabilitation: a sonification feasibility study." In: *Annals of the New York Academy of Sciences* 1337.1 (2015), pp. 69–76. DOI: 10.1111/nyas.12691.
- [106] S.Y. Park, S.Y. Lee, H.C. Kang, and S.M. Kim. "EMG analysis of lower limb muscle activation pattern during pedaling: Experiments and computer simulations." In: *International Journal of Precision Engineering and Manufacturing* 13.4 (2012), pp. 601–608. ISSN: 2005-4602. DOI: 10.1007/s12541-012-0077-4.
- [107] C. Prakash et al. "Passive Marker Based Optical System for Gait Kinematics for Lower Extremity." In: *Procedia Computer Science* 45 (2015). International Conference on Advanced Computing Technologies and Applications (ICACTA), pp. 176–185. ISSN: 1877-0509. DOI: <https://doi.org/10.1016/j.procs.2015.03.116>.
- [108] L. Yu et al. "Adaptive method for real-time gait phase detection based on ground contact forces." In: *Gait & Posture* 41 (Oct. 2014). DOI: 10.1016/j.gaitpost.2014.10.019.
- [109] J. Conte Alcaraz, S. Moghaddamnia, and J. Peissig. "Mobile quantification and therapy course tracking for gait rehabilitation." In: *2017 22nd International Conference on Digital Signal Processing (DSP)*. 2017, pp. 1–5. DOI: 10.1109/ICDSP.2017.8096106.
- [110] S. Gill, N. Seth, and E. Scheme. "A Multi-Sensor Matched Filter Approach to Robust Segmentation of Assisted Gait." In: *Sensors* 18.9 (2018). ISSN: 1424-8220. DOI: 10.3390/s18092970. URL: <https://www.mdpi.com/1424-8220/18/9/2970>.
- [111] M. Meghji et al. "An Algorithm for the Automatic Detection and Quantification of Athletes' Change of Direction Incidents Using IMU Sensor Data." In: *IEEE Sensors Journal* 19.12 (2019), pp. 4518–4527. ISSN: 2379-9153.
- [112] N.M. Rad, T. Van Laarhoven, C. Furlanello, and E. Marchiori. "Novelty Detection using Deep Normative Modeling for IMU-Based Abnormal Movement Monitoring in Parkinson's Disease and Autism Spectrum Disorders." In: *Sensors* 18.10 (2018). ISSN: 1424-8220. DOI: 10.3390/s18103533.



- [113] J.L.S. Waugh et al. "Online Learning of Gait Models From Older Adult Data." In: *IEEE Transactions on Neural Systems and Rehabilitation Engineering* 27.4 (2019), pp. 733–742. ISSN: 1558-0210.
- [114] J. Kavanagh. "Lower trunk motion and speed-dependence during walking." In: *Journal of neuroengineering and rehabilitation* 6 (May 2009), p. 9. DOI: 10.1186/1743-0003-6-9.
- [115] S. Qiu et al. "MEMS Inertial Sensors Based Gait Analysis for Rehabilitation Assessment via Multi-Sensor Fusion." In: *Micromachines* 9.9 (2018). ISSN: 2072-666X. DOI: 10.3390/mi9090442. URL: <http://www.mdpi.com/2072-666X/9/9/442>.
- [116] N.V. Boulgouris and Z.X. Chi. "Gait Recognition Using Radon Transform and Linear Discriminant Analysis." In: *IEEE Transactions on Image Processing* 16.3 (2007), pp. 731–740. ISSN: 1941-0042. DOI: 10.1109/TIP.2007.891157.
- [117] D. Kobsar and R. Ferber. "Wearable Sensor Data to Track Subject-Specific Movement Patterns Related to Clinical Outcomes Using a Machine Learning Approach." In: *Sensors* 18.9 (2018). ISSN: 1424-8220. DOI: 10.3390/s18092828. URL: <https://www.mdpi.com/1424-8220/18/9/2828>.
- [118] C. Mao, Y. Li, and F. Sun. "Accelerometer-Based Gait Recognition Using PCA LDA Algorithms." In: *2018 IEEE 23rd International Conference on Digital Signal Processing (DSP)*. 2018, pp. 1–4.
- [119] J. Conte Alcaraz, S. Moghaddamnia, M. Fuhrwerk, and J. Peissig. "Efficiency of the Memory Polynomial Model in Realizing Digital Twins for Gait Assessment." In: *2019 27th European Signal Processing Conference (EUSIPCO)*. 2019, pp. 1–5. DOI: 10.23919/EUSIPCO.2019.8903143.
- [120] G. Mayer-Kress, Y.T. Liu, and K. M. Newell. "Complex systems and human movement." In: *Complexity* 12.2 (2006), pp. 40–51. DOI: 10.1002/cplx.20151. eprint: <https://onlinelibrary.wiley.com/doi/pdf/10.1002/cplx.20151>. URL: <https://onlinelibrary.wiley.com/doi/abs/10.1002/cplx.20151>.
- [121] A. Salarian et al. "A Novel Approach to Reducing Number of Sensing Units for Wearable Gait Analysis Systems." In: *IEEE Transactions on Biomedical Engineering* 60.1 (2013), pp. 72–77. ISSN: 1558-2531. DOI: 10.1109/TBME.2012.2223465.
- [122] R. Ferber, S.T. Osis, J.L. Hicks, and S.L. Delp. "Gait biomechanics in the era of data science." In: *Journal of Biomechanics* 49.16 (2016), pp. 3759–3761. ISSN: 0021-9290. DOI: <https://doi.org/10.1016/j.jbiomech.2016.10.033>.
- [123] R.C. Deo. "Machine Learning in Medicine." In: *Circulation* 132.20 (2015), pp. 1920–1930. DOI: 10.1161/CIRCULATIONAHA.115.001593.
- [124] T. Zebin, P.J. Scully, and K.B. Ozanyan. "Human activity recognition with inertial sensors using a deep learning approach." In: *2016 IEEE SENSORS*. 2016, pp. 1–3. DOI: 10.1109/ICSENS.2016.7808590.
- [125] F.J. Ordóñez and D. Roggen. "Deep Convolutional and LSTM Recurrent Neural Networks for Multimodal Wearable Activity Recognition." In: *Sensors* 16.1 (2016). ISSN: 1424-8220. DOI: 10.3390/s16010115. URL: <https://www.mdpi.com/1424-8220/16/1/115>.

- [126] H.T.T. Vu et al. "ED-FNN: A New Deep Learning Algorithm to Detect Percentage of the Gait Cycle for Powered Prostheses." In: *Sensors* 18.7 (2018). ISSN: 1424-8220. DOI: 10.3390/s18072389. URL: <https://www.mdpi.com/1424-8220/18/7/2389>.
- [127] Z. Ding et al. "The Real Time Gait Phase Detection Based on Long Short-Term Memory." In: *2018 IEEE Third International Conference on Data Science in Cyberspace (DSC)*. 2018, pp. 33–38. DOI: 10.1109/DSC.2018.00014.
- [128] T. Zebin, N. Peek, A. Casson, and M. Sperrin. "Human activity recognition from inertial sensor time-series using batch normalized deep LSTM recurrent networks." In: vol. 2018. July 2018. DOI: 10.1109/EMBC.2018.8513115.
- [129] M. Gholami et al. "Lower Body Kinematics Monitoring in Running Using Fabric-Based Wearable Sensors and Deep Convolutional Neural Networks." In: *Sensors* 19.23 (2019). ISSN: 1424-8220. DOI: 10.3390/s19235325. URL: <https://www.mdpi.com/1424-8220/19/23/5325>.
- [130] M. Błażkiewicz and A. Wit. "Artificial neural network simulation of lower limb joint angles in normal and impaired human gait." In: *Acta of bioengineering and biomechanics* 20 4 (2018), pp. 43–49.
- [131] M. Mundt et al. "Prediction of lower limb joint angles and moments during gait using artificial neural networks." In: *Medical & Biological Engineering & Computing* 58 (Dec. 2019). DOI: 10.1007/s11517-019-02061-3.
- [132] A. Findlow et al. "Predicting Lower Limb Joint Kinematics Using Wearable Motion Sensors." In: *Gait & Posture* 28.1 (2008), pp. 120–126. ISSN: 0966-6362. DOI: <https://doi.org/10.1016/j.gaitpost.2007.11.001>.
- [133] J.Y. Goulermas et al. "Regression Techniques for the Prediction of Lower Limb Kinematics." In: *Journal of Biomechanical Engineering* 127.6 (July 2005), pp. 1020–1024. ISSN: 0148-0731. DOI: 10.1115/1.2049328.
- [134] J. Hannink et al. "Sensor-Based Gait Parameter Extraction With Deep Convolutional Neural Networks." In: *IEEE Journal of Biomedical and Health Informatics* 21.1 (2017), pp. 85–93. ISSN: 2168-2208. DOI: 10.1109/JBHI.2016.2636456.
- [135] H. Wu, Q. Huang, D. Wang, and L. Gao. "A CNN-SVM Combined Regression Model for Continuous Knee Angle Estimation Using Mechanomyography Signals." In: *2019 IEEE 3rd Information Technology, Networking, Electronic and Automation Control Conference (ITNEC)*. Mar. 2019, pp. 124–131. DOI: 10.1109/ITNEC.2019.8729426.
- [136] Sadiq A. and Eyad A. "Behavioral modeling of RF front end devices in Simulink." PhD thesis. Mar. 2008. DOI: 10.13140/RG.2.1.1870.4881.
- [137] M. G. Pandy. "Simple and Complex Models for Studying Muscle Function in Walking." In: *Philosophical Transactions: Biological Sciences* 358.1437 (2003), pp. 1501–1509. ISSN: 09628436.
- [138] J. Hannink et al. "Sensor-Based Gait Parameter Extraction With Deep Convolutional Neural Networks." In: *IEEE Journal of Biomedical and Health Informatics* 21.1 (2017), pp. 85–93.
- [139] R. H. Flake. "Volterra series representation of nonlinear systems." In: *Transactions of the American Institute of Electrical Engineers, Part II: Applications and Industry* 81.6 (1963), pp. 330–335. DOI: 10.1109/TAI.1963.6371765.

- [140] L. Ding. "Digital Predistortion of Power Amplifiers for Wireless Applications." PhD thesis. School of Electrical and Computer Engineering, Georgia Institute of Technology, Mar. 2004.
- [141] Hyunchul Ku and J. S. Kenney. "Behavioral modeling of nonlinear RF power amplifiers considering memory effects." In: *IEEE Transactions on Microwave Theory and Techniques* 51.12 (2003), pp. 2495–2504.
- [142] D. X. Liu et al. "Gait Phase Recognition for Lower-Limb Exoskeleton with Only Joint Angular Sensors." In: *Sensors* 16.10 (2016). ISSN: 1424-8220. DOI: 10.3390/s16101579. URL: <http://www.mdpi.com/1424-8220/16/10/1579>.
- [143] J. Conte Alcaraz, S. Moghaddamnia, N. Poschadel, and J. Peissig. "Machine Learning as Digital Therapy Assessment for Mobile Gait Rehabilitation." In: *2018 IEEE 28th International Workshop on Machine Learning for Signal Processing (MLSP)*. Sept. 2018, pp. 1–6. DOI: 10.1109/MLSP.2018.8517005.
- [144] M. Ma et al. "An Adaptive Zero Velocity Detection Algorithm Based on Multi-Sensor Fusion for a Pedestrian Navigation System." In: *Sensors* 18.10 (2018). ISSN: 1424-8220. DOI: 10.3390/s18103261. URL: <http://www.mdpi.com/1424-8220/18/10/3261>.
- [145] S. K. A. Kork et al. "Biometric database for human gait recognition using wearable sensors and a smartphone." In: *2017 2nd International Conference on Bio-engineering for Smart Technologies (BioSMART)*. Aug. 2017, pp. 1–4. DOI: 10.1109/BIOSMART.2017.8095329.
- [146] H. Saito and T. Watanabe. "Kalman-filtering-based joint angle measurement with wireless wearable sensor system for simplified gait analysis." In: *IEICE TRANSACTIONS on Information and Systems* 94.8 (2011), pp. 1716–1720.
- [147] F. Rosenblatt. *Principles of neurodynamics: perceptrons and the theory of brain mechanisms*. Report (Cornell Aeronautical Laboratory). Washington: Spartan Books, 1962.
- [148] A. J. Al-mahasneh, S.G. Anavatti, and M. Pratama. "Applications of General Regression Neural Networks in Dynamic Systems." In: *Digital Systems*. IntechOpen, Nov. 2018.
- [149] D. Specht. "A general regression neural network." In: *IEEE transactions on neural networks / a publication of the IEEE Neural Networks Council* 2 (Feb. 1991), pp. 568–76. DOI: 10.1109/72.97934.
- [150] K.S. Narendra and K. Parthasarathy. "Identification and control of dynamical systems using neural networks." In: *IEEE Transactions on Neural Networks* 1.1 (Mar. 1990), pp. 4–27. ISSN: 1941-0093. DOI: 10.1109/72.80202.
- [151] R. Gupta, I.S. Dhindsa, and R. Agarwal. "Continuous angular position estimation of human ankle during unconstrained locomotion." In: *Biomedical Signal Processing and Control* 60 (2020), p. 101968. ISSN: 1746-8094.
- [152] X Ma, Y. Liu, Q. Song, and C. Wang. "Continuous Estimation of Knee Joint Angle Based on Surface Electromyography Using a Long Short-Term Memory Neural Network and Time-Advanced Feature." In: *Sensors* 20.17 (2020).
- [153] H. Liu and X. Song. "Nonlinear system identification based on NARX network." In: *2015 10th Asian Control Conference (ASCC)*. May 2015, pp. 1–6.

- [154] O. Costilla Reyes et al. "Deep Learning in Gait Analysis for Security and Healthcare." In: (Oct. 2019), pp. 299–334. DOI: 10.1007/978-3-030-31760-7\_10.
- [155] X. Glorot and Y. Bengio. "Understanding the difficulty of training deep feed-forward neural networks." In: *AISTATS*. Vol. 9. JMLR Proceedings. 2010, pp. 249–256.
- [156] M.F. Møller. "A scaled conjugate gradient algorithm for fast supervised learning." In: *Neural Networks* 6.4 (1993), pp. 525–533. ISSN: 0893-6080. DOI: [https://doi.org/10.1016/S0893-6080\(05\)80056-5](https://doi.org/10.1016/S0893-6080(05)80056-5). URL: <http://www.sciencedirect.com/science/article/pii/S0893608005800565>.
- [157] D.P. Kingma and J.L. Ba. "Adam: A Method for Stochastic Optimization." In: *International Conference on Learning Representations* (Dec. 2014).
- [158] I. Goodfellow, Y. Bengio, and A. Courville. *Deep Learning*. Cambridge: MIT Press, 2016.
- [159] F. J. Morales and D. Roggen. "Deep Convolutional and LSTM Recurrent Neural Networks for Multimodal Wearable Activity Recognition." In: *Sensors (Basel, Switzerland)* 16 (2016).
- [160] S.-M. Lee, S. M. Yoon, and H. Cho. "Human activity recognition from accelerometer data using Convolutional Neural Network." In: *2017 IEEE International Conference on Big Data and Smart Computing (BigComp)*. 2017, pp. 131–134. DOI: 10.1109/BIGCOMP.2017.7881728.
- [161] James S. Bergstra, Rémi Bardenet, Yoshua Bengio, and Balázs Kégl. "Algorithms for Hyper-Parameter Optimization." In: *Advances in Neural Information Processing Systems* 24. Ed. by J. Shawe-Taylor et al. Curran Associates, Inc., 2011, pp. 2546–2554.
- [162] L. Zhang and P.N. Suganthan. "A survey of randomized algorithms for training neural networks." In: *Information Sciences* 364-365 (2016), pp. 146–155. ISSN: 0020-0255. DOI: <https://doi.org/10.1016/j.ins.2016.01.039>.
- [163] Ossama A.-H., li D., and Dong Y. "Exploring Convolutional Neural Network Structures and Optimization Techniques for Speech Recognition." In: Aug. 2013.

---

## PUBLICATIONS

---

Javier Conte Alcaraz, Sanam Moghaddamnia and Jürgen Peissig. “Efficiency of Deep Neural Networks for Joint Angle Modeling in Digital Gait Assessment.” In: *EURASIP Journal on Advances in Signal Processing*, February 2021.

Javier Conte Alcaraz, Sanam Moghaddamnia, Maxim Penner and Jürgen Peissig. “Monitoring the Rehabilitation Progress Using a DCNN and Kinematic Data for Digital Healthcare.” In: *IEEE 28th European Signal Processing Conference (EUSIPCO)*, Amsterdam, Netherlands, August 2020.

Javier Conte Alcaraz, Sanam Moghaddamnia, Martin Fuhrwerk and Jürgen Peissig. “Efficiency of the Memory Polynomial Model in Realizing Digital Twins for Gait Assessment.” In: *IEEE 27th European Signal Processing Conference (EUSIPCO)*, A Coruña, Spain, September 2019.

Javier Conte Alcaraz, Sanam Moghaddamnia, Nils Poschadel and Jürgen Peissig. “Machine Learning as Digital Therapy Assessment for Mobile Gait Rehabilitation.” In: *IEEE 28th International Workshop on Machine Learning for Signal Processing (MLSP)*, Aalborg, Denmark, September 2018.

Javier Conte Alcaraz, Sanam Moghaddamnia and Jürgen Peissig. “Mobile Quantification and Therapy Course Tracking for Gait Rehabilitation.” In: *IEEE 22nd International Conference on Digital Signal Processing (DSP)*, London, UK, August 2017.

Nils Poschadel, Sanam Moghaddamnia, Javier Conte Alcaraz, Marc Steinbach and Jürgen Peissig. “A Dictionary Learning Based Approach for Gait Classification.” In: *IEEE 22nd International Conference on Digital Signal Processing (DSP)*, London, UK, August 2017.

Javier Conte Alcaraz, Sanam Moghaddamnia and Jürgen Peissig. “An Android-based Application for Digital Gait Performance Analysis and Rehabilitation.” In: *IEEE 17th International Conference on E-health Networking, Application & Services (HealthCom)* Boston, USA, October 2015.



---

## CURRICULUM VITAE

---

Name Javier Conte Alcaraz  
Day of birth 29. Januar 1989

### Education

10/2018 to 03/2021 **Ph.D.** student Leibniz Universität Hannover  
Thesis title: Intelligent Signal Processing for Digital  
Healthcare Monitoring

09/2007 to 09/2014 **M.Sc.** in Telecommunications Engineering  
Universidad Politécnica de Cartagena, Murcia, Spain  
Thesis title: Android-based App for Gait Pattern  
Analysis: Implementation and Performance  
Validation

### Work Experience

10/2014 to 03/2021 **Leibniz Universität Hannover**, Institute of  
Communications Technology  
*Research Assistant*

10/2013 to 07/2014 **Studentenwerk**, Hannover  
*Internet Administrator*

10/2014 to 03/2021 **International Office LUH**, Hannover  
*ERASMUS Assistant Coordinator*

### Teaching Experience

10/2014 to 03/2021 **Leibniz Universität Hannover**, Faculty of Electrical  
Engineering and Computer Science

10/2014 to 03/2021 Laboratory: "Transmissions Technologies"  
Academic year of Exercises on "Electroacoustic I"  
2015 to 2016

01/2016 to 03/2021 Exercises on "Modulation tethods"

01/2018 to 03/2021 Exercises on "Digital transmissions"  
Academic year of Certificate on "LUH Professional teaching"  
2018 to 2019

#### COLOPHON

This document was typeset using the typographical look-and-feel classicthesis developed by André Miede. The style was inspired by Robert Bringhurst's seminal book on typography "*The Elements of Typographic Style*".

*Final Version* as of June 15, 2022 (classicthesis).